The application of cosmogenic exposure dating to glacial landforms: Examples from Antarctica and Patagonia.

Christopher Fogwill

(BSc Hons)

Thesis submitted for the degree of Doctor of Philosophy.

Department Of Geography, University of Edinburgh.

This thesis was brought to you by the numbers
26 and 10
and the letters
Al and Be……

Abstract

Through the measurement of the concentrations of the *in situ* cosmogenic nuclides ^{10}Be and ^{26}Al within rock surfaces, this thesis has attempted to solve previously intractable problems regarding the timing and magnitude of glaciation during the last glacial cycle in the vicinity of the Drake Passage. In southernmost Patagonia we have been able to constrain the timing of two major advances of the formerly expanded Patagonian Ice Sheet during the last glacial interglacial transition. In the past these have been in question due to the paucity of radiocarbon dates, in the extremely arid conditions prevailing to the east of the southern-most Andes. The timing of deglaciation over 16^0 of latitude appears to be synchronous, although the magnitude of glaciation differed markedly from latitude to latitude. In southernmost Patagonia maximum ice extent was achieved before 26 ka BP, and deglaciation occurred rapidly at around 17 ka Bp. This is indistinguishable from that of the last glacial period in the Northern Hemisphere. This is interesting as it at a time when insolation was rising to its maximum in the southern hemisphere. The similarity of glacial chronologies from mid-latitudes in both hemispheres indicate that global atmospheric signaling is a major driving mechanism of climate.

Results from Antarctica indicate a much more complex picture, with the Antarctic Peninsula and the Shackleton Range Mountains producing very different patterns of deglaciation. These data suggest that glaciation of the Antarctic Peninsula has been forced predominately by eustatic sea level fluctuations, with a complex spread of ages, suggesting ice surface thinning at times of rapid sea level rise. The pattern of deglaciation is very different in the Shackleton Mountains of Antarctica where Quaternary glacial fluctuations have been characterised by extreme stability, with no evidence of substantial ice thickening suggested by some hypotheses. The concentrations of radionuclides demonstrate that these summits have not been covered by ice for significant periods during the Quaternary. The implication is that this periphery of the East Antarctic Ice Sheet has not thickened by more than 400 m in the last 3 million years. Although these are only preliminary results, they place important constraints on glacial modelling studies and research regarding ice thickening of the Filchner Ice Shelf during glacial maxima. In turn these data have implications for ice-sheet controls of the global seawater budget during the last glacial interglacial cycle.

Preface

This work was funded by the UK Natural Environmental Research Council (NERC), with the Accelerator Mass Spectometry (AMS) analysis undertaken by the Carnegie Fund for Scottish Universities. The results represent my scientific contributions to glacial research in Patagonia and Antarctica, based in Edinburgh.

Due to the geographical spread of sites, together with the specialised nature of terrestrial *in situ* cosmogenic analysis and AMS the results presented here reflect the contributions of outside experts. However, all of the work included in this thesis has been written by myself, and I am fully responsible for all of the data analysis, the glacial history, palaeoclimatic interpretation and conclusions.

I would like to identify the efforts of several individuals who have made each chapter possible. All of the analyses by AMS were completed by Dr Peter Kubik at the Paul Scherer Institute / ETH tandem facility Zürich Switzerland. The samples from the Shackleton Range were taken by Dr Andy Kerr, as part of the joint European EUROSHAK Expedition. The samples from the Antarctic Peninsula were obtained by Dr Mike Bentley, during his NERC funded Fellowship based in Edinburgh. It is acknowledged that 14 out of the 29 sample analysed within this project were run by Dr Mike Bentley. These were included in this thesis as the interpretation of this region is impossible without their inclusion. These samples are identified in the text, the age interpretations from the AMS analyses has been undertaken by Chris Fogwill. Therefore the eventual interpretation is based on my age estimates, together with Dr Mike Bentleys field interpretations. All other aspects of the laboratory analyses were completed by the author in the cosmogenic laboratories in Edinburgh.

Acknowledgements

This work has been several years in the making since its inception as part of the Patagonia Project in 1997, by Prof. Chalmers Clapperton, Prof. David Sugden, Dr Bob McCulloch and Dr Nick Hulton. I am very grateful to Chalmers Clapperton for the opportunity to conduct this research initially at Aberdeen and am sorry that he was unable to be involved through to completion. I would like to thank Prof. David Sugden and Dr Bob McCulloch for encouraging me to transfer to Edinburgh, and for their help and support throughout my time here.

My travels and work in South America were assisted and vastly improved by friends and strangers alike, maybe I can repay you all in kind one day, but for now please accept my gratitude and a smile. Thanks go out to Liam O'Hara, Simon Parfett, Beatrice Castro and "the family Castro", Keith Turner, Tony Dummer, Sr. John Rees (especially for the new passport!), Bob McCulloch, Mike Bentley, Amerindia Expeditions, all the staff at Hotel Explora and Sr. Guilleramo Santana and the Park Rangers and employees of CONAF in Torres del Paine.

Both the laboratory work and the sample analyses would not have been possible without the direct involvement and repeated explanations of Dr Susan Ivy-Ochs and Dr Peter Kubik of ETH and PSI, Zürich Switzerland. I would also like to say Danke and cheers to Dr Silvio Tshudi, and all of the tandem crew, who have always tried their hardest to get the best results from some pretty marginal samples. From an Edinburgh perspective, I would like to say a big thank you to Dr William Phillips, without your help and unceasing enthusiasm many of the technical aspects of the thesis would not have been possible. This gratitude must be extended to Dr Bob McCulloch as well, who provided both practical, technical and theoretical support to every aspect of this work, as well as always fighting my corner as my supervisor. For help with columns, rock crushing and all the rest, my glass is raised to Jeremy Everest, Alan Davidson and Jessica Oragano, I know your pain!

Outside the world of cosmogenics I would like to extend my thanks to many members of the Geography Department here in Edinburgh who have helped through both technical assistance, discussions and the occasional beer. Nice one to Keith Morrison and Ross Purves for all things

technical and never being at all cynical about my work. My understanding of all things glacial has been greatly improved through discussions with Dr Doug Benn, Dr Mike Bentley, Keith Turner and Jeremy Everest and above all Prof. David Sugden. A special thanks must go to Sarah Davies, for reading chapters and also putting up with me taking over half the house with papers, drafts of my thesis, and increasingly raised levels of stress together with dirty mountain bikes, skis, climbing gear, and other stuff.

On a more personnel note I would like to say a big thank you to all of my family, who have always been great, always understanding, even though I've never really been able to explain what I'm doing properly! This thesis would had never come together with out both their emotional and financial support. Big thanks and love go out to Mum, Dad, Kate and my brand new niece Mia, sometimes Devon and Bristol has seemed further away than Patagonia.

Finally, Id like to say there is no way this thesis would have got to this stage without the help, encouragement and love of a certain Frances Mary Taylor. For all of your help and words of encouragement I am so grateful, even if at times I haven't always shown it! I know I wobble sometimes- like the earth on its axis! (sorry for the climate gag), but I am so grateful to you and can't wait for soon. There is so much to look forward to, and I hope I can look forward to it with you!

Declaration

This thesis is the result of my own work. Where the work of others has been used it has been duly acknowledged.

Table of contents

List of figures

List of Tables

CHAPTER 1

Introduction

1.1 Rationale and Strategy

This thesis explores the application of terrestrial *in situ* cosmogenic nuclide (TCN) analysis as a technique of exposure age estimation and as a tool for constraining long term landscape history in mid-latitude and polar glacial environments. To this end I have analysed the concentrations of the long-lived radioisotopes ^{10}Be and ^{26}Al in a total of 33 target surfaces which have been obtained from previously mapped glacial landforms from the field areas shown in Figure 1.1. These localities have been previously studied in terms of their geomorphology and glacial history, but all still await detailed chronologies. This work attempts to constrain the age of moraines and erratics related to the late glacial expansion of the Patagonian Ice Sheet and of glacial expansion in currently ice free areas rising above the present Antarctic Ice Sheet.

The need to constrain the temporal and spatial extent of terrestrial glacial fluctuations reflects the importance of glaciers as indicators of variations in local and regional climate over time. The knowledge of detailed chronologies of ice sheet variations can provide evidence to ground truth or constrain theoretical ice sheet and general circulation models, with the eventual aim of defining a climatic envelope that might have been responsible for the observed pattern of glaciation (Alverson *et al.*, 2000). At present the lack of understanding of the past dynamics of these ice sheets impedes the prediction of their future response to environmental change. This is particularly important today with rising global temperatures related to increasing levels of CO_2 and other greenhouse gases. Some researchers have suggested that this could cause ice sheets such as the West Antarctic Ice Sheet to collapse, resulting in a rise in global sea level and a change in the climate patterns of the southern hemisphere and the global system (Mercer, 1978).

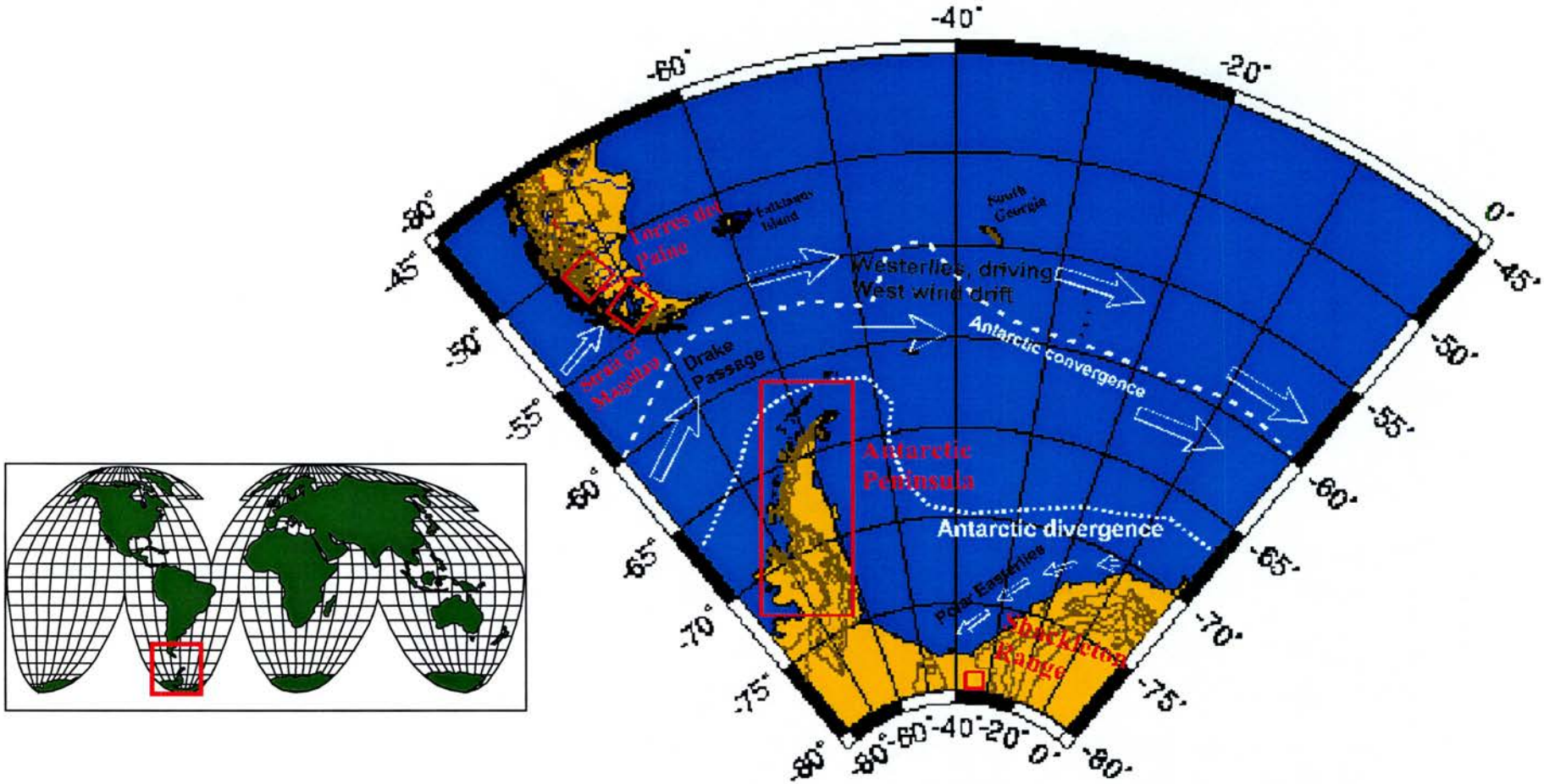

Figure 1.1. Location of study area, together with detailed polar stereographic projection showing the principal Antarctic ocean and atmospheric circulation patterns prevailing today. The main study areas are outlined in red. Near the Antarctic continent a westward flowing current, the East Wind Drift, is driven by the polar easterly wind system. Ekman transport produces a zone of divergence, Antarctic divergence, between the East Wind Drift and the West Wind Drift that circles Antarctica with an easterly flow. The cold West Wind Drift water converges with warmer water in each of the major ocean basins to the north at the Antarctic Convergence. Image courtesy of www.stemnet.nf.ca/cite/maps.htm

In the past the terrestrial record of glacial fluctuations has received relatively little attention by climate theorists, due to its fragmentary nature and sparse chronological control (Broecker and Denton, 1990). This has improved markedly in the past decades with careful application of radiocarbon dating to glacial deposits world-wide, although debate still continues due to an increased understanding of "problems with interpreting ice-margin fluctuations from existing lithostratigraphy and from the reworked wood samples that afford most of the chronological control" (Broecker and Denton, 1990. From Lowell, 1995, page 1542). This problem is compounded in the regions covered by this thesis due to the lack of formation and preservation of organic material suitable for radiocarbon dating.

Recently many workers have attempted to apply the TCN technique to glacial deposits in an effort to obtain event ages for the emplacement of these features (Phillips *et al.*, 1990; Gosse *et al.*, 1995; Ivy-Ochs, 1996; Ivy-Ochs *et al.*, 1999). This is different from many of the more traditional approaches applied to glaciogenic deposits, since it measures the exposure time since the actual event, as opposed to events occurring pre- or post-glaciation as is the case with radiocarbon and tephra-stratigraphy. Recent advances in accelerator mass spectrometry (AMS), and understanding of production rates and local scaling factors of *in situ* cosmogenic nuclides, have made the case for the application of TCN to Quaternary glacial chronological problems more accepted and robust (Stone 2000, Dunai 2000, Gosse and Phillips, 2001). It provides an independent estimate of elapsed time since initial emplacement or exposure of a rock surface, the history of which can be described in terms of its geomophological evolution. Therefore, it allows "the direct evidence of glacier movements on the continents to be fitted to the emerging picture of global palaeoclimate. The timing of glacial fluctuations can be elucidated in detail and world wide, regional, or local synchroneity or nonsynchroneity can be revealed" (Ivy-Ochs 1996, page 1).

1.2 Background: Interhemisperic climate change during the last glacial /interglacial transition

Attempts to model the forcing mechanisms of global climate change, during the last glacial interglacial transition (LGIT) are reliant on a sound knowledge of the spatial and temporal patterns of environmental change. Recent studies have highlighted that there is uncertainty regarding the interhemispheric timing of climate change during this period, with different lines of evidence pointing to puzzling patterns of interhemispheric synchrony and asynchrony between the climate records of the northern and southern hemisphere despite antiphased solar insolation. Conflicting hypotheses rely on data from both different proxy records of climate change and from different geographical localities. Therefore, it is often difficult to relate these records to mechanisms (McCulloch *et al.*, 2000). Indeed it could be that these apparent leads and lags are out-of-phase oscillations at a particular time scale.

In general these interhemispheric hypotheses fall into three camps, focussed on very different forcing mechanisms. The first, based primarily on data from marine cores, invokes changes in the thermohaline circulation of the North Atlantic Ocean that drives global oceanic circulation. This hypothesis suggests that the North Atlantic Ocean in its glacial configuration was extremely sensitive to variations in temperature and meltwater fluxes related to the extensive Northern Hemisphere Ice sheets of the Last Glacial Stage. As such, during times of rapid deglaciation, large volumes of surface meltwater caused the suppression of the Atlantic thermohaline system. Thus the northern and southern hemispheres are linked through the heat engine of the ocean conveyor (Broecker and Denton, 1990), with the North Atlantic acting as the driving mechanism of climate during the LGIT.

A second hypothesis, based on analysis of ice core data from Antarctica, points to changes in the southern hemisphere preceding those in the northern hemisphere. Analysis of atmospheric gases, such as methane and carbon dioxide, trapped within the ice demonstrates that atmospheric warming in continental Antarctica began before culmination of the coldest part of the Last Glacial Maximum in the Northern Hemisphere (Blunier *et al.*, 1998). Interhemispheric correlation of ice core records further strengthens this hypothesis, with Greenland seemingly lagging Antarctica in so-called Dansgard-Oeschger cycles (Blunier *et al.*, 1998). These

variations are punctuated by the late glacial Antarctic Cold Reversal (ACR) in the Antarctic terrestrial record, an event which pre-dates the equivalent northern hemisphere Younger Dryas (YD) cooling event by at least 1800 years (Blunier *et al.*, 1998). These interpretations have strengthened earlier conclusions based on the analysis of the marine record of the southern hemisphere, which indicate an early warming of the Southern Ocean together with the suggestion that high frequency low amplitude climatic variations in the Southern Hemisphere preceded those in the north by thousands of years (Hays *et al.*, 1976; Pichon *et al.*, 1992; Charles *et al.*,1996; Labeyrie *et al., 1996).* Attempts to invoke mechanisms for these apparent leads and lags have varied from a polar see-saw in which the source of polar deep water varies between the North Atlantic and the Southern Ocean (Broecker, 1998), to changes in the Southern Ocean influencing oceanic circulation in the North Atlantic (Toggweiler and Samuels, 1995). Alternatively it could be argued that this evidence supports variable responses, depending on the stage of the glacial interglacial cycle.

A third hypothesis points to the synchrony of glacier fluctuations and associated palaeoecological records between the terrestrial Northern and mid-latitude Southern Hemispheres. This data suggests symmetry of the structure and timing of the last glacial-interglacial transition between sites as geographically diverse as the Chilean Lake District, New Zealand, Ecuador and the North Atlantic (Clapperton *et al.*, 1997, Lowell *et al.*, 1995, Denton *et al.*, 1999). Denton *et al.*(1999), invoke instantaneous atmospheric mechanisms of change to account for this apparent symmetry, suggesting that variations in water vapour in the tropics initiated these changes. This interpretation has been backed by recent data from the analysis of the Taylor Dome Ice Core in coastal Antarctica, and by records of atmospheric CO_2 fluctuations in Argentine Patagonia, which indicates synchrony between these sites and the rapid fluctuations recorded in the North Atlantic (Steig *et al.*, 1998; White *et al.*, 1994).

Each of these hypotheses is based on the interpretation of different proxy records at different locations, and thus it is difficult to establish the nature of the mechanisms at work. The problem is compounded by the geographical distribution of the proxy records on which these hypotheses are based, being heavily biased to the northern hemisphere, particularly NW Europe and North America (McCulloch and Davies, 2001). Therefore the thrust of this thesis is to focus on dating glacier fluctuations in a range of southerly latitudes. The intention is to seek a high-resolution record of glaciation for areas on either side of the Drake Passage, and extending into continental

Antarctica. Such a study may help reveal the timing of changes in the southern hemisphere, and in particular any migration of the southern westerlies during glacial cycles. Modelling studies suggest that the westerlies may exert a powerful control on the large scale meridional circulation and heat transport of the oceans (Toggweiler and Samuels, 1995). These studies indicate that the topography of the Drake Passage influences the West Wind Drift, the magnitude of which is dependent on the strength and position of the westerlies. Thus variations in the strength and location of the westerlies could have a direct effect on upwelling and in turn the production of deep water in both hemispheres. Intensification of the westerlies could also lead to an increase in ocean ventilation which could cause cooling in the southern hemisphere while at the same time initiating increased ocean turnover and warming in the North Atlantic (Gnanadesikan and Halberg, 2000).

Improving the chronology of glaciation at sites surrounding the climatically important Drake Passage may reveal the nature and timing of global environmental change. It will be possible to compare these terrestrial records with the marine and ice core records in adjacent latitudes. Such information should make it possible to distinguish between regional and global environmental change, thus improving our understanding of how the ocean-atmosphere system interacts between the two hemispheres. Both southern Patagonia and the Antarctic Peninsula still represent unknowns, yet they are positioned at a climatically important localities with regard to the previously identified hypotheses. Previous workers have demonstrated that both Patagonia and the ice-free areas surrounding the Antarctic Peninsula and the Weddell Sea embayment contain rich records of terrestrial Quaternary glaciation (Clapperton and Sugden, 1982, Clapperton *et al.*, 1995, Marden 1993). Although the glacial controls differ markedly between these regions, they are similar in that there is a distinct lack of a robust chronology of Quaternary glaciation.

1.3 The Organisation of the thesis

The thesis is arranged into seven chapters, with chapters 3 to 6 representing stand-alone paperes due to their differing climatic and glaciological controls. Chapter 2 aims to provide the methodological details used, including the basic principles of the technique, the extraction of the

isotopes ^{10}Be and ^{26}Al from quartz, the field methodology, and data interpretation based on the isotopic concentrations measured by AMS. The thesis does not aim to provide a complete review of the theoretical and applied areas of terrestrial *in situ* cosmogenic nuclides, which has been covered in depth by other workers. The most comprehensive is that of Gosse and Phillips (2001).

Chapter 3 investigates the timing of deglaciation of the formerly expanded Patagonian Ice Sheet in the Magellan region, centred on the southernmost Andes of Fuego-Patagonia, from its limits at the Last Glacial Maximum (LGM) (Clapperton *et al.*, 1995). Previous workers have identified a rich record of glacial landforms and sediments related to the Pleistocene expansion of the southern most Patagonian Ice Sheet (Caldenius. 1932, Ferugilio. 1950, Mercer, 1976 and Marden, 1993). However, controversy exists over the timing of these expansions, mainly due to the extreme aridity to the east of the ice sheets that prevented the instantaneous build up of organic material suitable for radiocarbon dating (Marden 1993, McCulloch *et al.* 2000).

Chapter 4 investigates the nature and chronology of deglaciation of the expanded Patagonian Ice Sheet, which drained through the region of Torres Del Paine during the Last Glacial Interglacial Transition. There is a rich record of glacial landforms and sediments related to the Pleistocene expansion of the Patagonian Ice sheets (Caldenius, 1932; Ferugilio, 1950, Mercer, 1976 and Marden, 1993). Controversy still exists over the timing of these expansions again mainly due to the role and significance of radiocarbon dated sequences in the prevailing dry climate (Marden 1993, McCulloch *et al.* 2000). This problem has lead to recent open discussions regarding the interpretation of minimum radiocarbon dates from glacial sequences in this central region (McCulloch *et al.*, 2000 and Wenzen. 2001, McCulloch *et al.* 2001).

Chapter 5 aims to ascertain the timing of deglaciation of the ice-free areas surrounding George VI Sound on the Antarctic Peninsula through the measurement of the TCNs ^{10}Be and ^{26}Al in erratic boulders. Past attempts to elucidate the temporal and spatial extent of the ice domes which built up over this region have proved difficult due to the lack of direct chronological control (Bentley and Anderson, 1998). The position of this area, at the transition between cyclonic pressure systems and the continental Antarctic high-pressure cell provides an ideal location for testing recent hypotheses linking climatic change between mid- and high-latitude systems.

Chapter 6 studies the evolution of the presently ice-free massif of the Shackleton Range which provides a unique insight into the history and therefore the past and present health of the East Antarctic Ice Sheet. The Shackleton Range lies at the junction of the East Antarctic Ice Sheet (EAIS) and the Ronne-Filchner Ice Shelf (RFIS). The history of past glaciation and landscape evolution could provide critical evidence on two major debates in Antarctic evolution and glaciology (Kerr and Hermichen, 1998). The first concerns uncertainty in the former extent of grounded ice in the area of the Weddell Sea embayment at the Last Glacial Maximum, for which only a few constraints exist (Denton et al., 1992; Elverhoi, 1981; Cararra, 1981; Kerr and Hermichen, 1998; Bentley and Anderson, 1998). The second is that the region may also shed light on the Pliocene-Pleistocene evolution of the East Antarctic Ice Sheet, for which no direct chronology currently exists in the this region. The question of whether the East Antarctic Ice Sheet has been a stable feature of Antarctica since achieving its modern configuration, or whether its size has varied significantly since the Pliocene is critical to our understanding of both Antarctica and its global climatic significance, and has been the subject of much controversy (Sugden *et al.*, 1993; Webb and Harwood, 1987).

1.4 References

Alverson K, Oldfield F. 2000. Past global changes and their significance for the future, an introduction. In Alverson KD, Oldfield F, Bradley RS. Eds. Past global changes and their significance for the future. Quaternary Science Reviews. 19: 1-5.

Bentley MJ, Anderson JB. 1998. Glacial and marine geological evidence for the ice sheet configuration in the Weddell Sea-Antarctic Peninsula region during the Last Glacial Maximum. Antarctic Science 10. 3. 309-325.

Blunier T, Chappellaz J, Schwander J, Dällenbach A, Stauffer B, Stocker TF, Raynaud D, Jouzel J, Clausen HB, Hammer CV, Johnsen SJ. 1998. Asynchrony of Antarctic and Greenland climate during the last glacial period. Nature 394: 739-743.

Broecker WS. 1998. Paleoceanographic circulation during the last deglaciation: a bi-polar seesaw? Paleoceanography 13:119-121.

Broecker WS. and Denton GH. 1990. The role of ocean-atmosphere reorganizations in glacial cycles. Quaternary Science Reviews 9: 305-343.

Caldenius C. 1932. Las glaciations cuaternarias en la Patagonia y Tierra del Fuego. Geografiska Annaler 14. 1-64.

Cararra P. 1981. Evidence for a former large ice sheet in the Orville Coast- Ronnie Ice Shelf Area, Antarctica. Journal of Glaciology. 27. 487-491.

Charles CD, Lynch-Stieglitz J, Ninneman US, Fairbanks RG. 1996. Climate connections between the hemispheres revealed by deep sea sediment core / ice core correlations. Earth and Planetary Science Letters 142: 19-27.

Clapperton CM, Sugden DE, Kauffman D, McCulloch RD. 1995. The last glaciation in central Magellan Strait, southernmost Chile. Quaternary Research 44: 133-148.

Clapperton CM, Hall M, Mothers P, Hole MJ, Still JW, Helmens KF, Kuhry P, Gemmell AMD. 1997. A Younger Dryas ice cap in the equatorial Andes. Quaternary Research 47: 13-28.

Clapperton CM and Sugden DE. 1982. Late Quaternary glacial history of George VI Sound area, West Antarctica. Quaternary Research 18: 243-267.

Denton GH, Anderson BG, Rutford RH, Anderson BG. 1992. Glacial history of the Ellswoth Mountains, West Antarctica. Geological Society of America Memoir. 170. 403-432.

Denton GH, Heusser CJ, Lowell TV, Moreno PI, Anderson BG, Heusser LE, Schlüchter C, Marchant DR. 1999. Interhemispheric linkage of paleoclimate during the last glaciation. Geografiska. Annaler 81A(2): 107-153.

Dunai TJ. 2000. Scaling factors for production rates of in situ produced cosmogenic nuclides: a critical reevaluation. Earth and Planetary Science Letters 176. 157-169.

Elverhøi A. 1981. Evidence for a late Wisconsin glaciation of the Weddell Sea. Nature. 293. 641-642.

Ferugilio E. 1949-50. Descripcion geologica de la Patagonia. Buenos Aires, Direccion General Yacimientos Petroloiferos Fiscals. Vols. 1,2,3.

Gnanadesikan A, Hallberg RW. 2000. On the relationship of the Circumpolar current to southern hemisphere winds in coarse-resolution ocean models. Journal of Physical Oceanography. 30. 2013-2034.

Gosse JC, Evenson EB, Klein J, Lawn B, Middleton, R. 1995. Precise cosmogenic ^{10}Be measurements in western North America: Support for a global Younger Dryas cooling event. Geology 23 (10), 877-880.

Gosse JC, and Phillips FM. 2001. Terrestrial in situ cosmogenic nuclides: theory and application. Quaternary Science Reviews 20: 1475-1560.

Hays JD, Lozano JA, Shackleton N, Irving G. 1976. Reconstruction of the Atlantic and western Indian Ocean sectors of the 18,000 B.P.Antarctic Ocean. Memoir of the Geological Society of America 145: 337-372.

Ivy –Ochs S. 1996. The dating of rock surfaces using the in situ produced ^{10}Be, ^{26}Al, and ^{36}Cl, with examples from Antarctica and the Swiss Alps. Ph. D. Thesis, Swiss Federal Institute of Technonology, Zurich. 196pp.

Ivy-Ochs S, Schlüchter C, Kubik PW, Denton GH. 1999. Moraine exposure dates imply sychronous Younger Dryas glacier advance in he European Alps and in the Southern Alps of New Zealand. Geografiska Annaler, Series A: Physical Geography 81(2), 313-323.

Kerr A, Hermichen WD. 1998. Glacial modification of the Shackleton Range, Antarctica. Terra Antarctica. 6(3) 353-360.

Labeyrie L, Labracherie M, Gorfti N, Pichon JJ, Vautravers M, Arnold M, Duplessy J-C, Paterne M, Michel E, Duprat J, Caralp M, Turon J-L. 1996. Hydrographic changes of the Southern Ocean (southeast Indian Sector) over the last 230 kyr. Paleoceanography 11: 57-76.

Lowell TV, Heusser CJ, Anderson BG, Moreno PI, Hauser A, Heusser LE, Schlüchter C, Marchant DR, Denton GH. 1995. Interhemispheric correlation of Late Pleistocene glacial events. Science 269, 1541-1549.

Marden CJ. 1993. Late Quaternary glacial history of the South Patagonian Icefield, at Torres Del Paine, Chile. Ph. D Thesis, University of Aberdeen. 298pp

McCulloch RD, Bentley MJ, Purves RS, Hulton NRJ, Sugden DE, Clapperton CM. 2000. Climatic inferences from glacial and palaeoecological evidence at the last glacial termination, southern South America. Journal of Quaternary Science 15: 409-417.

McCulloch RD, Davies SJ. 2001. Late-glacial and Holocene palaeoenvirnmental change in the Strait of Magellan, southern Patagonia. Palaeogeography, Palaeoclimatology, Palaeoecology. 173. 143-173.

McCulloch RD, Sugden DE. 2001. Climatic inferences from glacial and palaeoecological evidence at the last glacial termination, southern South America: a reply Journal of Quaternary Science. 16 (3) 291-294.

Mercer JH. 1976. Glacial history of southernmost South America. Quaternary Research. 6. 125-166.

Mercer JH. 1978. West Antarctic ice sheet and CO_2 greenhouse effect: a threat of disaster. Nature 271. 321-325.

Phillips FM, Zreda MG, Smith SS, Elmore D, Kubik PW, Sharma P. 1990. Cosmogenic chlorine-36 chronology for glacial deposits at Bloody Canyon, Eastern Sierra Nevada. Science 248: 1529-1532.

Pichon JJ, Labeyrie LD, Bareille G, Labracherie M, Duprat J, Jouzel J. 1992. Surface water temperature changes in the high latitudes of the southern hemisphere over the last glacial-interglacial cycle. Paleooceanography 7: 289-318.

Steig *et al.*, 1998. Synchronous climate changes in Antarctica and the North Atlantic. Science. 282. 92-95.

Stone JO. 2000. Air pressure and cosmogenic isotope production. Journal of Geophysical Research. 105. B10. 23,753-23,759.

Sugden DE, Marchant DR, Denton GH. 1993. The case for the stable East Antarctic Ice Sheet: The background. Geografiska Annaler. 75A(4). 151-154.

Toggweiler JR, Samuels B. 1995. Effect of Drake Passage on the global thermohaline circulation. Deep sea research Pt 1. Oceanographic Research 51: 238-247.

White JWC, Ciais P, Figge P, Kenny R, Markgraf V. 1994. A high-resolution record of atmospheric CO2 content from carbon isotopes in peat. Nature. 376. 153-156.

Webb PN, Harwood DM. 1987. The Sirius formation of the Beardmore Glacier region. Antarctic Journal of the U.S. 22. 8-12.

Wenzen G. 2001. Climatic inferences from glacial and palaeoecological evidence at the last glacial termination, southern South America: comment. Journal of Quaternary Science. 16 (3) 291-294.

CHAPTER 2

Methodology

2.1 Introduction

The application of terrestrial *in situ* cosmogenic nuclides (TCN) is revolutionising the study of landscape evolution and Quaternary geochronology. Major recent developments in the analytical aspects allow the routine measurement of extremely low concentrations of cosmogenic nuclides (Gosse and Phillips, 2001). This provides the Earth Scientist with an extensive set of tools, with which to study surface processes in any lithology, anywhere on earth, and over time scales ranging from 10^3 to 10^7years.

This chapter outlines the aspects of TCN analysis as used in Quaternary glacial geochronology using the radioisotopes ^{10}Be and ^{26}Al. This will be achieved by introducing the principles of the *in situ* production of cosmogenic nuclides followed by a discussion of the major issues of the application of this technique to the glacial environment. This is followed by a detailed description of the methodology followed in this thesis, including field sampling, specific details of the chemical extraction procedure, and data interpretation and analysis.

2.2 Principles of surface exposure dating

The following section introduces the theoretical aspects of TCNs, including both the primary sources and their production within target surfaces. This leads on to a discussion of the correction factors that are required in the application of this technique, and the use of single and

multiple isotopes to constrain surface exposure histories. This does not aim to be a comprehensive review, but rather to offer the reader a reference to the factors affecting sampling and data interpretation. For a more comprehensive technical review of the technique see Gosse and Phillips (2001).

Production of terrestrial in situ cosmogenic nuclides

The Earth is constantly bathed in cosmic radiation, which upon entering the upper atmosphere produces a shower of secondary particles which can in turn produce nuclides from target atoms in earth surface materials. The primary cosmic ray spectrum consists of high energy galactic cosmogenic rays (GCRs) (1-100GeV), and solar cosmic rays (10-100MeV). The cosmic ray flux is made up of three principal components, protons, α-particles and a small percentage of heavier particles (Gosse and Phillips, 2001). On entering the atmosphere these particles produce a shower of secondary particles, consisting of neutrons, protons and muons, which have the capability of producing cosmogenic isotopes within target nuclei within the Earth's atmosphere. These can include soils, sediments, ice, water and within the atmosphere, the most well known being meteoritic ^{14}C. With their much higher energies, GCRs secondry neutrons are the major component in production of TCNs at the earth surface.

For cosmogenic ^{10}Be and ^{26}Al, the ideal target mineral is quartz (SiO_2). ^{10}Be is primerally produced from both O and Si and ^{26}Al principally from Si (Gosse and Phillips, 2001). Previous studies have shown that, with its simple, stoichimetric chemistry and relative resistance to chemical weathering, quartz is an ideal target in comparison to other minerals (Nishiizumi *et al.*, 1986; Ivy-Ochs, 1996). The use of quartz is also advantageous as it allows the simultaneous preparation of samples for the analysis of the isotopes ^{26}Al and ^{10}Be.

The simple relationship between the measured *in situ* amount of ^{10}Be and ^{26}Al and the time a surface has been exposed for is related by equation 2.1 (Lal, 1991),

$$N = \frac{P}{\lambda + \frac{\rho\varepsilon}{\Lambda}}\left(1 - e^{-(\lambda + \rho\varepsilon/\Lambda)T}\right) + N_o e^{-\lambda T} \qquad \text{Eq 2.1}$$

where, N is the measured number of atoms per gram of the TCN within the sample, and N_0 is the number of atoms per gram prior to exposure. For this application it is assumed that N_0 is zero, therefore removing this second term from the equation. P is the local production rate of the TCN within the sample, T is the exposure time in years(a^{-1}), λ is the decay constant of the radionuclide ($^{10}Be=4.59*10^{-7}$; $^{26}Al=9.63*10^{-7}$), ρ is the rock density ($2.7g/cm^3$), and E is the erosion rate (cm/a^{-1}). The final constant, Λ, is the attenuation length in the rock surface in question ($150g/cm^2$) (Lal, 1991). For the application of this technique to surface exposure dating two principal assumptions are made in this age model. The rate of erosion (E) is assumed to be zero, and the rate of production (P) is assumed to be constant through time.

From equation 2.1, it can be seen that in order to obtain an accurate model of the exposure time (T), it is critical that the derivation of each term is well understood, and that all the associated errors are propagated in the eventual age and error calculation. The most contentious element is the estimation of the production rate (P) of the TCN in question. The spatial and temporal derivation of this variable has recently been the subject of much recent debate within the earth sciences and atmospheric physics community, and is discussed in detail in the section (2.7.1).

2.3 The application to Quaternary glacial geochronological problems

The opportunity to directly quantify the time at which an erratic or bedrock surface has been exposed to incoming cosmic radiation has been enthusiastically welcomed by the geomorphological community. The technique allows the direct measurement of both denudation rates and exposure histories, providing hitherto unquantifiable information about the rates and timing of surficial processes. The application of TCNs to the direct dating of the formation of landforms related to the advance and retreat of glaciers has provided a significant contribution to Quaternary glacial geochronology. One of the major benefits of the technique is to provide exposure estimates directly (Tschudi, 2000). Glacial landscapes provide an ideal setting for TCN studies, with much exposed bedrock representing glacial erosion, and polish and striations indicating surface preservation and minimal erosion since glaciation (Gosse *et al.* 1995 a, b). Features such as this can provide direct evidence to uphold the assumptions regarding erosion and nuclide inheritance, made regarding the nuclide build-up model described in section (2.2.1).

This together with the importance of glacial chronology to understanding Quaternary climate change has lead many workers to focus on glacial chronology (Nishiizumi *et al.*, 1989; Brook and Kurtz, 1993; Gosse *et al.*, 1995 a, b; Ivy-Ochs *et al.*, 1995, Ivy-Ochs, 1996).

Many workers have applied the technique of TCN on boulders located on moraines and erratics (Gosse *et al.*, 1995 a, b; Ivy-Ochs *et al.*, 1996). However, the use of these has been called into question by some workers since they do not necessarily reflect the event age, rather they reflect the accumulated exposure due to an often complex emplacement history (Hallet and Putkonen, 1994). Some of the most precisely constrained glacial advances are those from highly dynamic cirque glaciers. Here dynamic and erosive glacial systems have cleared out the glacial trough numerous times, thus providing fresh material with little or no problems related to inheritance (Gosse *et al.*, 1995 a, b; Ivy-Ochs *et al.*, 1996). Hallet and Putkonen (1994) argue that there is no simple relationship between a boulder exposure age and the age of a moraine; rather the boulder age reflects the competing effects of moraine erosion and boulder weathering. The auther suggests that these contrasting views are a result of the application of this technique in a variety of glacial environments and to different types of sample, demonstrating the need for both careful sampling and interpretation of the TCN data with reference to the sample and the landform in question.

2.4 Field Methods

Due to the site-specific nature of exposure dating, sample selection is critical to obtain useful information on the problem in question. Only a sound understanding of the geomophological process under investigation will elucidate its history and obtain meaningful results.

Prior to sampling, the geomorphology of the area is clearly mapped and there are firm constraints on the extent of glaciation through time. This is for two major reasons. First it ensures that optimal sample selection is carried out to answer the question in hand. Secondly, it ensures correct interpretation of the eventual data. This was one of the prime factors controlling the field localities chosen for this project. The sites eventually chosen have all been either been mapped geomorphologically or had previously been visited and identified as suitable localities

for the application of this technique. Other factors affecting the choice of locality and cosmogenic nuclides used included:

- The availability of exposed bedrock and erratics of a suitable size

- The local and regional geology. Are suitable lithologies available? In the case of the isotopes ^{10}Be and ^{26}Al rocks containing a high percentage of quartz are required

If these criteria were met, then the site was suitable for the application of this technique. However, before any sampling took place estimates of the mass of quartz required to allow analysis of the problem by AMS. Equation 2.2 demonstrates the relationship between altitude, latitude, expected age and the mass of quartz required to obtain a detectable ratio of ^{9}Be to cosmogenic ^{10}Be (Tschudi, 2000):

$$W = \frac{c.\frac{N_A}{m_{be}}.r}{\frac{P_{Be}}{\lambda}.(1-e^{-T.\lambda)})} \qquad \text{Eq 2.2}$$

where, W is the mass of quartz required, c is the mass (mg) of ^{9}Be to be added during processing, N_A is Avogadros number, m_{Be} is the atomic mass of ^{9}Be, r is the limiting AMS ^{10}Be/^{9}Be ratio, P_{Be} is the local production rate for the sample site in atoms/a^{-1} /g SiO_2, λ is the decay constant for ^{10}Be (a^{-1}), and T is the expected exposure time in years. This equation is derived from equation 1, and is demonstrated graphically in Figure 2.1. Although only an estimate, this provides a ball park figure ensuring that a significantly large sample was taken to ensure a detectable ratio from the AMS. It was only necessary to calculate this for ^{10}Be analyses as the production rate is lower than that of ^{26}Al and thus a larger mass of quartz is required. It should be re-emphasised that this takes no account of topographic scaling or sample thickness correction factors, nor of the percentage of quartz available within a specific lithology.

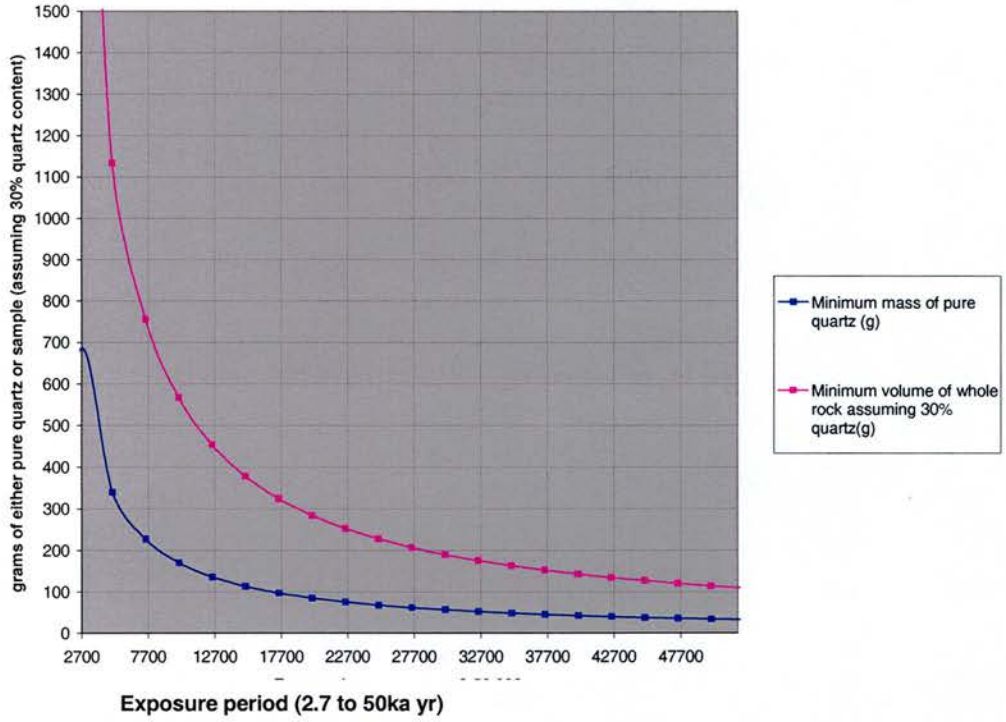

Figure 2.1. Relationship between mass of quartz and age to ensure a measurable ratio by AMS ($^{10}Be/^{9}Be$ ratio $>10^{-12}$). In this example this has been calculated for a typical Patagonia sample at 80 m altitude, with a local ^{10}Be production rate of $5.89\pm0.24 at/g/a^{-1}$. To demonstrate how much sample is required in the field, the weight of whole rock required is calculated assuming a quartz content of 30%. It must be noted that these data do not account for any variables such as shielding or unknown factors. However this does provide a useful guide in the field.

Locating suitable surfaces for sampling can often be harder than at first imagined. However, as described in the previous section it is worth-while taking time and only choosing the best samples in order to minimise any problems with eventual interpretation of the TCN data. In this study glacial erratics, boulders, and bedrock were sampled. The minimum size of sampled boulder or erratic was greater than $1m^3$, in order to reduce interference from problems such as exhumation or post depositional movement and long-term snow or soil coverage. Once selected, the sample was described in detail in relation to its surface morphology, any features such as striations or exfoliation, and the relationship of the boulder to the surrounding landforms and features. This information was backed up with photographs and field sketches on both macro and micro (using a hand lens) scales, to ensure the accurate interpretation of the sample. These details can provide information such as probable degrees of erosion and also highlight problems during eventual age determination. Boulders or erratics that displayed obvious exfoliation were ignored, as were boulders found on steep surfaces due to the likelihood of them rolling after deposition.

Sampling was undertaken on the upper horizontal surface of the boulder or erratic in question, using a hammer and chisel to remove the upper most surface of the sample. Where possible this was taken as a single block, allowing more careful processing of the sample prior to extraction of the TCN's ^{10}Be and ^{26}Al. However, harder lithologies only provided surface chips and sore fingers. The size and most inportantly the thickness of each sample was recorded to allow the calculation of the change of shielding with depth. The samples were carefully labelled and sealed to avoid any chance of cross contamination during transport back to the laboratories for analysis.

2.5 Extraction Procedure of ^{10}Be and ^{26}Al from pure Quartz

The procedure used in these analyses basically followed those outlined in Ivy-Ochs (1996) and Kohl and Nishiizumi (1992). These have been refined following the work of Cockburn (1998). Some minor additional steps were undertaken to cope with the very large sample masses required, particularly at low elevation, mid-latitude sites and with the relatively young exposure

times in question. A detailed outline of the protocol followed can be found in Appendix 1, and the major steps can be followed in Figure 2.2.

2.5.1 Sample description

Once the sample had been collected and returned from the field, it was further described it terms of its micro-morphology; this included the nature and thickness of any weathering rind, polish or oxidation. These details were recorded together with an accurate sketch of the sample. The latter is especially important, as in reality samples are very rarely flat square blocks and often require sawing into shapes that can be described geometrically and modelled simply mathematically. Therefore the sketch acts as a record of the original sample.

2.5.2 Rock crushing and sieving

In order to extract the quartz fraction from the whole rock sample, it must be sawn and crushed to a suitable size range, depending on the typical size of quartz grain. This can be estimated by analysis of a thin section of the rock under a petrological microscope. Most lithologies contained enough quartz in the 250-500μm fraction. However in some cases it was necessary to use the 125-250 μm fraction to obtain sufficient quartz. Once crushed, the samples were thoroughly washed through a sieve, to remove any particles finer than those required, and then water-washed in a beaker until the water ran clean, thus removing any light organic material and unwanted platy mica minerals contained within the samples.

2.5.3 Heavy liquid mineral separation using lithium hetropolytungstates (LST) solution

Due to the high percentages of feldspars and heavy opaque minerals found in the rocks from both Patagonia and Antarctica, a stage of liquid density separation was used in order to concentrate the quartz within the sample. The theory behinde this technique is simple, the LST liquid is a concentrated solution of lithium hetropolytungstates in water, whos density can be varied by the addition or evaporation of water. By adjusting the density of this solution it is possible to keep quartz and feldspars floating, whilst heavy minerals sink (density >2.7 g/ml). A second stage of seperation can be undertaken to sink the quartz fraction whilst keeping the feldspar fraction floating. This involves reducing the density of the solution to just less than that of quartz, this can be achieved by using a large piece of pure quartz, and adding water until it begins to sink just below the surface of the first solution. The sample can be added to this

solution and the quartz and feldspar fractions seperated. This technique saves both time and expense during the following stage of quartz etching.

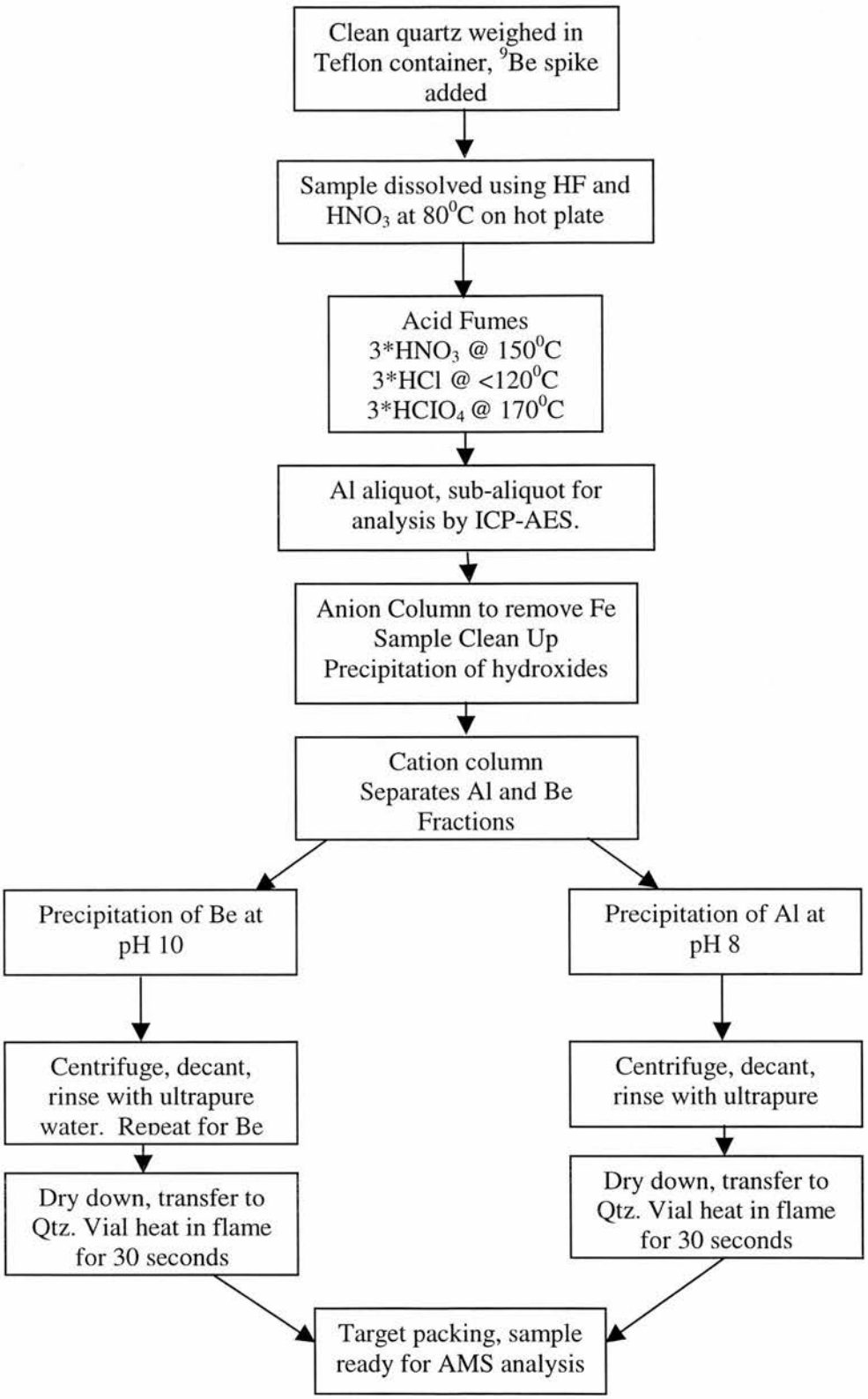

Figure 2.2. Flow diagram of extraction procedure for the cosmogenic nuclides ^{10}Be and ^{26}Al

2.5.4 Production of a pure quartz separate

Once a quartz concentrate has be obtained it must be processed to leave pure quartz and ensure that no non-cosmogenic Be or Al exists in the sample. To avoid any contamination of meteoric Be, every step from this point was undertaken using 18MΩ water (Elga reverse osmosis water purification system). Unwanted accessory minerals and meteoritic Be held within the weathering surface of the quartz grains are removed with a weak solution of analytical grade hydrofluoric (20ml) and nitric (10ml) acid in 1 litre of ultrapure 18mΩ water for each 7.5grams of quartz concentrate. This is done in a 1 litre Nalgene© screw top container, which is placed in an ultrasonic bath overnight. This is repeated four times, and thoroughly rinsed between stages to remove any breakdown product of the process. The quality of the quartz is checked visually under a binocular microscope, and any undissolved mafic minerals removed by hand picking. This process is repeated multiple times on separate fractions until enough pure clean quartz is obtained to satisfy the required mass required by Equation 2.

2.5.5 Sample dissolution

Using a chemically cleaned Teflon container, the total sample mass was accurately recorded using a micro-balance. This stage is critical to the eventual measurement of the isotopic ratios of the known non-cosmogenic isotope to the unknown cosmogenic isotope by AMS. Once the known mass of sample is in solution, the concentrations of Be and Al can be measured by Inductively Coupled Plasma Atomic-Emission Spectroscopy (ICP-AES). Once the mass has been recorded the isotopic ratios are fixed and until the measurement by ICP the sample must be treated quanititvly, to ensure there is no change of this isotopic ratio as this would affect the eventual age calculation. Quartz normally contains enough natural ^{26}Al not to require the addition of a known spike of ^{26}Al. However, natural levels of ^{9}Be are <2ppm of the quartz sample (Tschudi, 2000); thus a known spike of ^{9}Be must be made to allow measurement of the unknown cosmogenic ^{10}Be by AMS. This was done using a calibrated 0.1-100µl Eppendorf pipette, to transfer an accurate volume of a well mixed Merck Standard Be solution (concentration 1000±5mg/l). The volume of carrier required can be reduced, provided the chemical processing is demonstrated to be working well. The majority of samples were run using a carrier spike of 0.5ml, although due to the lack of quartz available and young ages expected for some samples this had to be reduced to 0.35ml. This has the effect of reducing the

required ratio of the isotopes by AMS, and in turn increasing the precision of the eventual measurement.

The sample were dissolved in a concentrated 2:1 solution of hydrofloric acid (48% analytical grade), and nitric acid (40% analytical grade), covering the sample. Great care was taken at this stage to avoid any initial violent reaction between the acid and the quartz grains. The samples were then placed on a hot plate, at 90^0C. Above this temperature rapid evaporation of the HF and HNO_3 outweighs the increased speed of the reaction. In this solution and at this temperature, approximately 5g of SiO_2 are digested in a 24hr period, thus requiring up to 10 days for a 50 gram sample to dissolve (Ivy-Ochs, 1996). Once in solution, the samples are fumed, in turn with HNO_3, HCl and $HClO_4$. Each sample is fumed to dryness three times with each acid. This stage breaks down fluorides and attacks insoluble accessory minerals from within the individual quartz grains. It is noted that some insoluble grains remained after this process, especially with large samples.

To increase efficiency samples were dissolved in batches of seven samples and one blank, with four Teflon containers on each hot plate. At least one process blank was run with each sample batch. The blank contains the carrier solution and the same acid loading as the samples with which it is run, and is measured by AMS at the same time as the samples concerned. This provides a check for contamination of any non-cosmogenic ^{10}Be or ^{26}Al which has entered the system during processing. This can occur easily, from chemical loading, unclean labware, atmospheric dust particles and possible sample cross contamination where very low ratios are attempting to be measured. Using 0.5ml of carrier solution, typical measured blank ratios are between 0.02 to $0.04*10^{-12}$ for ^{10}Be/^{9}Be.

2.5.6 Analysis by ICP-AES

Once the sample has been dissolved, accurate determination of the Al concentration of the sample is required. This is not constant due to the inhomogeneous nature of individual quartz grains, so it must be estimated from the total sample rather than on a sub-aliquot of quartz grains.

The aliquot was taken as soon as the final fume had dried down. The sample was re-dissolved with <5ml 1:1 HNO_3, and carefully transferred into a clean and dry 100ml measuring flask, filled with water and mixed thoroughly. From this a 2ml sub-sample was taken using a calibrated Ependorf pipette, and in turn transferred to a second 100 ml measuring cylinder. This was then be filled to the 100ml mark and then analysed by ICP-AES. In some cases, where large samples (>80grams) were used some insoluble material was left in the bottom of the Teflon containers. This was mainly insoluble zircons and rutile. These were well rinsed with acid to avoid them acting as a sink for either Be or Al following the procedure of Ivy-Ochs (1996). They were then removed, dried, weighed accurately and sent for analysis by X-Ray Diffraction (XRD). The weight of this insoluble material was then be removed from the total sample weight.

As well as providing an independent estimation of Al content, analysis of the Be content was also undertaken. This provided a second check to ensure the quality of the original sample. In particular it showed that there was no excess ^{9}Be (indicating contamination), and that no Be had been lost during sample transfer, chemistry or to any solid material removed at the end of the dissolution.

The measured concentration of Al and Be from the aliquot(in ppm) analysed from ICP-AES was used to calculate the sample concentration (in mg/l) of the original sample mass, this is the total Al/Be concentration. These values vary from tens to hundreds of ppm depending on the quartz in the original sample. However if these values are very high it is likely that feldspar grains have not been removed by the etching procedure. It is important to note, that although the ICP-AES measurement error is <1% (Kubik *et al.*, 1998), the error on the ^{26}Al concentration from the sub-aliquot is >5%. Therefore this must be accounted for in the eventual exposure age calculation (Tschudi, 2000).

2.5.7 Sample clean up

Although a clean mono-mineralic sample of quartz was produced prior to dissolution, other accessory minerals were often present in the samples. This is due to the non-homogeneous nature of quartz, which often contains other trace elements within its lattice. One of the principle trace elements in quartz is iron (Fe), which is also an interfering cation, together with B^{+}, Ca^{2+},Mg^{3+},Na^{+} and K^{+} (Ivy-Ochs, 1996). These trace elements must be removed from the

samples prior to separation of the Al and Be fractions by cation exchange column later in the procedure. Failure to remove these cations before separation reduces the efficiency of the later cation exchange procedure due to their high affinity with the column resin compared to that of the Al or Be (Ochs and Ivy-Ochs 1997). Also these elements could interfere with the eventual AMS measurement of samples by reducing the purity of the sample by reducing the beam current or acting as interfearing isobars (Cockburn, 1998). Several techniques are available to remove these elements, including MIBK (methyl isobutyl ketone), an organic extraction technique, as described in Ivy-Ochs (1996), or an anion exchange column (Cockburn, 1998) as used here.

2.5.8 Anion exchange column

Samples varied in their Fe content, this could be clearly seen by the colour of the sample in a 9M HCl solution. This varied from clear, demonstrating low iron content, to bright yellow, indicating a high iron content. All samples were eluted through Bio-rad 20ml PFA columns packed with anylitical grade AG 1-X8 (chloride form, 100-200 dry mesh size) (Cockburn, 1998). The originally dry resin, was mixed with 18mΩ ultrapure water to obtain a water-equilibrated state. The 20ml column was packed with resin, through settling through a column of 18mΩ ultrapure water, thus ensuring no air pockets and even packing of the resin to ensure even flow. The Be and Al fractions were eluted with 9M HCl into a clean Teflon container. Any Fe in the sample could be seen clearly in the low pH (0.5M HCl) eluted volume as light to dark yellow solution. This was stored for future reference, while the elutant containing the Al and Be was dried down at 100^0C.

2.5.9 Hydroxide precipitation

A second sample clean-up stage was required to remove Mg^{3+}, Ca^{2+},Na^+, K^+ and B^+, in particular. This was achieved following the procedure outlined by Ochs and Ivy-Ochs (1997), which demonstrated that both Be^{2+} and Al^{3+} precipitate at pH8, where as these other interfering cations are kept in solution. To this end the dry sample was taken up into acid solution and transferred into a 15ml centrifuge tube. Using NH_4OH, the solution was slowly adjusted to pH8, thus precipitating the amorphous $Be(OH)_2$ and $Al(OH)_3$. Once complete, this solution and solid precipitate is left for 24 hours to ensure completion of the reaction. The sample was then centrifuged, and the solution containing the unwanted cations transferred into a separate bottle

for future reference. The clean hydroxide precipitate was returned to a solution by the addition of 1M HCl, ready for separation into Al and Be fractions.

2.5.10 Cation exchange column

This second ion exchange stage of the process ensured separation of the Al and Be fractions of the sample. This procedure follows those described by Ivy-Ochs (1996). As with the Anion stage, Bio-rad 20ml PFA columns were used, and packed with AG 1-X8 cation resin, analytical grade, hydrogen form, 100-200 dry mesh size.

The only alterations from the procedure described by Ivy-Ochs (1996), were for large sample masses. The differing affinities of Al and Be, and the high concentration of natural Al compared to Be can cause the Al fraction to flood the cation exchange column and cause Al to be eluted into the Be fraction of the sample. This substantially affects the purity of the Be fraction, reducing analytical accuracy during measurement by AMS. This was overcome by multiple runs of the cation column exchange procedure on the Be fraction of sample masses greater than 40 grams (Ivy-Ochs, pers com). Samples greater than 60 grams were run three times, to ensure high purity of the eventual target. An alternative approach to this problem is to increase the volume of the column itself (Tschudi, 2000). This would require a change in the volumes of elutants used, which must be calculated for the specific column volume. As no samples in this study were greater than 100 grams, 20ml columns were always used, with multiple runs as described above.

2.5.11 Precipitation

Once separate, the Al and Be fractions were precipitated as described in section 2.5.7. This acts as a final sample clean up, and prepares the sample for oxidation from the hydroxide. Once again the samples were left overnight to complete precipitation, then centrifuged at 3000 rpm for 15 minutes.

The purity of the Be fraction at this point was checked by visual reference in its precipitate form. The mass of solid material should be similar to the corresponding amount of carrier added at the start of dissolution. The Al and Be hydroxide fractions can be viewed in the centrifuge tubes. If the $Be(OH)_2$ volume is substantially more than expected, then the cation column procedure must be repeated, as it is likely that there is Al contaminating the Be fraction.

If the samples are pure they are water washed. This was achieved by removing the solution left from the precipitation stage, and replacing it with 18MΩ ultrapure water. The sample must then be thoroughly mixed, in order to break down the solid precipitate and remove the soluble boron (^{10}B) (Finkel and Suter, 1993), and sodium hydroxide (Na(OH)). Boron removal is especially critical for the measurement of Be, as it is an interfering isobar.

2.5.12 Oxidation

The hydroxides were dried down in a specially designed heater block, still in their polypropylene centrifuge tubes at 40^0C. Once dry, the sample became a small pellet, which was easily detached from the side wall of the centrifuge tube. The colour of these pellets ranged from off-white to dark brown. Each sample was then transferred to a hand blown quartz vial, using a clean micro-spatula or tweezers. Any item coming into contact with the sample or the transfer equipment was cleaned between samples.

The samples were then oxidised individually using a butane / propane gas mix. The sample was introduced slowly into the flame to avoid any violent reaction. As the sample was lowered into the flame, it often changed colour prior to glowing red, indicating the change from hydroxide to oxide form. The sample was held in the flame for at least 20 seconds once glowing to ensure complete oxidation. The sample was then left to cool to room temperature in a clean, dust free area.

2.5.13 Target preparation

Target preparation is normally undertaken at the accelerator facility as each AMS requiries different targets and conductive packing material. For this study the targets were prepared at ETH/PSI Tandem facility in Zurich. The BeO and Al_2O_3, were mixed with fine, clean copper powder, in a ratio of approximately 1:4. The copper acts as a conductor, helping sputtering of the target by the negative ion source. The remainder of the target is packed with the pure copper material. Once more, it is critical at this stage to ensure no contamination from either other samples or external sources occurs. The target preparation is now complete, and ready for analysis by AMS.

2.6 Analysis by AMS

Due to their extremely low natural abundancies the long-lived radioisotopes ^{10}Be and ^{26}Al cannot be measured by conventional mass spectrometry, and with their long half life it would take years to count a typical sample by conventional decay counting (Elmore and Phillips, 1987; Finkel and Suter, 1993). Therefore the measurement of ^{10}Be and ^{26}Al, with sufficient analytical sensitivity to measure the build up of *in situ* cosmogenic nuclides can only be practically achieved by AMS. This technique which was developed in the late 1970s and has the ability to measure as little as 10^5 atoms and radioisotope/stable element ratios of the order of 10^{-14}. The physics behind this technique is reviewed in detail by Finkel and Suter (1993) and Elmore and Phillips (1987), and the specifics of ^{10}Be and ^{26}Al measurement are covered in Klein *et al.* (1982), Middleton *et al.* (1983) and Raisbeck *et al.* (1987).

For this study all of the isotopic ratios were measured using the AMS at the ETH/PSI tandem facility at ETH-Zurich, Honggerberg (Finkle and Suter, 1993). Therefore the remainder of this discussion will specific to this facility. In general the tandem facility still corresponds to the description of Synal *et al.* (1997), it is principally made up of three sections. The first is the low energy section containing the ion source, where negative ions are created by a caesium sputter source, and specific isotopes seperated by mass. This ion beam feeds into the tandem accelerator, where the ions are accelerated through a two-stage process. Initially the ion beam is accelerated once to the high voltage terminal in the tandem unit where it passes through a foil slit or narrow gas filled canal where the ions are stripped of several of their electrons and become positively charged molecules. This causes the molecules to become unstable and break up into their constituent atoms. They are then accelerated a second time and injected into the mass spectrometer on the high energy side of the accelerator. At this stage the unwanted isobaric interference elements such as ^{10}B in the case of ^{10}Be, and ^{26}Mg in the case of ^{26}Al, can be either removed or identified by the detection system, which is based on the nuclear properties of high energy ions (Ivy-Ochs, 1996; Finkle and Suter, 1993).

Rather than measure the absolute isotopic ratios the ETH/PSI AMS measures the unknown samples against known standards. Then the measured ratios of the unknowns are normalised to the standards. These standards are described with reference to the ETH/PSI AMS in Ivy-Ochs

(1996). These standards have their own blanks that are subtracted and not included in the eventual error calculation (Finkle and Suter, 1993). The eventual one sigma error from the AMS measurement, is a product of the counting statistics, reproducibility derived from the standard measurements and repeated measurements of the samples. This normally gives a precision of between 3 and 10%.

2.7 Data interpretation and analysis

The estimation of the surface exposure age of a sample is a two stage process based on the calculation of a site specific production rate (P_s) and the determination of the concentration (N) of cosmogenic isotope based on the measurement by AMS. This process can be seen as a flow diagram in Figure 2.3.

2.7.1 Site specific production rate calibration

The critical variable in the calculation of the apparent exposure ages is the estimation of production rate of the TCN in question. The primary incoming cosmic ray flux varies over the surface of the earth, being primarily controlled by the geomagnetic field and the atmosphere, which act as filters. Therefore the chosen reference production rate (P_0) must be scaled for geomagnetic latitude and altitude above sea level. In this study the reference production rate (P_0) used is that of Kubik *et al.* (1998), which was determined experimentally. This value agrees well with the revised rates of Nishiizumi *et al.* (1989) and Nishiizumi *et al.* (1986), which were also determined using the altitude/ latitude scaling functions of Lal (1991). However, there is strong evidence that the relative muon contribution to total production is much lower than the 16% assumed by Lal (1991) (Heisinger, 1997; Stone 2000). For this study the values of Kubik *et al.* (1998) have been modified to provide an accurate representation of both the stopped and fast muon components (Heisinger, 1997; Stone 2000). Therefore the new reference production rate is a product of three variables, production by spallation of 5.22±0.22 atoms/g(quartz)/yr, together with a value of 0.12 atoms/g(quartz)/yr for stopped muons and 027 atoms/g(quartz)/yr for fast muons (Schaller *et al.*, 2001). This results in a total surface production rate (P_0), at sea level and high latitude (SLHL) for ^{10}Be of 5.37±0.22 atoms/g(quartz)/yr. This value was chosen

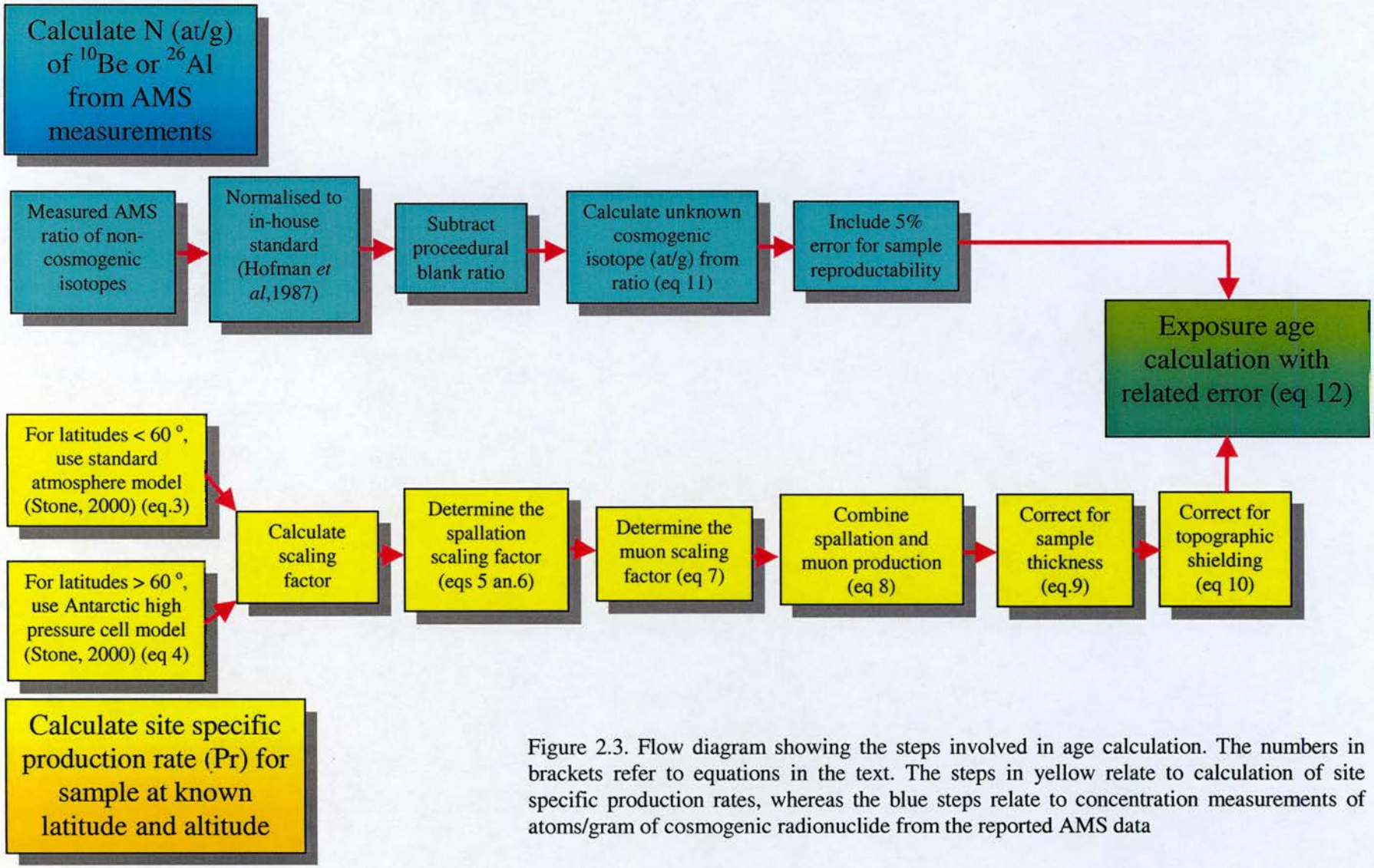

Figure 2.3. Flow diagram showing the steps involved in age calculation. The numbers in brackets refer to equations in the text. The steps in yellow relate to calculation of site specific production rates, whereas the blue steps relate to concentration measurements of atoms/gram of cosmogenic radionuclide from the reported AMS data

based on the availability of all relevant data necessary for the calculations, and also with a distinct lack of well constrained calibrated sites in the southern hemisphere.

The reference production rate (P_0) is quoted at sea level, and high latitude (>60°) (SLHL). This value must be scaled for the known elevations and latitudes of the samples in question. There is still open discussion regarding the methods of undertaking this exercise, due to the non-uniform relationship between altitude and atmospheric pressure over the earth's surface. The original, and still widely-used scaling factors published by Lal (1991) uses a model of the standard atmosphere relationship between altitude and atmospheric pressure. This masks regional differences in mean annual pressure and spatial variations in isotope production rates. Recent studies have attempted to model more realistic spatial variations in modern surface air pressure and its influence on the production rates of TCN's (Stone, 2000; Dunai, 2000). Through comparing these various models it was decided to use the model proposed by Stone (2000), for two principle reasons. It has been tested in a low altitude calibration site (Scotland), and at the lattitudes this study was undertaken at did not produce significantly different results (±5%) to the model of Dunai (2000), which used a complex temperature function which is open to question. Therefore in this study the scaling of P_0 for the latitude and altitude of each sample has been undertaken following the procedure described by Stone (2000). This provides scaling factors for latitude and altitude based on those of Lal (1991), with two changes. First they are recalculated in terms of atmospheric pressure as opposed to altitude. Second, the relative contributions of spallogenic and muogenic production are changed using the modified values of Kubik *et al.* (1998), quoted earlier. Thus the site-specific production rate (P) is calculated by the following steps:

a) Determine the atmospheric pressure at the site.

This is done by using the standard atmosphere hydrostatic equation of Lide (1999), to approximate the pressure altitude relationship for mid-latitudes (Equation 2.3).

$$P(z) = Ps \exp\left\{-\frac{gM}{R\xi}\left[\ln T_s - \ln(T_s - \xi z)\right]\right\} \qquad \text{Eq 2.3}$$

Where P_s is sea level pressure (1013.25 hPa (1033.2 gwt. cm^{-2})), T_s is sea level temperature (T_s=288.15 K), and ξ is the adiabatic lapse rate (ξ=0.0065 Km^{-1}), Z is altitude (m). The constant M is the molar weight of air, g is the acceleration due to gravity, and R is the gas constant: giving gM/R=0.03417K m^{-1}.

This equation however is not representative of extremes in the global atmospheric pressure field, such as Antarctica where a better approximation is equation 2.2. This equation is based on work by Radok *et al.* (1996), in which he derived a pressure-altitude relationship for Antarctica. Stone (2000) fitted this equation to published Antarctic pressure data as follows in Equation 2.4.

$$P_{Ant}(z) = 989.1\exp\left[-\frac{z}{7588}\right] \qquad \text{Eq 2.4}$$

b) Determine the scaling factor for spallation from polynomials published by Stone (2000)

Equation (2.5) is similar to Lal's (1991) polynomial fit, providing scaling factors as a function of atmospheric pressure at seven index latitudes.

$$S_\lambda(P) = a + b\exp[-P/150] + cP + dP^2 + eP^3 \qquad \text{Eq 2.5}$$

The values of a,b,c,d and e are provided in 10^0 increments in Table 1 for latitudes of 0^0-60^0 (Table 1 of Stone 2000). In order to calculate for latitudes that are not increments of 10, linear interpolation between the bracketing values was undertaken. This preserves some of the artefacts of Lal's (1991) curve fitting procedure. However, due to the related unknowns the error introduced here is less than 1% and therefore insignificant.

Table 1 of Stone (2000), reçalculated from those of Lal (1991), as a function of atmospheric pressure.

Latitudeλ	a	b	c	d	e	$M_{\lambda,1013.25}$
0	31.8518	250.3193	-0.083393	7.4260E-05	-2.2397E-08	0.587
10	34.3699	258.4759	-0.089807	7.9457E-05	-2.369E-08	0.600
20	40.3153	308.9894	-0.106248	9.450E-05	-2.823E-08	0.678
30	42.0983	512.6857	-0.120551	1.1752E-04	-3.8809E-08	0.833
40	56.7733	649.1343	-0.160859	1.5463E-04	-5.0330E-08	0.933
50	69.0720	832.4566	-0.199252	1.9391E-04	-6.365E-08	1.000
60	71.8733	863.1927	-0.207069	2.0127E-4	-6.6043E-08	1.000

c) Determine the muon scaling factor

The production by negative muon capture increases less steeply with altitude than production by spallation and therefore must be scaled independently. This is achieved by equation 2.6.

$$M_{\lambda}(P) = M_{\lambda,1013.25} \exp[(1013.25 - P)/242] \qquad \text{Eq 2.6}$$

The value sof $M_{\lambda,1013.25}$ are provided for 10^{o} latitude increments in Table 4 and are taken directly from Lal (1991). As previously described these values can be interpolated between for intermediate latitudes. It is noted however that all of the study sites in this thesis were at latitudes greater that 50^{0} degrees, where $M_{\lambda,1013.25}$ will be equal to 1.

d) Combine the production due to spallation and muon capture

Equation 2.7 allows the calculation of the scaling factor of the isotope for the production due to spallation and muon capture as a function of atmospheric pressure ($F_{\lambda}(P)$).

$$F_{\lambda}(P) = f_{sp} S_{\lambda}(P) + (1 - f_{sp}) M_{\lambda}(P) \qquad \text{Eq 2.7}$$

where S_{λ} and M_{λ} are the scaling factors derived from equations 2.3 and 2.6, and f_{sp} is the fraction of spallogenic and muon capture at the surface at sea level. Values for f_{sp} differ for different

isotopes, but recent studies indicate much lower values than those originally used by Lal (1991). In this study the values used for f_{sp} for ^{10}Be and ^{26}Al are 0.974 and 0.978 respectively (Stone, 2000).

This series of steps provides a scaling factor ($F_\lambda(P)$), corrected for the sample's altitude and latitude which can then be easily converted to an effective local production rate (P), as seen in Equation 2.8.

$$P = F_\lambda(P).P_0 \qquad \text{Eq 2.8}$$

Where P_0 is the reference production. This value of the total incoming signal must be corrected for self-shielding, due to the sample geometry and topographic shielding.

e) Correction for sample thickness

The local production rate (P) of any sample must be corrected to reflect the fact that the sample will attenuate the cosmic radiation, so that deeper material will have a lower effective production rate than material closer to the surface. In this study the depth-corrected production rate is given by the integral of the effective production rate over the sample thickness. Taking Po as 1 provides the formula for the thickness scaling factor (Equation 2.9):

$$P(otox) = Po\frac{\Lambda}{\rho x}\left(1 - e^{\frac{-\rho x}{\Lambda}}\right) \qquad \text{Eq 2.9}$$

where x is sample thickness (cm), ρ is rock density (g/cm^3), and Λ is the absorption free path length for spallation (g/cm^2), a value of 150 g/cm^2 was used for all samples in this study. The sample thickness correction ($P_{(o\ to\ x)}$), is a unitless number with a value less than 1 (Gosse and Phillips, 2001).

f) Topographic shielding correction

Partial shielding of a target surface either by itself in the case of an angled surface or by nearby topographic features results in a decrease in the production rate at the site. This must be

subtracted from the site specific production rate (P). The relationship between the shielding angle and the reduction in effective production over time is complex, as the variation of the incident flux is not uniform from 0° to 90° from vertical. In fact incident energy is minimal below 45°, therefore only small corrections are required for low shielding angles, with even a flat surface on the bottom of a conical pit with 45° walls still receiving 80% of the radiation incident upon an unobstructed surface (Gosse and Phillips, 2001). This effect can be quantified by integrating the free access of cosmogenic radiation for the angular dependence of incident cosmic rays by the relationship in Equation 2.10 (Nishiizumi *et al.*, 1989; Cerling and Craig, 1994).

$$F(\theta) = \sin^{2.3}\theta \qquad \text{Eq 2.10}$$

The data for this is gathered easily in the field, recording the surface dip compared to the horizontal, the azimuth angle (θ) and the profile of features blocking the cosmic rays in all directions (2π) around the sample. This data is integrated to calculate the blocked cosmogenic signal for all sectors which is then summed to provide a geometric correction.

2.7.2 Calculating unknown concentration of the isotope from AMS measurement

The AMS measures the ratio of atoms of ^{10}Be to ^{9}Be within the sample. However, this may not be a true reflection of just the cosmogenic to non-cosmogenic components. Other sources include process contamination from the laboratory and background levels from the accelerator itself. Therefore the process of calculating the concentration of the isotope in question (N) must be described in detail.

a) AMS analysis

The results of the analysis by AMS from the PSI/ETH tandem facility at ETH Zurich are reported as the ratio of ^{10}Be / ^{9}Be or ^{26}Al/^{27}Al in each sample. This result is normalised to an in-house standard, which in the case of ^{10}Be / ^{9}Be is a secondary standard from the original material used by Hofmann *et al.* (1987) to determine a half-life of ^{10}Be of 1.51 My. For ^{26}Al/^{27}Al the standard material used is a secondary standard based on the reference material of Sarafin (1985). The measured ratios are also ascribed an error which is a combination of counting statistics and

the reproducibility derived from the standard measurements and repeated measurements of the samples.

b) Correct measured ratio for appropriate laboratory chemistry blank

The reported ratio includes any additional isotopic signal from either chemical loading during processing or contamination. Therefore laboratory blanks are always run alongside samples. The blanks are loaded with identical volumes of acid as the samples and exposed for the same times and processed in exactly the same way. In this way the measured blank ratio can be subtracted directly from the reported sample ratio. The calculation of N, the concentration of the unknown cosmogenic isotope is shown in equation 2.11.

$$N = \frac{\left(Cv/1000\right)N_A}{A_i}.\left(R_{measured} - R_{Blank}\right) \Big/ m_{ps} \qquad \text{Eq 2.11}$$

Where C_v is the carrier mass in ml, N_A is Avogadros Number ($6.02214*10^{23}$atoms mol^{-1}), A_I is the atomic weight of the isotope (values used 9.01218g mol^{-1} for ^{10}Be and 26.98154g mol^{-1} for ^{26}Al). The values of $R_{measured}$ and R_{blank} are those taken directly from the reported AMS ratios. Dividing all of this by the mass of the sample provides the concentration of the unknown isotope in atoms/gram.

2.7.3 Exposure age calculation

The final calculation of an exposure age for the sample from the corrected site specific production rate (P) and the corrected concentration of the isotope in question (N) is seen in Equation 2.12. This is based on the assumption that the sample has no previous exposure.

$$t = \frac{1}{\lambda + \frac{\rho E}{\Lambda}} \log\left[1 - \frac{N\lambda + \frac{\rho E}{\Lambda}}{P}\right] \qquad \text{Eq 2.12}$$

where P is the production rate for the sample location, corrected for thickness and shielding (atom/g/yr), λ is the decay constant ($4.59*10^{-7}yr^{-1}$ for ^{10}Be, $9.63*10^{-7}$ $yr^{-1}$for ^{26}Al), E is the

erosion rate (cm/yr), ρ is the rock density (2.7g/cm^3), and Λ is the absorption mean free path length for spallogenic production in rock (150g/cm^2). The errors related to both the production rate determination and the measurement of N, the isotope concentration by AMS are added quadratically. An additional 5% error was added quadratically for sample reproducibility, creating a total uncertainty of between 13 to 15% for most samples (Ivy-Ochs, 1996). A further 5% error was included in the calculation of Al exposure ages based on the analysis by ICP-AES measurement described earlier (Tschudi, 2000). The resultant error is conservative, as it includes the statistical errors of the AMS measurements (Kubik *et al.*, 1998). It is noted that errors related to uncertainties in the half-life, and analytical uncertainties such as carrier concentration are not included, as the samples are prepared together and are of the same istopic system (Gosse and Phillips, 2001).

2.8 Data interpretation

Once the unknown concentration of the TCN and the exposure age has been calculated then interpretation of the results can begin. In this study, two approaches have been followed. Although both ^{10}Be and ^{26}Al are extracted simultaneously through the procedure outlined in this chapter, the advantages of analysing both nuclides must be weighed up depending on the age range and the question under investigation. It has been demonstrated that a single nuclide can provide precise constraints on well preserved boulders on moraines or glacial landforms (Gosse *et al.*, 1995a). The use of a single nuclide (in this case just ^{10}Be), to constrain the age of a surface is dependent on the assumption based on field observations of minimal erosion and no inherited nuclide signal. This assumption is made when attempting to constrain the ages of boulders and erratics from glacial advances thought to be related to the Last Glacial Interglacial Transition in southernmost South America. Due to the likely time frame of the formation of these landforms (Clapperton *et al.*, 1995), analysis of multiple isotopes (^{10}Be and ^{26}Al) will not provide any additional information regarding sample histories in this region. Therefore in this region only the single isotope ^{10}Be has been measured by AMS, the ^{26}Al samples were however prepared and archived in case of problems with the analysis of the single isotope. Thus the data provided from the AMS measurement was simply interpreted as an exposure age estimate from the more precise ^{10}Be AMS analysis (Gosse *et al.*, 1995 a, b)

In the Antarctic Peninsula and Shackleton Range, where due to the unknown age of overriding glaciation and the possibility of repeated periods of glaciation both the ^{10}Be and ^{26}Al fractions of each of the samples were measured routinely by AMS. This approach allowed further interpretation of the AMS data and verification of both exposure ages and sample exposure history. This approach was first proposed by Lal and Arnold (1985), and is based on fact that the half-lives differ markedly, causing the eventual concentration of different nuclides to vary depending upon periods of exposure and burial of the sample. This can be identified through the analysis of the ratio of $^{26}Al/^{10}Be$ plotted against the log of measured ^{10}Be concentration (scaled to production at sea level and high latitude), this is termed an erosion island graph (Lal 1991). Figure 2.4 shows the curve produced when these variables are plotted, eventually reaching an end point when both nuclides have reached saturation, after long exposure periods when production and decay are equal. This point of saturation gradually decreases as the erosion rate increases. By plotting this relationship for a number of erosion rates the "steady-state erosion island" (Lal, 1991), is produced. The steady-state term is used to describe samples plotting within this area as having a simple exposure history affected only by erosion (Klein *et al.*, 1986; Lal, 1991). Samples which plot above the upper line of this region are termed to be in the forbidden zone (Lal and Arnold, 1985), and could reflect one of three possible scenarios. It could either indicate possible higher production rates at some point in the past, such as a period of time at higher elevation (i.e. down slope movement (Gosse and Phillips, 2001)). Alternatively it could indicate an inherited component from prior exposure for one isotope, or possibly a sample processing error such as failure to remove feldspar or other contamination.

Samples which plot on the uppermost line of the curve ($\varepsilon=0$), show no evidence of burial or erosion during the exposure period, and have no previous inherited signal from an earlier exposure period. Therefore the concentration can be interpreted directly as an exposure age.
Samples that plot within the area of steady-state erosion can in theory be interpreted as a combination of erosion and exposure and their position can be used to infer an erosion rate for the sample, together with an age estimate, which can also be calculated. If this is accepted, the ages will differ proportionally to exposure time, with the isotope with the shorter half-life being the younger exposure age.

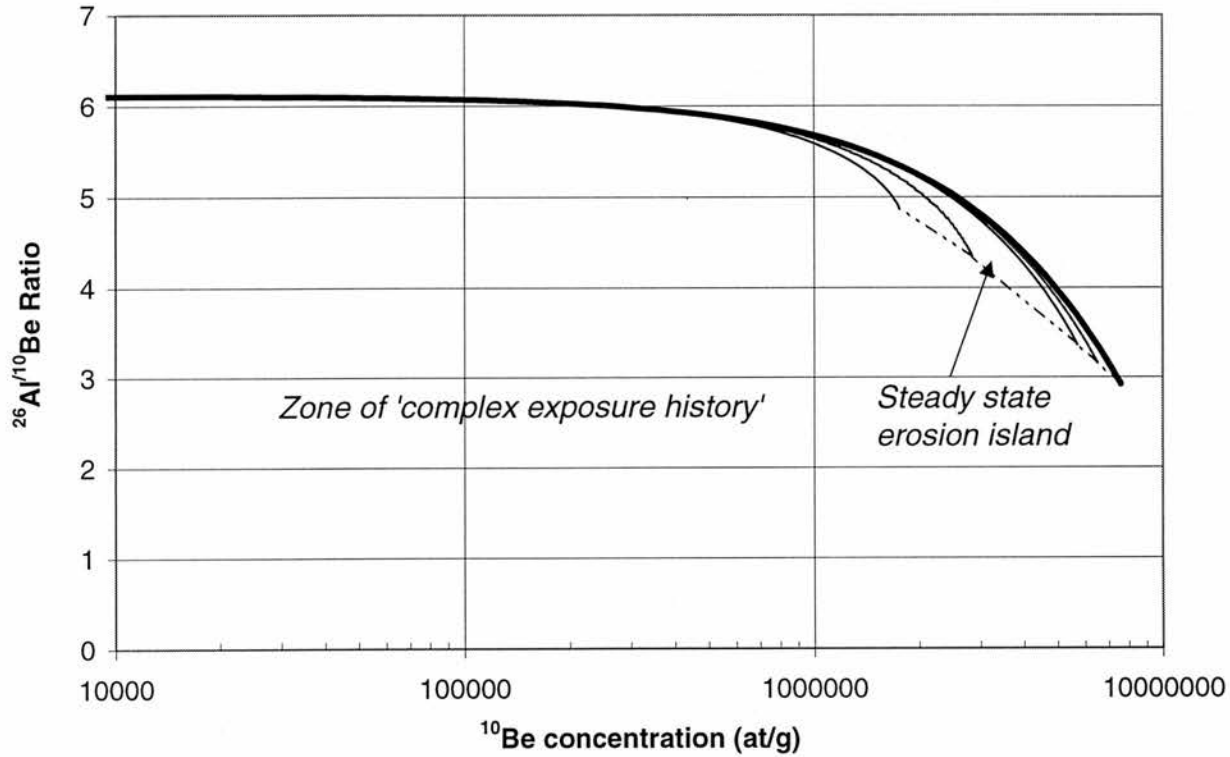

Figure 2.4. Erosion Island plot of $^{26}Al/^{10}Be$ against ^{10}Be, all concentrations have been nornmalised to sea level high latitude. The upper most line represents nuclide build up with no surface erosion, saturation with respect to the isotope occurs at the lower right hand end of this line. The point of saturation decreases with increasing erosion rate. The lines inside the the area of steady state erosion show the evolution of the ratio with time for different erosion rates. The lower dashed line connects the final ratios for each erosion rate and is not actually a line of evolution.

The final scenario is for samples plotting below the line of steady state erosion, thus indicating complex burial history. This can be complete burial or a reduction in incoming cosmogenic signal by a shielding medium such as snow, sediment, ice or water. This will result in a change in the $^{10}Be/^{26}Al$ ratio due to differential rates of radioactive decay (Gosse and Phillips, 2001). If re-exposed the ratio will once more increase; therefore these samples can only be interpreted as have been shielded from cosmic rays at least once, but it could be explained by an infinite number of trajectories involving multiple periods of exposure, subaerial erosion, burial or plucking. Recent studies have attempted to model burial periods with TCNs; however these are based on the assumption of rapid deep burial and are therefore limited in applications (Granger and Muikar, 2001). It is difficult to reconcile detailed and complex sample histories when sample reproducibility is around 5% (Ivy-Ochs 1996). However this approach does offer an opportunity to put forward possible models for a sample's history.

2.9 Use of a multiple isotopes to constrain uplift

A further application of TCN data is for it to provide constraints on long term uplift of the samples or surface in question. This is possible as the production rate of a cosmogenic radionuclide increases exponentially with decreasing atmospheric pressure (Lal, 1991; Brook *et al.*, 1995). Therefore the concentration of a radionuclide can be used to set limits on the amount and rate of uplift which has taken place to the surface over the exposure period. Cosmogenic radionuclides are especially useful for this purpose, as the final saturation concentration is altitude dependent. Using cosmogenic radionuclides to constrain uplift has distinct advantages over other techniques such as fission track dating or ^{40}Ar-^{39}Ar thermochronology, as it allows uplift to be described relative to sea level (or atmospheric shielding), as opposed to denudation and inferred tectonic uplift (Brook *et al.*, 1995).

This approach was first explored and developed by Brown *et al.* (1991), and Brook *et al.* (1993, 1995). In brief it allows the differentiation between long periods of exposure at lower elevations and shorter periods of exposure at higher elevations, or a combination of these two. The model (Equation 2.13), uses the altitudinal dependence of the radionuclide production rate. Thus allowing the calculation of the concentration of ^{10}Be accumulated through different uplift rates

with time, from sea level or any other altitude to its present altitude. The model requires the derivation of the change in atmospheric shielding throughout the period of uplift. This is an important factor, as it significantly affects the rate of build up. As described within section 2.7.1, in this study the atmospheric scaling model described by Stone (2000) was used.

$$N = \left(\frac{Ps}{\left(\frac{U}{\Lambda_a}\right) + \left(\lambda + \frac{E}{\Lambda_a}\right)} \right) \left(e^{\left(U/\Lambda_a\right)t} \right) - \left(e^{-\left(\lambda + E/\Lambda_a\right)} \right) + N_0 e^{-\lambda t} \qquad \text{Eq 2.13}$$

The application of this model provides estimates of maximum uplift rates to raise the surface in question to their present altitudes over the exposure period. As noted by Brook *et al.* (1995), "Our approach only provides a "one way" test. High concentrations of radionuclides are inconsistent with high uplift rates, but low concentrations do not indicate high uplift rates due to the possible effects of erosion." This model also allows an estimate of the minimum age from uplift to be calculated, as described by Ivy-Ochs (1996). By taking the maximum uplift rate, which is limited by the current altitude of the surface in question it is possible to suggest the maximum exposure time required to uplift the surface in question from sea level to its present altitude.

2.10 Conclusions

This chapter has outlined how the TCNs ^{10}Be and ^{26}Al are produced *in situ* in terrestrial rocks, and how their analysis can reveal constraints on the timing of glaciation over time scales of tens of thousands to several million years. Despite an overall uncertainty in production rate determination of around 10%, this technique offers the opportunity to place quantitative constraints on the emplacement of geomorphic features that have previously been unobtainable.

2.11 References

Brook EJ, Kurtz MD. 1993. Surface-exposure chronology using in situ cosmogenic ^{3}He in Antarctic quartz sandstone boulders. Quaternary Research 39. 1-10.

Brook EJ, Brown ET, Kurz MD, Ackert RP, Raisbeck GM, Yiou F. 1995. Constraints on age, erosion and uplift of Neogene glacial deposits in the Transantarctic Mountains using-*in situ* cosmogenic ^{10}Be and ^{26}Al. Geology, V. 23. P 1063-1066.

Brown ET, Edmond JM, Raisbeck GM, Yiou F, Kurz MD, Brook EJ. 1991. Examination of surface exposure ages of Antarctic moraines using *in situ* produced ^{10}Be and ^{26}Al.. Geochimica et Cosmochemica Acta. V. 55. 2269-2283.

Cerling TE, Craig H. 1994. Geomophology and in situ cosmogenic isotopes. Annual Review of Earth and Planetary Sciences 22. 273-317.

Clapperton CM, Sugden DE, Kauffman D, McCulloch RD. 1995. The last glaciation in central Magellan Strait, southernmost Chile. Quaternary Research 44: 133-148.

Cockburn, H.A.P. 1998. Landscape evolution in Namibia and Antarctica: Quantifying denudation rates using in-situ cosmogenic isotope analysis. Unpublished PhD thesis, The University of Edinburgh, 246pp.

Dunai TJ. 2000. Scaling factors for production rates of in situ produced cosmogenic nuclides: a critical reevaluation. Earth and Planetary Science Letters. 176, 157-169.

Elmore D, Phillips FM. 1987. Accelertor mass spectrometry for measurement of long-lived radioisotopes. Science 236. 543-550.

Finkle R, Suter M. 1993. AMS in the earth sciences: technique and applications. Advances in Analytical Geochemistry. V.1. 1-114.

Gosse JC, Evenson EB, Klein J, Lawn B, Middleton R. 1995a. Precise cosmogenic ^{10}Be measurements in western North America: Support a global Younger Dryas cooling event. Geology. V. 23. 877-880.

Gosse JC, Klein J, Evenson EB, Lawn B, and Middleton R. 1995b. Beryllium-10 dating of the duration and retreat of the last Pindale glacial sequence. Science. 268. 1329-1333.

Gosse JC, Phillips FM. 2001. Terrestrial in situ cosmogenic nuclides: theory and application. Quaternary Science Reviews 20. 1475-1560.

Granger D E., Muzikar P. 2001. Dating sediment burial with cosmogenic nuclides: Theory, techniques, and limitations, Earth and Planetary Science Letters. 188,. no. 1-2. 269-281.

Hallet B, Putkonen, J. 1994. Surface dating of dynamic landforms:young boulders on ageing moraines: Science. V.265. 937-940.

Heisinger B. 1997. In situ production of radionuclides at great depths. Nuclear Instruments and Methods. B. 123. 341-346.

Hofmann HJ. Beer J, Bonani G. von Gunten HR. Raman S, Suter S, Walker RL, Wölfli W, Zimmermann D. 1987. Half-life and AMS standards: Nuclear Instruments and Methods. B29. 32-36.

Ivy-Ochs S, Schlüchter C, Kubik PW, Dittrich-Hannen B, Beer J. 1995. Minimum ^{10}Be exposure ages of early Pliocene for the Table Mountain plateau and the Sirius Group at Mount Fleming, Dry Valleys, Antarctica. Geology 23. 1007-1010.

Ivy –Ochs S. 1996. The dating of rock surfaces using the in situ produced ^{10}Be, ^{26}Al, and ^{36}Cl, with examples from Antarctica and the Swiss Alps. Ph. D. Thesis, Swiss Federal Institute of Technonology, Zurich. 196pp.

Ivy-Ochs S, Schlüchter C, Kubik PW, Beer J, and Kerschner H. 1996. The exposure age of an Egsen moraine at Julier Pass measured with the cosmogenic radionuclides ^{10}Be, ^{26}Al and ^{36}Cl. Eclogae Geologicae Helvetiae 89. 1049-1063.

Klien J, Middleton R, Tang H-Q. 1982. Modifications of an FN Tandem for quantitave measurements of ^{10}Be. Nuclear Instruments and Methods 193. 601-616.

Klein J, Giegengack R, Middleton R, Sharma P, underwood JR, Weeks WA. 1986. Revealing histories of exposure using in situ produced ^{10}Be and ^{26}Al in Libyan desert glass. Radiocarbon 28. 547-555.

Kohl CP and Nishizumi K. 1992. Chemical isolation of quartz for measurement of *in situ* produced cosmogenic nuclides. Geochemica et Cosmochemica Acta. 56. 3583-3587.

Kubik PW, Ivy-Ochs S, Masarik J, Frank M, Schlüchter C. 1998. ^{10}Be and ^{26}Al production rates deduced from an instantaneous event within the dendro-calibration curve, the landslide of Köfels Ötz Valley, Austria, Earth and Planetary Science Letters 161. (1-4). 231-241.

Lal D, Arnold JR. 1985. Tracing quartz through the environment. Proceedings of the Indian Academy of Science (Earth Planetary Science Section) 94. 1-5.

Lal D. 1991. Cosmic ray labeling of erosion surfaces: in situ nuclide production rates and erosion rates. Earth and Planetary Science Letters 104, 424-439.

Middleton R, Klein J, Raisbeck GM, Yiou F. 1983. Accelerator Mass Spectrometry with ^{26}Al. Nuclear Instruments and Methods in Physics Research 218. 430-438.

Nishiizumi K, Finkle RC, Klein J, Kohl CP. 1986. Cosmogenic production of ^{7}Be and ^{10}Be in water targets. Journal of Geophysical Research 101. 22,225-22,232.

Nishiizumi K, Winterer EL, Kohl CP, Lal D, Arnold JR, Klein J, Middleton R. 1989. Cosmic ray production rates of ^{10}Be and ^{26}Al in quartz from glacilly polished rocks. Journal of Geophysical Research 94 (B12). 17,907-17,915.

Ochs M, Ivy-Ochs S. 1997. The chemical behavior of Be, Al, Fe, Ca, and Mg during AMS target preparation from terrestrial silicates modelled with chemical speciation calculations. Nuclear Instruments and Methods in Physics Research B 123, 235-240.

Radok U, Allison I, Wendler G. 1996. Atmospheric surface pressure over the interior of Antarctica. Antarctic Science. 8. 209-217.

Raisbeck GM, Yiou F, Bourles D, Lorins C, Jouzel J, Barkov, NI. 1987. Evidence for two intervals of enhanced ^{10}Be deposition in Antarctic Ice during the last glacial period. Nature 326. 273-277.

Sarafin R. 1985. Anwendung radiochemister methoden und der Beschleuniger Massenspectrometrie zur Bestimmung der tiefenbhängigen, langlebigen Spallations-Radionuklide ^{10}Be, ^{26}Al, ^{36}Cl und ^{53}Mn in Steinmeteoriten und Gedanken zum noch ungeklärten Urspring der Shergottite. Ph.D. dissertation Universtät zu Köln. pp132.

Schaller M, von Blanckenburg F, Hovius N, Kubik PW. 2001. Large-scale erosion rates from in situ produced cosmogenic nuclides in European river sediments. Earth and Planetary Science Letters 188. 441-458.

Stone JO. 2000. Air pressure and cosmogenic isotope production. Journal of Geophysical Research. 105. B10. 23,753-23,759.

Synal HA, Bonani G, Dobeli M, Ender RM, Gartenmann P, Kubik PW, Schnabel C, Suter M. 1997. Status report of the PSI/ETH AMS facility. Nuclear Instruments and Methods B123. 62-68.

Tschudi T. 2000. Surface exposure dating: A geologist's view, with examples from both hemispheres. . Ph. D. Thesis, Swiss Federal Institute of Technonology, Zurich. 125pp.

CHAPTER 3

Application of surface exposure dating to deposits of the Last Glacial Interglacial Transition in Patagonia, southern most Chile: Magellan Region.

3.1 Abstract

The timing of the Last Glacial Maximum in the Magellan region of Patagonia is ascertained using the concentrations of cosmogenic ^{10}Be from erratics from glacial landforms. Three advances were identified, related to landforms created by the expansion of the Patagonian Icefield as discrete ice lobes that flowed north east down the Strait of Magellan from a source area in the Cordillera Darwin. An advance at 26,011±1,380 ^{10}Be yr BP, is marked by a large thrust moraine complex produced by the advance of ice into glacifluvial and glacilacustrine sediments. Deglaciation was only punctuated by short periods of stabilisation or advance of the retreating ice lobe at 20,851±1,340, and 18,734±1,315 ^{10}Be yr BP. The timings of these events are recorded by small low angle moraines and marginal drainage channels incised proximal to the position of the stable ice front. Both periods of stabilisation have been constrained through the analysis of the concentrations of cosmogenic ^{10}Be contained in two large rockfall deposits related to these landforms.

These data indicate that the Last Glacial Maximum in southernmost South America has resulted in multiple advance stages, with the greatest extent occurring at ca. 26 ka years. This strengthens the conclusions from other sectors of Patagonia that suggests maximum ice extent was synchronous between the mid-latitude southern hemisphere and the northern hemisphere.

3.2 Introduction

This paper investigates the timing of deglaciation of the formerly expanded Patagonian Ice Sheet centred on the southernmost Andes of Fuego-Patagonia, from its inferred limits at the Last Glacial Maximum (LGM) (Clapperton *et al.*, 1995) (Figure 3.1). Previous workers have identified a rich record of glacial landforms and sediments related to the Pleistocene expansion of the southernmost Patagonian Ice Sheet (Caldenius, 1932; Ferugilio. 1950; Mercer, 1976 and Marden, 1993). However, uncertainty still exists over the timing of these expansions.

The southernmost Andes provide one of the only topographic barriers to the circulation of the southern westerlies at this latitude, therefore producing an energetic climate regime. It has been suggested that glacial dynamics in this region are controlled by the location, moisture content and intensity of the westerlies, which are themselves controlled by global pressure gradients (Denton *et al.*, 1999, Hubbard, 1997, Hulton *et al.*, 1994, 2000). Therefore, fluctuations in the extent of glaciers in this region should reflect changes in major climatic systems of the southern hemisphere, and provide insights into local precipitation and temperature conditions (Clapperton *et al.*, 1995). The link with climate has been demonstrated further north in the Chilean Lake District, where glacier advances occurred simultaneously with ice rafting events in the North Atlantic (Denton *et al.*, 1999). This correlation suggests that glacial advances during the LGM at 40^0S were a result of global climate forcing mechanisms as opposed to regional controls such as surges of the Laurentide Ice Sheet or switches in ocean thermohaline circulation (Lowell *et al.*, 1995; Broecker and Denton, 1990; Denton *et al.*, 1999).

Recent studies have suggested diverse and tentative chronologies of glaciation of this southern sector of the ice sheet, but these hypotheses have proved difficult to test due to the paucity of a detailed radiocarbon chronology bracketing ice advances in this region (Clapperton *et al.*, 1995, McCulloch *et al*, 2000). This in part can be seen as the difficulty of interpreting minimum radiocarbon dates to constrain glacial retreat (McCulloch *et al.*, 2001; McCulloch and Davies, 2001). Chronologies based wholly on the analysis of organic material that has built up since deglaciation are at the mercy of both the rate at which it is possible for the formation of organic material to occur, and the preservation of this material *in situ*. This problem is compounded in this region by the presence of contamination by old carbon in the form of lignite within core

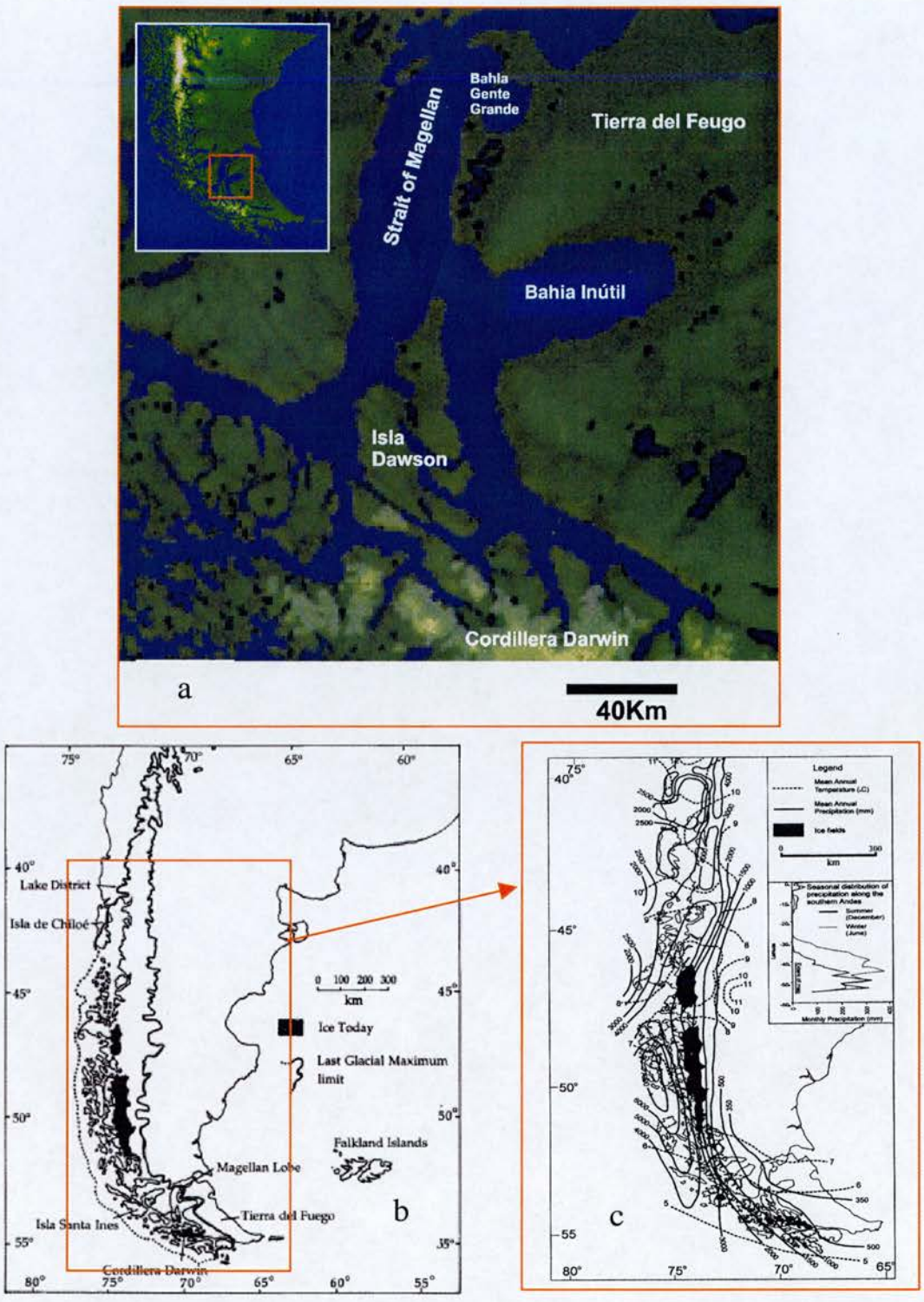

Figure 3.1. Location maps of the Magellan field area showing, a, The Magellan Region with Ice lakes and topography from G-topo 30 data, b, the proposed extent of ice during the LGM (Hollin and Schilling, 1981),c, Distribution of present glaciers and climatic features together with data showing the seasonal migration of the westerlies (inset) (McCulloch *et al.*, 2000).

material (McCulloch and Davies, 2001). Such issues have been highlighted recently with open discussions regarding this problem, especially in the central latitudes of the former Patagonian Ice Sheet (45-50^0 South) (Wenzens, 1999; McCulloch *et al.*, 2000; Wenzens, 2001; McCulloch *et al.*, 2001). The complex pattern of deglaciation of the southernmost sector of Patagonia could therefore be simply a product of the interpretation of the available chronological and morphostatigraphical records. With this in mind the application of an alternative chronological technique such as analysis of the terrestrial *in situ* cosmogenic nuclide ^{10}Be could improve the glacial chronology of this region (Ivy-Ochs, 1996; Gosse and Phillips 2001). New direct dating can be used to investigate the linkages between regional and global climate and the geomophological record of ice advance and retreat during from the Last Glacial Maximum.

3.3 The topography and climate

The landscape of the Magellan region of Patagonia reflects late Cenozoic structural trends, with orogenic mountains aligned NW-SE and WNW-ESE extending to tilted and dissected plateaux descending to the north and eastwards towards the Atlantic seaboard of Argentina (Clapperton *et al.*, 1995). The study area is characterised by moraine rimmed embayments and channels (Raedake, 1978), which record repeated advances of ice lobes flowing northwards from source areas in the Cordillera Darwin (Porter *et al.*, 1992; Clapperton *et al.*, 1995) (Figure 3.1).

The high summits of the Cordillera Darwin are still glaciated under modern conditions, sustained by the persistent moisture laden westerly air streams. The topographic barrier of the southernmost Andes creates a substantial rainshadow across the Magellan Region, with mean annual precipitation totals exceeding 2000mm in the Cordillera Darwin, falling to less than 350mm in the central area of the Straits of Magellan (Romero, 1985)(Figure 3.1). The combination of these topographic and climatic factors cause the alpine glaciers and ice sheets of the Cordillera Darwin and Isla Santa Inès to terminate at sea level, with the steep rise in the equilibrium line altitude (ELA) north-eastwards over Tierra del Feugo.

3.4 Geomorphology and glacial history

Caldenius (1932) plotted the position of most major moraine systems throughout Patagonia and Tierra del Fuego. He attempted to construct a chronology for these advances by teleconnecting glacial lake varves found in Patagonia to the Swedish varve chronology of De Geer (1927 and 1929). Using this system, Caldenius ascribed the largest outer most moraine limits to the late-glacial stadial events, the Finiglacial, Gotiglacial and the Daniglacial. In this seminal publication Caldenius was able to trace these limits throughout Patagonia. Subsequent work has demonstrated that, although the limits are broadly correct, the chronology is unresolved between different regions and even individual lobes of the once expanded Patagonian Ice Sheet (Clapperton *et al.*, 1995; Denton *et al*,. 1999; McCulloch *et al.*, 2001). To date there is still considerable disagreement between the chronologies of glaciation of this region even over short distances.

The geomorphology of deposits thought to relate to the global LGM in the region of the Strait of Magellan and Tierra del Feugo have been investigated by many workers since Caldenius (Auer, 1956; Bruggen, 1950; Feruglio, 1959-50, Raedeke, 1978; Uribe, 1982; Clapperton, 1989, Porter, 1989; Porter *et al.*, 1992; Clapperton *et al.*, 1995; Benn and Clapperton, 1999). This work has described a complex pattern of drift, which is marked on both sides of the Strait of Magellan by belts of moraine ridges and marginal meltwater channels that are continuous for tens of kilometres. In the area surrounding the Straits these moraines are typically composed of ice-thrust glacifluvial and glacilacustrine sediments facies forming sharp-crested ridges up to 20m in height. The most comprehensive descriptions of the sediment landform associations are those of Benn and Clapperton (1999). Their detailed analysis of the internal structure and the morphology of these moraine belts indicate that they are thrust ridge complexes, recording ice-marginal and proglacial glacitectonic deformation. The presence of a thick overlaying drape of poorly stratified diamictons and outwash gravels unconformably overlying ice-thrust sediments, indicates extensive melt-out from thick debris rich basal ice layers.

The work of Benn and Clapperton focused on the sediments located on either sides of the central region of the Strait of Magellan, and accepted the chronology of the limits as described by Clapperton *et al.* (1995) (Figure 3.2). On the basis of this work the LGM limit was described as

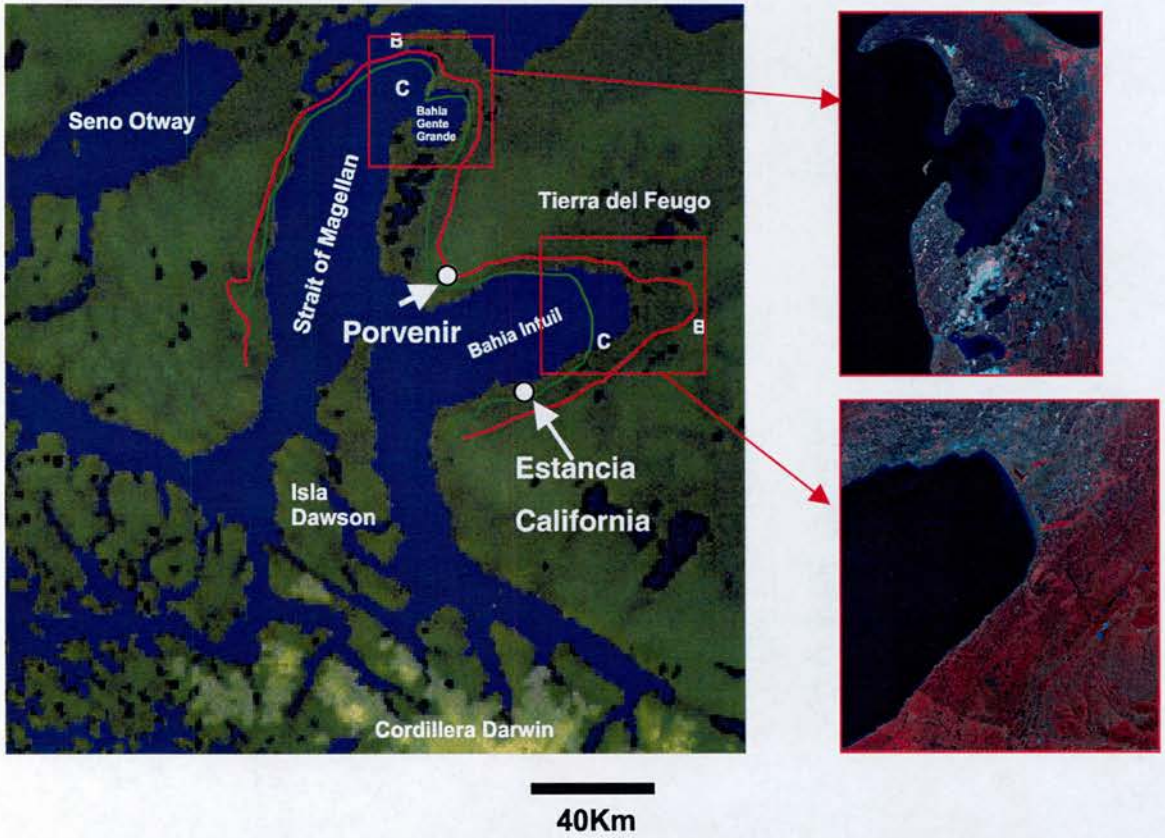

Figure 3.2. Glacier limits around the central and southern Magellan Straits, identified by Clapperton *et al.* (1995). The localities Porvenir and Estancia California are the localities where basal radiocarbon dates are available. At Porvenir the minimum constraint on ice withdrawal is 20,834 cal yr BP, and 16,591 cal yr BP at Estancia California. With detail of the Landsat Thematic Imagery which was used to construct the summary geomophological maps of these areas in Figures 3.3 and 3.4.

advance B, with the limit within this being described as "glacial event C", an advance following recession from the LGM. The ice proximal flanks of these moraine belts are characterised by extensive hummocky kame and kettle topography, which is particularly prevalent on the Peninsulas Jaun Mazia and Gente Grande surrounding Bahia Gente Grande (Figure 3.5). This kame and kettle topography commonly contains isolated moraines and chains of kettle holes aligned parallel to the former ice margin. The limits of advance B and C are separated by extensive systems of lateral meltwater channels and kame terraces that have deposited large volumes of sediment. The measurement of the concentrations of ^{10}Be in boulders on the tops of these large thrust moraines will indicate the time of their emplacement by advancing ice.

The work of Clapperton *et al.* (1995), extended the limits of advance B and C around the Magellan Lobe south to the lobe affecting the embayment of Bahia Inútil (Figure 3.2). However, it should be noted that this region lies outside areas covered by aerial photographic coverage, and that geomorphological mapping relies on Landsat imagery with little ground truthing. The work of Raedeke (1978) best describes the geomorphology of the area, identifying large moraine limits 30km to the east of the end of modern embayment. This was correlated with advance B by Clapperton *et al.* (1995), while the limits of glacial event C were placed well within Bahia Inútil, some 40km behind the advance B (Figure 3.2). The work of Raedake (1978), identified a large number of erratic blocks at two localities at the eastern end of this embayment. Figure 3.4 shows the localities of these boulder fields in relation to the local geomophology, and Figure 3.6 demonstrates typical boulders. Fieldwork was undertaken during 1999, in order to improve the geomorphological understanding of this area and to allow sampling of the erratics identified by Raedake, for TCN exposure analysis.

The erratics identified by Raedake (1978) were deposited on extensive areas of kame and kettle topography, which is generally chaotic, but with small morainic mounds aligned parallel to the main concentration of both groups of erratics (Figure 3.6). Due to their size, mono-lithogenic composition, concentration and surface morphology these deposits were interpreted as a rockfall deposited on to the accumulation zone of the glacier. There is limited evidence of secondary glacial reworking, suggesting that most boulders have been transported passively within the glacier (Boulton, 1978). The source area for these large erratics is likely to be the granitic massif of the Cordillera Darwin, the source area of the ice lobes affecting this locality, located around 200km to the south west (Figure 3.1).

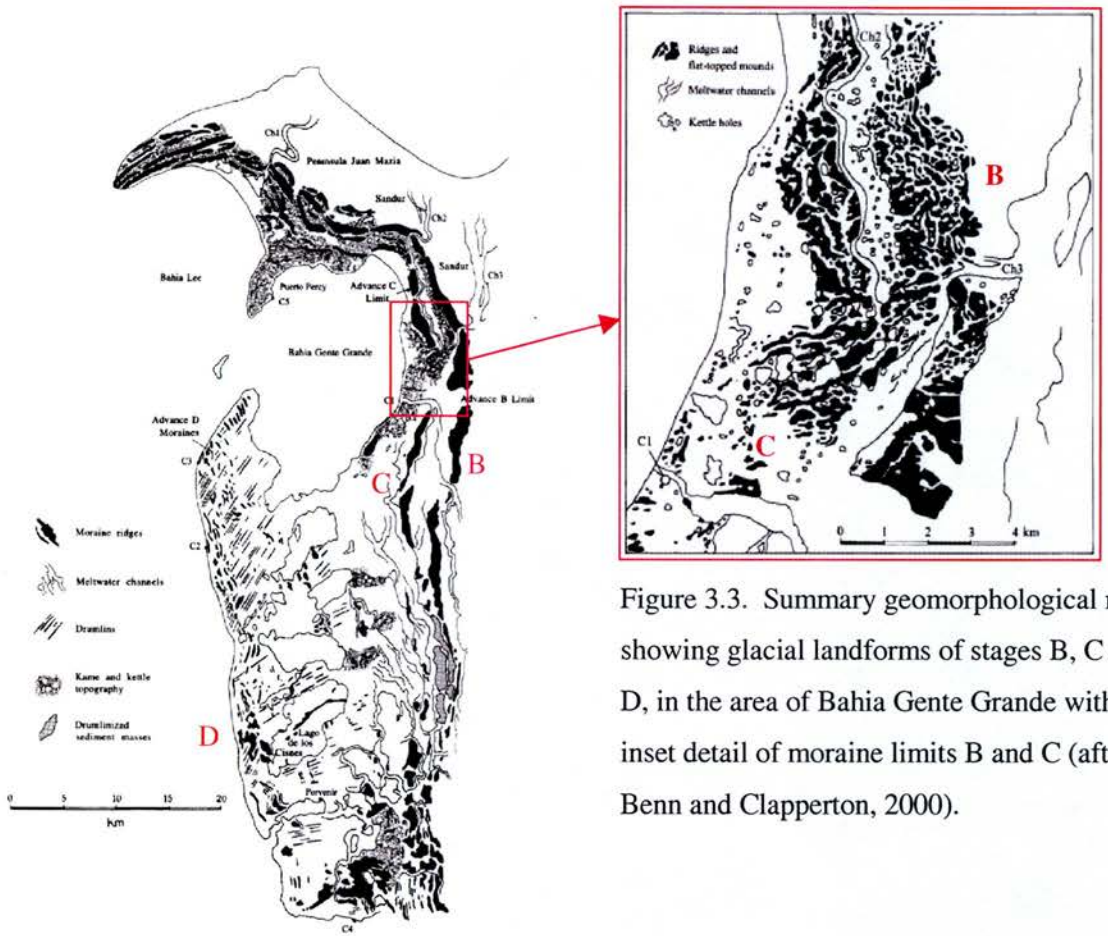

Figure 3.3. Summary geomorphological map showing glacial landforms of stages B, C and D, in the area of Bahia Gente Grande with inset detail of moraine limits B and C (after Benn and Clapperton, 2000).

From detailed ground truthing at the eastern end of Bahia Inútil it is clear that there are no significant terminal moraines related to the ascribed limit of glacial stage B of Clapperton *et al.* (1995). Rather the landscape at the end of Bahia Inútil is characterised by a series of small-scale (2-3m) low angled moraine limits. These are separated by large tracts of kame and kettle topography, which is incised by numerous abandoned drainage channels which run approximately parallel to the coast until points at which they are seen to deflect north draining into the embayment. Figure 3.4 demonstrates the positions of these channels on the southern shores of Bahia Inútil in comparison to the locations of the boulder fields described by Raedeke (1978). Although the size of the channels vary, they are all at least 20m in depth and greater than 30m wide.

The auther suggests that the these channels and small reticulate moraines record periods of stabilisation or even advance during general decay of an ice margin within this embayment, with the channels being incised by meltwater routed around the edge of the stable ice front. Therefore by measuring the exposure times of these rockfall erratics it may be possible to place numerical constraints on ice extent in relation to these features. The location of the two erratic boulder fields close to the glacial limits B and C of Clapperton *et al.* (1995), allow the timing of these periods of stabilisation or advance to be ascertained.

3.5 Current chronology

At present the timings of these advances are constrained by a number of minimum radiocarbon dates of around 17 to 20 ^{14}C ka BP from rootlets and plant material located above inorganic blue grey clays (Clapperton, 1995). Recent work has demonstrated that it is likely that many of these dates are affected by lignite contamination (McCulloch and Davies, 2001). Therefore, for this study the only radiocarbon dates which are accepted are those described below, that have been pre-treated to remove this problem.

At present limits B and C are best constrained by two minimum radiocarbon dates from organic material directly above glacial blue grey clays from cores surrounding Bahia Inútil (McCulloch pers com). The locations of these can be seen in Figure 3.7. These cores provide very important

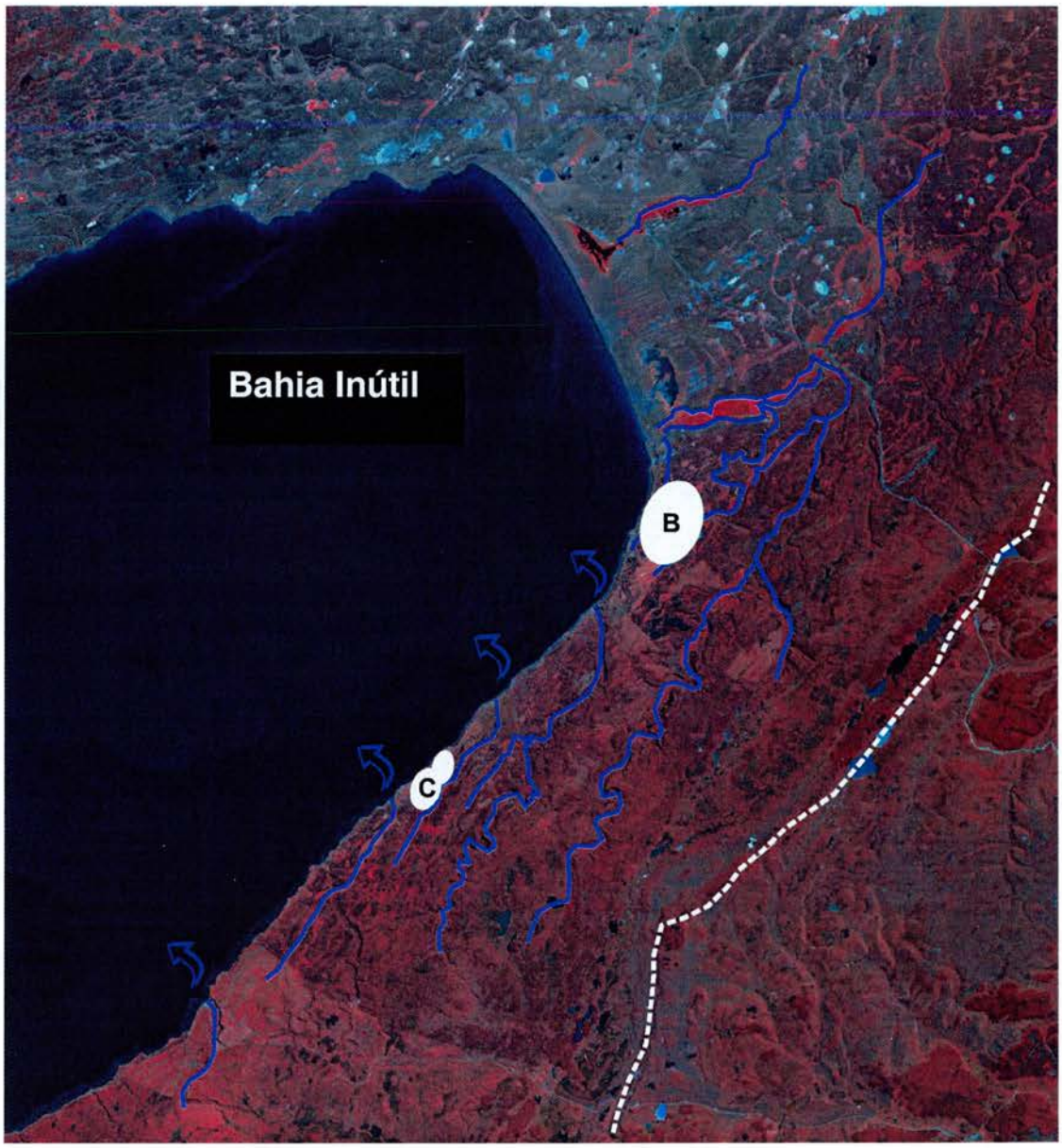

Figure 3.4. Landsat composite image of the eastern end of Bahia Inútil, that has been annotated to show the positions of incised drainage channels described in text. This image has not been georectified, but at its widest point is 25 km wide. The white areas represent the highest concentrations of erratic boulders described in text. They also represent the areas where small reticulate moraines are most common

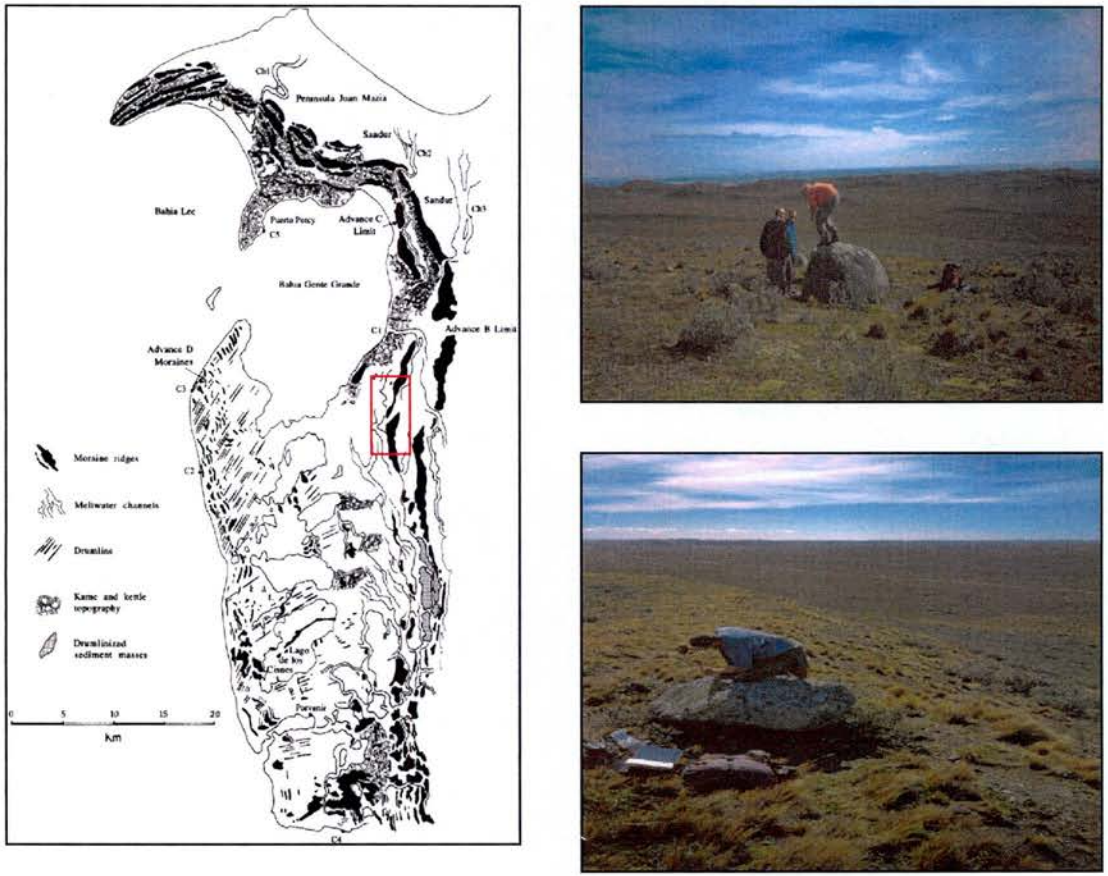

Figure 3.5. Summary geomorphological map of Bahia Gente Grande, with example photographs of the types of boulder samples taken from these large thrust moraines. Both Images are taken looking due north east, from the moraines described as C by Clapperton *et al.* (1995).

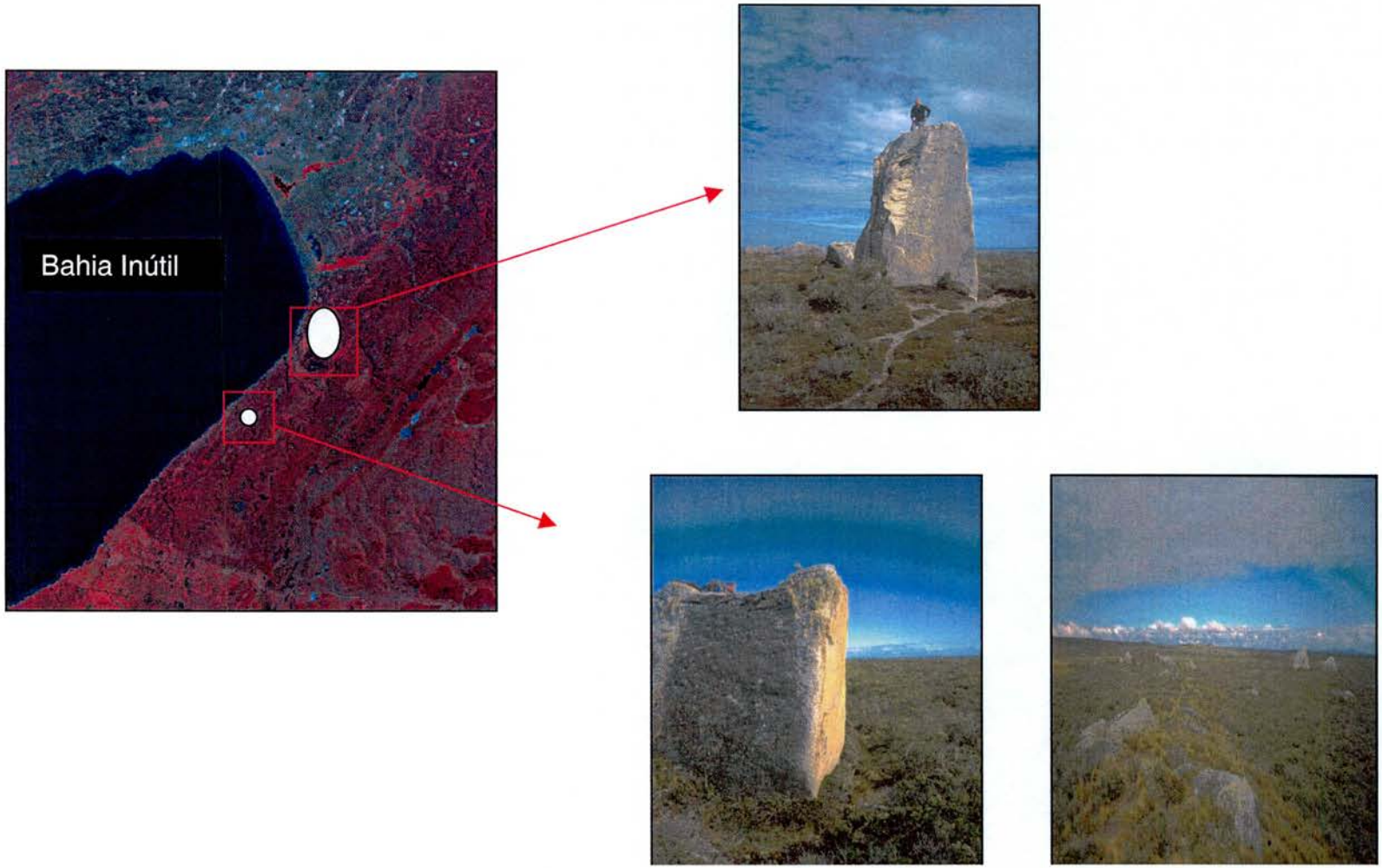

Figure 3.6. The locations of the two major rockfall deposits on the shores of Bahia Inútil. The upper photo show the typical size of these boulders (see figure for scale). The lower two images show the typical unweathered surfaces, and the concentrations of these boulders on the small reticulate moraines located within these deposits.

constraints on the withdrawal of glacial ice from these limits, suggesting that ice had receded from limit B in the area of Porvenir by 20,834 cal yrs BP. This is supported by the basal dates from a core on the southern shores of Bahia Inútil, at Estancia California, which indicate ice withdrawal from limit C by 16,591 cal yrs BP (McCulloch pers com). A further minimum constraint on these landforms is their stratigraphic relationship with a silicic tephra the Reclús, which has been tightly constrained in this region to 15,382 cal yr BP from multiple sites throughout southern Patagonia (McCulloch and Davies, 2001). The presence of the Reclús tephra within glacilacusterine sediments indicates that ice had withdrawn a considerable distance (greater than 80km) from these limits by the time the eruption of Volcán Reclús occurred. To improve this chronology sampling for TCN surface exposure dating of erratics related to these limits was undertaken during the field season in the austral summer of 1999.

3.6 Exposure dating

The exposure histories of the sampled rock surfaces in question were estimated by the measurement of the concentration of the TCN ^{10}Be. This radionuclide is produced in the upper few decimetres of rock surfaces exposed to cosmic ray bombardment, where the isotope is formed within the lattices of certain minerals (Lal, 1991, Gosse and Phillips 2001). Sampling was restricted to two localities, the area south east of Bahia Gente Grande, and the eastern end of Bahia Inútil (Figure 3.2). The critical difference between these localities is the type of samples found to constrain glaciation. The samples from the large terminal moraines east of Bahia Gente Grande are glacial erratics, which have been incorporated and transported subglacially to eventual emplacement on top of the large moraine systems when ice was actively creating these landforms. This differs from the samples taken from a large rockfall event in Bahia Inútil, which probably originated from the high mountains of the Darwin Cordillera and provides a minimum constraint on deglaciation from these limits. The sample descriptions together with the ages ascribed by Clapperton *et al.* (1995) are recorded in Table 3.2.

The concentration of ^{10}Be was measured in 11 boulders on top of the landforms described above. Samples were taken from suitably large boulders, by removing the uppermost centimetres of their top surfaces. By choosing the largest boulders from those available, any problems related

to exhumation or significant coverage by snow or vegetation were minimised. Sampling was restricted to boulders in stable positions on top of landforms, to avoid any post-depositional movement. As quartz is the ideal mineral for the application of ^{10}Be, only quartz rich granites and granodiorites were sampled

^{10}Be was selectively extracted from the quartz component of the whole rock sample following the standard procedures described by Kohl and Nishizumi (1992) and Ivy-Ochs (1996). Isotopic ratios were measured at the ETH tandem AMS facility in Zurich, Switzerland. Tables 3.1 and 3.2 list the cosmogenic ^{10}Be radionuclide data, the location and type of sampling site and the conventional exposure ages of each sample. In this study the reference production rate used is that of Kubik *et al* (1998), which has been determined experimentally. *In situ* production of cosmogenic ^{10}Be is a combination of three principle components, the most important being spallation, with fast and stopped muons making a less significant contribution to total production. There is strong evidence that the relative muon contribution to total production is much lower than the 16% originally assumed (see Heisinger, 1998 and Stone 2000 for discussion). This study incorporates the modified values of Kubik *et al* (1998) to provide a more accurate representation of the stopped and fast muon components (Heisinger, 1997; Stone 2000). Therefore the reference production rate for ^{10}Be used is a spallation component of 5.22±0.22 atoms/g (qtz)/yr, together with a value of 0.12 atoms/g (qtz)/yr for stopped muons and 0.027 atoms/g (qtz)/yr for fast muons (Schaller, 2001). This results in a total surface production rate (P_0), at sea level and high latitude (SLHL) for ^{10}Be of 5.37±0.22 atoms/g (qtz)/yr. This value was chosen for three reasons; (1) it is referenced to the calibrated radiocarbon timescale, hence the exposure ages given here should be directly comparable to calibrated radiocarbon ages (2) all relevant data necessary for the calculations are available (3) due to the lack of a suitable calibration site in the southern hemisphere on this time scale.

The reference production rate was scaled to that of each site following the methods outlined by Stone (2000). The total production at the site, was corrected for attenuation of cosmic radiation due to the thickness of the sample itself, and any shielding due to the surrounding topography following the procedures of Dunne *et al.* (1999). These correction factors were applied to model the effect of the reduced incoming cosmogenic signal on the total production at the sample site. Errors related to the AMS, the production rate and 5% for sample reproducibility are added quadratically, and calculated as a function of the eventual age. The effect of shielding from snow

or tephra were not included, as they represent unknowns over the exposure period. Their effect would lead to a increase in the eventual age, but it was felt that a model of this would be unrealistic with the likely degree af variation over the exposure period.

In order to provide a realistic age envelope, the ages have been calculated for the effect of surface erosion, at rates of 1mm, 3mm and 1cm per 1000 years. The rate of erosion will obviously vary with lithology and environmental conditions. Therefore, this is offered as a guide to the possible upper and lower age limits of the surface in question. The surface of some samples provide limitations on the magnitude of erosion, including striations and surface pitting, details of which are described in Table 3.2.

3.7 Results

The cosmogenic radionuclide data related to the AMS measurement are summarised in Table 3.1. This provides an uncorrected record of the original data allowing recalculation of the data independently of the age models used in this study. Total propagated errors related to the production rate, AMS analyses, and an additional 5% sample reproducibility range from 6.1 to 15.3%.

Table 3.2 presents the sample descriptions and cosmogenic radionuclide ages calculated by the procedure outlined. The analysis of multiple samples provides an internally coherent data set with which to fix the glacial limits both temporally and spatially. As these samples have been taken from erratics or boulders that were either in close proximity to one another or on top of a single landform making it possible to interpret them as error weighted mean ages of the landform. The auther suggests that the error weighted mean provides a more accurate representation of landform age, reducing the variation due to factors such as soil or snow cover or settlement of individual boulders.

Figure 3.8 demonstrates the exposure ages and the resultant error weighted means against proxy records of atmospheric temperature from ice core records from both Greenland and Antarctica. This figure also shows the exposure ages with reference to the available radiocarbon chronology

Table 3.1 Cosmogenic radionuclide data

sample ID	Latitude (^{0}S)	Longditude (^{0}E)	Altitude (m)	Sample mass (g)	Depth shielding factor[1]	topographic shielding factor[2]	Be carrier (mg)[3]	measured $^{10}Be/^{9}Be$ ratio[4]	± % error[5]	measured laboratory blank $^{10}Be/^{9}Be$[6]	±% error[7]	Blank corrected ratio[8]	^{10}Be atoms /g in sample[9]	± % error[10]	± % error inc. 5% sample reproducability[11]
BI:B1	53	69	80	76.3582	0.956	1.000	0.507	3.13E-13	11.1	2.48E-14	15.9	2.88E-13	127868.2	12.1	13.1
BI:B2	53	69	75	33.6177	0.965	0.994	0.507	1.6E-13	7.5	4.1E-14	16.8	1.19E-13	119923.2	11.6	12.7
BI:B3	53	69	85	57.2905	0.965	1.000	0.507	2.1E-13	7.5	2.48E-14	16.8	1.85E-13	109517.2	8.8	10.1
BI:B4	53	69	80	43.129	0.948	1.000	0.507	1.95E-13	9.3	4.1E-14	16.8	1.54E-13	120969.5	12.6	13.6
BI:C1	53	69	52	56.6195	0.948	0.991	0.507	1.86E-13	5.7	2.48E-14	15.9	1.61E-13	96454.78	7.0	8.6
BI:C2	53	69	48	19.2615	0.948	0.991	0.507	8.1E-14	9.1	2.48E-14	13.6	5.62E-14	98848.62	14.4	15.3
BI:C3	53	69	54	38.6121	0.948	0.991	0.355	1.91E-13	8	2.8E-14	17.5	1.63E-13	100012.1	9.8	11.0
BGG:C1	53	70	82	52.002	0.965	1.000	0.355	3.55E-13	5.1	2.8E-14	17.5	3.27E-13	148975.9	5.7	7.6
BGG:C2	53	70	100	22.977	0.965	1.000	0.355	1.69E-13	6.5	2.8E-14	17.5	1.41E-13	145383.2	8.5	9.9
BGG:C4	53	70	73	66.4962	0.965	1.000	0.355	4.08E-13	3.1	2.8E-14	17.5	3.8E-13	135386.4	3.6	6.1

1. Calculated using "flat" dependency of Masirik and Reedy (1995)

2. Calculated using the relationship $\sin^{2.3}\theta$, for 360^0 around the sample, where θ is the angle of the topographic obstruction from the horizontal (Gosse and Phillips 2000).

3. Carrier addition measured by calibrated pipette, and corrected for temperature and density.

4 & 5. Reported from AMS measurements, include errors related to "in-house" standard.

6 & 7. Removes possible effects of exposure and chemical loading of other samples, measured during same accelerator run.

8. Total blank corrected $^{10}Be/^{9}Be$ ratio.

9 & 10. Concentration of cosmogenic ^{10}Be in sample with errors propagated step-wise (atoms / gram).

11. Additional 5% error related to sample reproducability, based on multiple analyses on single samples by Ivy-Ochs (1996).

Table 3.2 Sample descriptions and cosmogenic radionuclide ages

Sample ID	Glacial stage [1]	Altitude(m)	Location [2]	Sample type [3]	Relitive Age [4]	10Be exposure age (yrs) [5]	±error (yrs)	Comments	Exposure age (yr) @E=1mm/ka	Exposure age (yr) @E=3mm/ka	Exposure age (yr) @E=1cm/ka	Mean landform age (yr) [6] (E=0)
BI:B1	C(B)	80	***Bahia Inutil***	E	>R, >A	**22,803**	**3,135**	Fresh surface suggests minimal erosion	23285	24339	29390	
BI:B2	C(B)	75	***Bahia Inutil***	E	>R, >A	**21,419**	**2,849**	Fresh surface suggests minimal erosion	21844	22767	27084	**20851±1340**
BI:B3	C(B)	85	***Bahia Inutil***	E	>R, >A	**19,244**	**2,101**	Fresh surface suggests minimal erosion	19586	20323	23644	
BI:B4	C(B)	80	***Bahia Inutil***	E	>R, >A	**21,759**	**3,081**	Fresh surface suggests minimal erosion	22198	23152	27642	
BI:C1	<C	52	***Bahia Inutil***	E	>R, >B	**19,057**	**1,988**	Fresh surface suggests minimal erosion	19392	20114	23357	
BI:C2	<C	48	***Bahia Inutil***	E	>R, >B	**18,521**	**2,927**	Fresh surface suggests minimal erosion	18838	19517	22546	**18734±1315**
BI:C3	<C	54	***Bahia Inutil***	E	>R, >B	**18,625**	**2,193**	Fresh surface suggests minimal erosion	18945	19633	22702	
BGG:C1	C	82	***Bahia Gente Grande***	Bm	>R, >A	**26,299**	**2,273**	Striations indicate low ersosion	26945	28374	35691	
BGG:C2	C	100	***Bahia Gente Grande***	Bm	>R, >A	**25,200**	**2,697**	Striations indicate low ersosion	25792	27097	33632	**26011±1380**
BGG:C4	C	73	***Bahia Gente Grande***	Bm	>R, >A	**24,106**	**1,780**	Striations indicate low ersosion	24647	25833	31655	

1. Glacial stages based on this work, Clapperton et al.'s (1995) original glacial stage is shown in parenthesis where the relative ages of moraines have been reinterpreted.
2. See text for descriptions, and Figures 3 and 4.
3. Sample type; Bm=Boulder perched on moraine, E=Erratic, B=bedrock surface
4. Available minimum constraints on landform; R=Reclus tephra (15,382 cal yr BP) (McCulloch and Davies, 2001), A=Minimum radiocarbon date of 20,834 cal yr BP above blue gray clays (McCulloch pers com), B=Minimum radiocarbon date of 16,591 cal yr BP at Estancia California (McCulloch pers com).
5. Calculated using a ^{10}Be production rate of 5.37±0.22 at/g/yr (Schaller et al., 2001), scaled following the methods outlined by Stone (2000), which are a reformulation of those of Lal (1991).
6. Error weighted mean of TCN ages from boulders from individual landforms

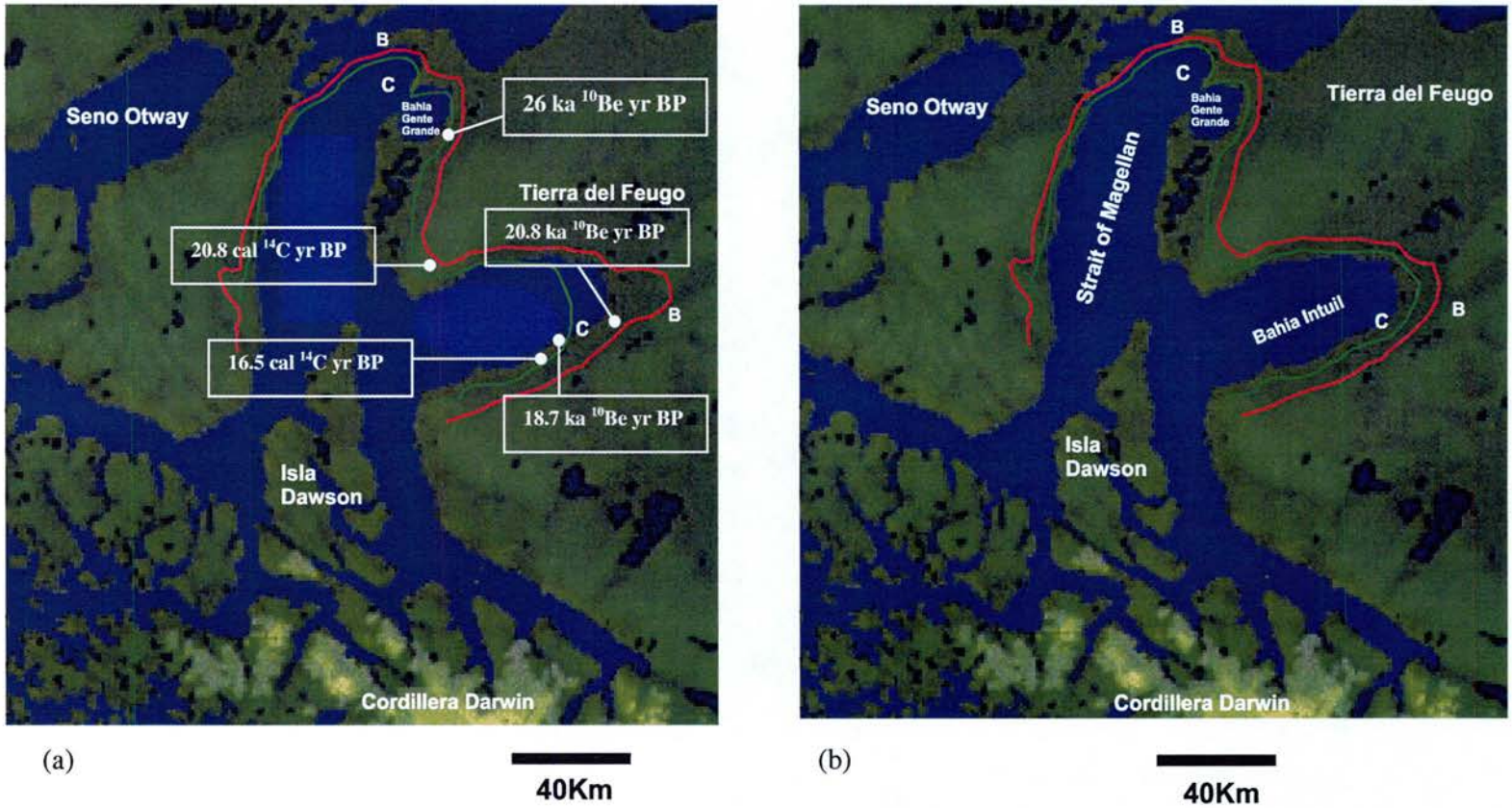

Figure 3.7. Comparison of the spatial and temporal relationships of glacial advances in this region based on (a) the work of Clapperton et al. (1995), with the available radiocarbon and new cosmogenic exposure data and (b) the suggested revision of these limits in light of this new data from this study.

discussed in Section 3.5, providing a visual comparison between these data, allowing discussion of it regional and global significance. It is noted that the exposure ages are quoted with zero erosion. This is possibly open to question. However the surfaces sampled do indicate minimal erosion, therefore, it is suggested an erosion rate of between 0 to 3 mm/ka should provide a realistic age envelope for these samples. Thus providing the following error weighted mean ages for the landforms if erosion is assumed to be between 0 to 3mm/ka respectively. The large thrust moraine in Bahia Gente Grande was emplaced between 26,011 and 27,201 ^{10}Be yr BP. The rockfall erratics at the far eastern end of Bahia Inútil were emplaced between 20,851 and 22,132 ^{10}Be yr BP. The second concentration of rockfall erratics in Bahia Inútil were emplaced between 18,734 and 19,819 ^{10}Be yr BP.

3.8 Discussion of results

By constraining the temporal and spatial pattern of deglaciation of this area it is possible comment on previous interpretations. To simplify this process this discussion will focus on the mean exposure ages of the landforms assuming zero erosion. As described above, these data fix deglaciation from these landforms, with the mean landform ages being internally consistent with the available minimum radiocarbon constraints (Figure 3.8). These data indicate that the large thrust moraine formed on the edge of Bahia Gente Grande was formed 26,011±1,380 ^{10}Be yr BP. This is much earlier than the two groups of rockfall erratics located on the southern shores of Bahia Inútil which were emplaced at 20,851±1,340 and 18,734±1,315 ^{10}Be yr BP respectively.

Figure 3.7a demonstrates the position of these landforms in time and space compared to the ascribed limits of Clapperton *et al.* (1995). If the interpretation of Clapperton *et al.* (1995) is accepted then it indicates that the exposure dates from the rockfall deposit located inside the limits of glacial stage B are too young for this scenario with a mean landform age of 20,851±1,340yrs. This is compared to the dates of boulders located on the moraine of stage C in the area of Bahia Gente Grande, which provide a mean landform exposure age of 26,011±1380yrs. (Figure 3.8). This difference is hard to reconcile with the interpretation of Clapperton *et al.* (1995) unless we invoke significant cover or erosion of the surfaces of the erratics of the rockfall deposit. Mechanisms could include the slow stagnation of ice at this

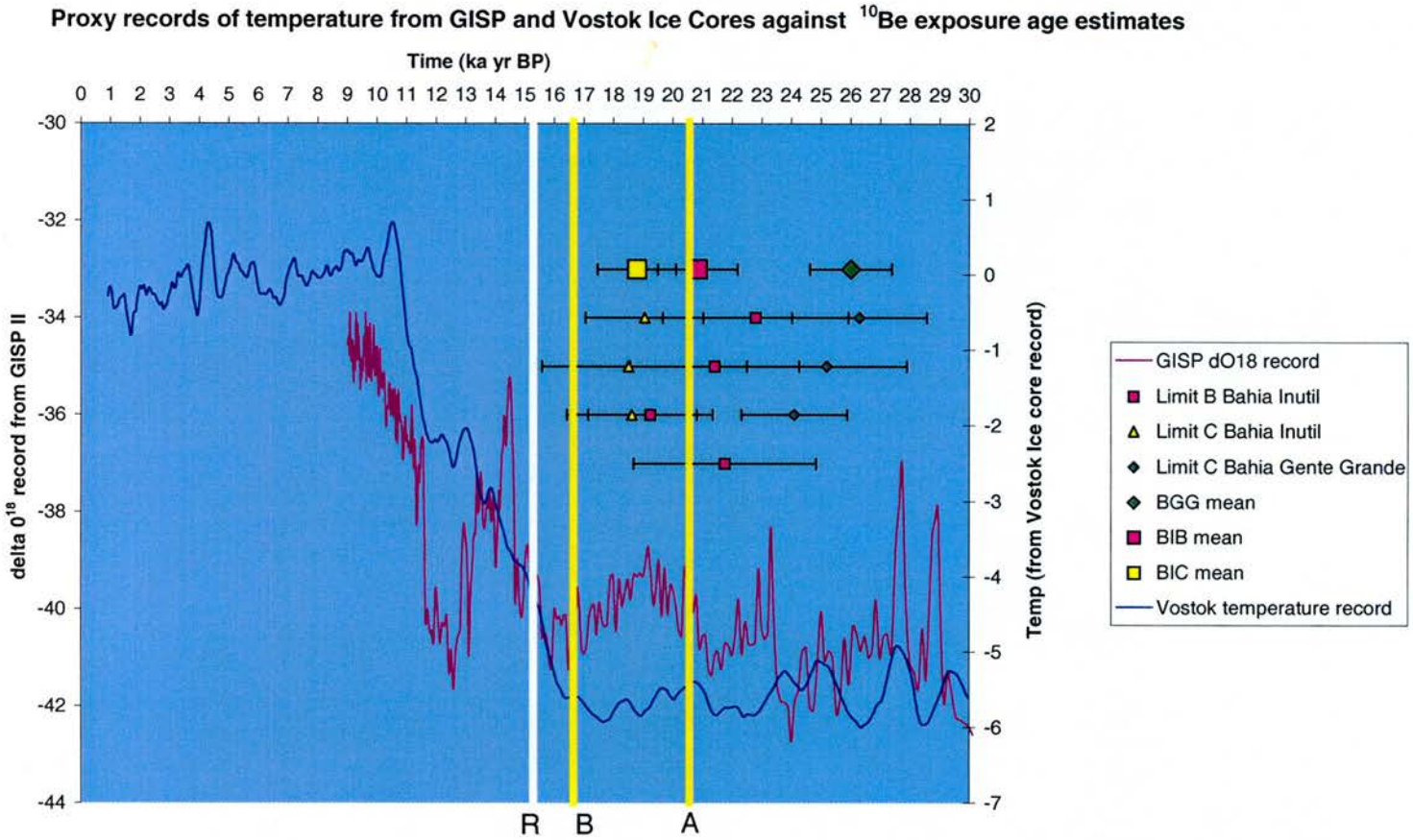

Figure 3.8. Exposure ages of boulders from the Magellan Region of Patagonia, seen against records of proxy atmospheric temperature from Greenland (GISP II, delta ^{18}O) and VOSTOK, Antarctica (proxy atmospheric temperature record). The calibrated age of the Reclus tephra (R) is also marked to demonstrate the time of eruption of this constraining tephra (15,382 cal yr BP)(McCulloch and Davies, 2001). A and B represent best available radiocarbon dated constraints on these limits, with A at 20,834 cal yr BP and B at 16,591 cal yr BP (McCulloch pers com). The exposure ages reflect minimums. Erosion and surface coverage have not been accounted for. Table 2 demonstrates the effects of erosion on these exposure ages.

limit, or significant sediment cover on top of these boulders, reducing the incoming signal of the cosmogenic energy. However, the field relationships do not back up either of these hypotheses. The size and surface morphology of these rockfall erratics also preclude nuclide loss due to either fire damage or significant weathering effects.

With the problems described with the previous interpretation, these data suggest a revision of the limits of Clapperton *et al.* (1995). This is outlined in Figure 3.7b. It suggests that the exposure age estimates related to the rockfall deposits represent two periods of relative stabilisation of the ice during deglaciation from a previously expanded state which formed the large thrust moraine, located to the east of Bahia Gente Grande. The absence of any significant moraines at the eastern end of Bahia Inútil, may reflect either a lack of material suitable for building the large moraines recorded in the central portion of the Strait of Magellan, or alternatively that the limit C may be recorded much further east in Bahia Inútil.

The implications of this revised interpretation are that the large thrust moraine described to the east of Bahia Gente Grande records the maximum limits of ice expansion at the LGM at around 26 ka yr BP within the Magellan Region. The rockfall erratics dated within Bahia Inútil record stillstands or advances of the ice margin receding from limit C at around 20.8 ka yr BP and 18.7 ka yr BP, marked by small reticulate moraines and meltwater channels.

3.9 Wider implications

Two important results can be drawn from the interpretations of the data presented here. Figure 3.7a and b demonstrate how the spatial and temporal relationships allow us to reassign the limits of advance C in Bahia Inútil from those described by Clapperton *et al.*(1995). This interpretation requires further testing by the detailed geomorphological mapping and analysis of the outer moraines systems described by Raedeke (1978). However given the exceptionally low mean altitude of the land area east of the end of Bahia Inútil, it does not seem impossible for the limits of advance B and C to be as close as they are in the central region of the Magellan Strait.

The second result relates to the emplacement of the moraine complex related to advance C in Bahia Gente Grande at 26,011±1,380yr Bp. This broadly agrees with the conclusions of Clapperton *et al.* (1995), suggesting that the greatest glacial expansion in the Magellan Region occurred relatively early in the last glacial cycle. Allowing a surface erosion rate of 3mm per 1000 years increases the mean exposure age by around 2000 years (Table 2). This limit is located just inside that of advance B, and is close in age based on morphological characteristics (Benn and Clapperton, 1999a). This implies that the maximum expansion of glacial ice in the Magellan Region occurred before 20,000 yr BP, reiterating the conclusions of Clappeton *et al.* (1995) that mountain glaciers were most extensive before the coldest period of the LGM. Perhaps this reflects the ability of the atmosphere to hold more moisture during warmer intervals, before maximum cooling was achieved. This effect could have been magnified by a northward shift in the precipitation bearing westerlies at this time, thus starving the accumulation area of this southern most sector of the Patagonian Ice Sheet, thus inducing rapid decay (Heusser, 1989; Hulton *et al.* 1994).

It is noted that the structure and timing of these events demonstrate that the LGM in the Magellan Region is characterised by multiple glacial stages between 26 to 18 ka yr BP, with the maximum ice extent being achieved prior to 26 ka yr BP. These results add further weight to recent work indicating that the timing of the most extensive glaciation was coeval throughout Patagonia (Denton *et al.*, 1999; Kaplan *et al.* In press). Strengthening hypotheses suggesting synchrony between glaciation in the mid-latitude southern hemisphere and maximum temperature depression in the northern hemisphere (Denton *et al.*, 1999). However, much more precise chronological control is required to quantify the degree of synchrony.

3.10 Conclusions

Through the inter-calibration between the TCN and available radiocarbon chronologies two principle conclusions made regarding the LGM in the Magellan Region.

- Maximum ice extent at the LGM was achieved before 26 ka yr BP, strengthening the conclusions from other sectors of Patagonia that maximum ice extent was synchronous between the mid-latitude southern hemisphere and the northern hemisphere.

• Recession from these limits was punctuated by several periods of stabilisation or advance two of which have been identified at 20.8 and 18.7 ka yr BP. These may well correspond with multiple glacial advances recorded further north in the Lakes Region of Chile.

3.11 References

Auer, V. 1956. The Pleistocene of Fuego-Patagonia Part 1: The ice and interglacial ages. Annales Academiae Scientarium Fennicae. Ser 3. 45.

Benn DI, Clapperton CM. 1999 a. Pleistocene glacitectonic landforms and sediments around central Magellan Strait, southernmost Chile: evidence for fast outlet glaciers with cold-based margins. Quaternary Science Reviews. 19. 6. 591-612.

Boulton GS. 1978. Boulder shapes and grain-size distributions of debris as indicators of transport paths through a glacier and till genesis. Sedimentology. 25. 773-799.

Broecker WS. and Denton GH. 1990. The role of ocean-atmosphere reorganisations in glacial cycles. Quaternary Science Reviews 9: 305-343

Bruggen J. 1950. Geologia. 2nd edition. Editorial Nascimento, Santiago, Chile.

Caldenius C. 1932. Las glaciations cuaternarias en la Patagonia y Tierra del Fuego. Geografiska Annaler 14. 1-64.

Cerling TE, Craig H. 1994. Geomophology and in situ cosmogenic isotopes. Annual Review of Earth and Planetary Sciences 22. 273-317.

Clapperton CM. 1989. Asymmetrical drumlins in Patagonia, Chile. Sedimentary Geology, 62. 387-398.

Clapperton CM, Sugden DE, Kauffman D, McCulloch RD. 1995. The last glaciation in central Magellan Strait, southernmost Chile. Quaternary Research 44: 133-148.

Cockburn HAP. (1998) Landscape evolution in Namibia and Antarctica: Quantifying denudation rates using in-situ cosmogenic isotope analysis. Unpublished PhD thesis, The University of Edinburgh, 246pp.

De Geer G. 1927. Late glacial clay varves in Argentina, measured by Dr. Carl Caldenius, dated and connected with the solar curve through the Swedish time scale. Geografiska Annaler. 9.

De Geer G. 1929. Gotiglacial clay varves in southern Chile, measured by Dr. Carl Caldenius, identified with synchronous varves in Sweden, Finland and the USA. Geografiska Annaler. 11.

Denton GH, Heusser CJ, Lowell TV, Moreno PI, Anderson BG, Heusser LE, Schlüchter C, Marchant DR. 1999. Interhemispheric linkage of palaeoclimate during the last glaciation. Geografiska. Annaler 81A(2): 107-153.

Dunne J, Elmore D, Muzikar P. 1999. Scaling factors for the rates of production of cosmogenic nuclides for geometric shielding and attenuation at depth on sloped surfaces. Geomorphology. 27. 3-11.

Feruglio E. 1949-50. Description geologica de la Patagonia. Buenos Aires. Direccion General Yacimentos Petroloiferos Fiscals.Vols 1,2,3.

Gosse JC, and Phillips FM. 2001. Terrestrial in situ cosmogenic nuclides: theory and application. Quaternary Science Reviews 20: 1475-1560.

Heisinger B. 1997. In situ production of radionuclides at great depths. Nuclear Instruments and Methods. B. 123. 341-346.

Heusser CJ. 1989. Climate and chronology of Antarctica and adjacent South America over the past 30,000 yr. Palaeogeogr. Palaeoclimatol, Palaeoecol. 118, 1-24.

Hollin JT and Shilling DH. 1981. Late Wisconsin-Weichselian mountain glaciers and small ice caps. In: The Last Great Ice Sheets. Eds. Denton GH, and Hughs TJ. Pp179-220. Wiley, New York.

Hofmann HJ. Beer J, Bonani G. von Gunten HR. Raman S, Suter S, Walker RL, Wölfli W, Zimmermann D. 1987. Half-life and AMS standards: Nuclear Instruments and Methods. B29. 32-36.

Hubbard AL. 1997. Modelling climate, topography and palaeoglacier fluctuations in the Chilean Andes. Earth Surf. Processes and Landforms. 22. 79-92.

Hulton N, Sugden DE, Payne A and Clapperton CM. 1994. Glacier modelling and the climate of Patagonia during the Last Glacial Maximum. Quaternary Research 31. 423-425.

Ivy –Ochs S. 1996. The dating of rock surfaces using the in situ produced ^{10}Be, ^{26}Al, and ^{36}Cl, with examples from Antarctica and the Swiss Alps. Ph. D. Thesis, Swiss Federal Institute of Technonology, Zurich. 196pp.

Kohl CP and Nishizumi K. 1992. Chemical isolation of quartz for measurement of *in situ* produced cosmogenic nuclides. Geochemica et Cosmochemica Acta. 56. 3583-3587.

Kubik PW, Ivy-Ochs S, Masarik J, Frank M, Schlüchter C. 1998. ^{10}Be and ^{26}Al production rates deduced from an instantaneous event within the dendro-calibration curve, the landslide of Köfels Ötz Valley, Austria, Earth and Planetary Science Letters 161. (1-4). 231-241.

Lal D. 1991. Cosmic ray labelling of erosion surfaces: in situ nuclide production rates and erosion rates. Earth and Planetary Science Letters 104, 424-439.

Lowell TV, Heusser CJ, Anderson BG, Moreno PI, Hauser A, Heusser LE, Schlüchter C, Marchant DR, Denton GH. 1995. Interhemispheric correlation of Late Pleistocene glacial events. Science 269, 1541-1549.

Marden CJ. 1993. Late Quaternary glacial history of the South Patagonian Icefield, at Torres Del Paine, Chile. Ph. D Thesis, University of Aberdeen. 298pp

Masarik J, Reedy RC. 1995. Terrestrial cosmogenic-nuclide production systematics calculated from numerical simulations. Earth and Planetary Science Letters. 136. 381-395.

Mercer JH. 1976. Glacial history of southernmost South America. Quaternary Research. 6. 125-166.

McCulloch RD, Bentley MJ, Purves RS, Hulton NRJ, Sugden DE, Clapperton CM. 2000. Climatic inferences from glacial and palaeoecological evidence at the last glacial termination, southern South America. Journal of Quaternary Science 15. 409-417.

McCulloch RD, Sugden DE. 2001. Climatic inferences from glacial and palaeoecological evidence at the last glacial termination, southern South America: a reply Journal of Quaternary Science. 16 (3) 291-294.

McCulloch RD, Davies SJ. 2001. Late-glacial and Holocene palaeoenvironmental change in the central Strait of Magellan, southern Patagonia. Palaeogeography, Palaeoclimatology, Palaeoecology. 173. 143-173.

Nishiizumi K, Finkle RC, Klein J, Kohl CP. 1996. Cosmogenic production of ^{7}Be and ^{10}Be in water targets. Journal of Geophysical Research 101. 22,225-22,232.

Porter SC. 1989. Character and ages of Pleistocene drifts in a transect across the Strait of Magellan. Quaternary of South America and Antarctic Peninsula. 7. 35-49.

Porter SC, Clapperton CM, Sugden DE. 1992. Chronology and dynamics of deglaciation along and near the Strait of Magellan. Southernmost South America. Sveriges Geologiska Undersokning. Ser. Ca 81. 233-239.

Raedake L. 1978. Formas del terreno y depositos cuaternarias. Tierra del Feugo central, Chile. Revista Geologica de Chile. 5.3-31.

Romero H. 1985. Geografica de Chile: geografia de los climas. Instituto Geografico Militar: Santiago.

Schaller M, von Blanckenburg F, Hovius N, Kubik PW. 2001. Large-scale erosion rates from in situ produced cosmogenic nuclides in European river sediments. Earth and Planetary Science Letters 188. 441-458.

Stone JO. 2000. Air pressure and cosmogenic isotope production. Journal of Geophysical Research. 105. B10. 23,753-23,759.

Uribe PC. 1982. Deglaciation en el sector central del estrcho de Magallanes: consideraciones geomorfologicas y chronologicas. Annals del Instituto de la Patagonia. 13. 103-111.

Wenzens G. 1999. Fluctuations of outlet glaciers in the southern Andes (Argentina) during the past 13,000years. Quaternary Research. 51. 238-247.

Wenzens G. 2001. Climatic inferences from glacial and palaeoecological evidence at the last glacial termination, southern South America: comment. Journal of Quaternary Science. 16 (3) 291-294.

CHAPTER 4

The Last Glacial Interglacial Transition in Patagonia, southern most Chile: Torres del Paine: Application of surface exposure dating.

4.1 Abstract

We use cosmogenic ^{10}Be surface exposure analysis of boulders on moraines to date the decay of the Patagonian Ice Sheet from its Last Glacial Maximum limits in the area of Torres del Paine. A short-lived re-advance occurred at 15,832±767 ^{10}Be yr BP, at a distance of over 50km from the modern ice margin. These data represent the first direct dating of a late glacial advance at this time in this central region of southern Patagonia. This finding is backed up by other proxy records in this region, suggesting that this event was followed by rapid deglaciation to within 15km of modern ice margin.

These results strengthen the hypothesis that a synchronous retreat stage occurred over 16° of latitude during the Late Glacial, as suggested from sites to the North and South of this region. The advance represents the ice extent at the end of the Last Glacial Maximum prior to the abrupt onset of deglaciation. This temporal and spatial fix provides further direct evidence that in this region any ice expansion after this time was minimal, restricted to within 16 km of the present day ice margin.

4.2 Introduction

Attempts to model the forcing mechanisms of global climate change, during the Last Glacial / Interglacial Transition (LGIT) are reliant on a sound knowledge of the spatial and temporal patterns of environmental change. Recent studies have highlighted that there is uncertainty regarding the interhemispheric timing of climate change during this period, with different lines of evidence pointing to patterns of interhemispheric synchrony and asynchrony between the northern and southern hemisphere. The principle hypotheses fall into three broad groups: (1) the pattern and timing of change was globally sychronous; (2) climate change in the northern hemisphere began earlier than the southern hemisphere; (3) the southern hemisphere led the northern hemisphere (McCulloch *et al.*, 2000).

The first hypothesis points to the synchrony of glacier fluctuations and associated palaeoecological changes between the terrestrial Northern and mid-latitude Southern Hemispheres. This data suggests symmetry of the structure and timing of the LGIT between sites as geographically diverse as the Chilean Lake District, New Zealand, Ecuador and the North Atlantic (Clapperton *et al.*, 1997, Lowell *et al.*, 1995, Denton *et al.*, 1999, White *et al.*, 1994). This hypothesis has been backed by recent data from the analysis of the Taylor Dome Ice Core from the coastal regions of Antarctica, the analysis of which indicates synchrony between this site and the rapid fluctuations recorded in the North Atlantic (Steig *et al.*, 1998). However, the evidence is not yet sufficiently constrained temporally and spatially to allow firm correlation with the high-resolution records of North America and north-west Europe. Therefore this work aims to constrain the nature and timing of global environmental change during the LGIT in a region which is currently poorly understood. Improved chronological data should make it possible to distinguish between local and global patterns of environmental change, thus improving our understanding of how the ocean-atmosphere system of the two hemispheres interact (McCulloch and Davies, 2001).

The southernmost Andes provides one of the only topographic barriers to the circulation of the southern westerlies at this latitude, therefore producing an energetic climate regime. It has been suggested that glacial dynamics in this region are controlled by the location, moisture content and intensity of the southern hemisphere westerlies, which are themselves controlled by global

pressure gradients (Hulton *et al.*, 1994, 2000; Hubbard, 1997; Denton *et al.*, 1999). During glacial phases the core of the westerlies and the related increase in moisture and temperature depression migrated northwards to latitudes of 45-50°S due to expansion of the polar cell. The evidence for this comes from well constrained glacial chronologies and modelling studies from more northern areas of the Chilean Lake District (Denton *et al.*, 1999). Under modern climate conditions, this latter area is only affected by small local glaciers, but has evidence of substantial glaciation during the LGIT (Hubbard, 1997; Denton *et al.*, 1999). Therefore, this study investigates the nature and chronology of deglaciation of part of the Patagonian Ice Sheet, which terminated in the region of Torres Del Paine during the LGIT (Figure 4.1). This reflects changes in the climate systems of the southern hemisphere (Clapperton *et al.*, 1995), and provides insights into the local precipitation and temperature conditions during deglaciation.

4.3 Evidence of past glaciation in central Patagonia

Previous workers have identified a rich record of glacial landforms and sediments related to the Pleistocene expansion of the central portion of the Patagonian Ice Sheet (Caldenius, 1932; Ferugilio, 1950, Mercer, 1976 and Marden, 1993). Caldenius (1932) plotted the position of most major moraine systems throughout Patagonia and Tierra del Fuego. By teleconnecting glacial lake varves found in Patagonia to the Swedish varve chronology of De Geer (1927, 1929) he attempted to construct a chronology for these advances. Using this system, Caldenius ascribed the largest outer most moraine limits to the late-glacial stadial events, the Finiglacial, Gotiglacial and the Daniglacial. In this seminal publication Caldenius was able to trace these limits throughout Patagonia.

Subsequent work has demonstrated that although the limits are broadly correct, the chronology is unresolved between regions and individual lobes of the once expanded Patagonian Ice Sheet. This is particularly true in the central latitudes of the Patagonian Icefield (45-50°S), where considerable disagreement exists over the extent of glaciation related to LGIT exists, because of the interpretation of minimum radiocarbon dated glacial sequences in this region (Marden 1993; McCulloch *et al.*, 2000; Wenzens, 2001; McCulloch *et al.* 2001). Chronologies based wholly on the analysis of organic material that has built up since deglaciation are at the mercy of both the

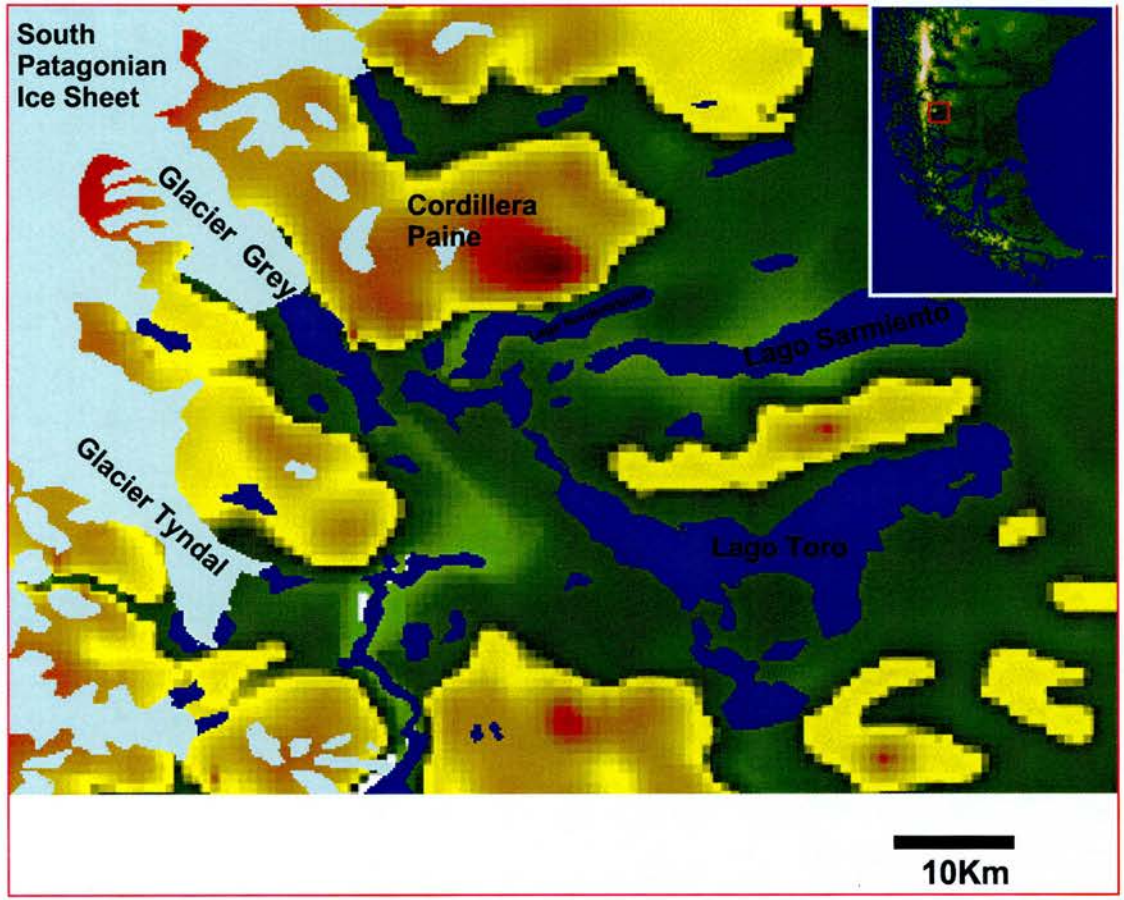

Figure 4.1. Location maps of the Magellan field area showing ice bodies, principle lakes and topography from the G-topo 30 data (The brighter yellows and reds indicate areas of higher relief, where as the green shades indicate low (<200m) relief, the yellow areas represent topography between 200-1000m, and the red areas represent topography greater than 1000m. It most be noted than the resolution of this data is ±30m. The location of the Torres del Paine area can be seen on the inset diagram of the whole of Patagonia

rate at which it is possible to form organic material, and the likelihood of preservation of this material *in situ*. Both these factors are called into question in the extremely arid conditions prevailing to the east of the Patagonian Ice Sheet. The resultant spatial and temporal pattern of deglaciation is further complicated in this region due to possible non-symmetrical expansion and contraction of portions of the icesheet at different latitudes through time. Reflecting the different controlling mechanisms on glacial expansion over such a large latitudinal range, making correlation between different regions complex (McCulloch *et al.*, 2000).

Consequently, this study aims to define the timing of the glacial fluctuations in Torres del Paine, through the application of terrestrial *in situ* cosmogenic nuclide analysis (TCN), using the radionuclide ^{10}Be. These temporal fixes may be used as direct evidence to answer recent open debates regarding the extent of ice in this region during the late glacial. Hypotheses based solely on the interpretation of minimum radiocarbon dated sequences have suggested that moraines relating to a Younger Dryas (Finiglacial) correlative advance are over 50 km from the present ice margin in Torres del Paine (Caldenius, 1932; Wenzens, 1999; Wenzens, 2001). This directly contradicts with other workers who suggest that any late glacial Younger Dryas correlative advance is restricted to within 15 km of the modern ice margin at this latitude (Marden, 1993; McCulloch *et al.*, 2000; McCulloch *et al.*, 2001). This hypothesis is based predominatly on the stratigraphic relationship between silisic tephra, the Reclús, and moraines and related outwash deposits. The Reclús tephra has been well dated by independent radiocabon analysis in areas to the south of this region, providing a mean age of 12,700^{14}C yr BP (15,382 cal. Yr BP). The presence of this tephra in sediments which have been actively bulldozed by advancing glacial ice at the southern end of Lago Grey, was used as direct evidence to uphold this latter hypothesis (Marden, 1994).

4.4 Physical setting

The area of Torres del Paine is in the Ultima Esperanza district of Chilean Patagonia (51° S, 73° W), and lies to the south east of the margin of the modern South Patagonian Icefield (Figure 4.1). Today the area has been classified as a world biosphere reserve by UNESCO, for its natural beauty and diverse wildlife. The geology of the area is dominated by the Late Miocene

intrusion of the pluton of the Cerro Toro formation into local Jurassic and Cretaceous clastic country rocks formed as part of a back arc basin prior to the orogenic events related to Andean uplift (Michael, 1983). More recent uplift and erosion has exposed this granitic pluton in Cordillera Paine where differential denudation has created a number of impressive peaks with steep granite walls, often capped with the contrasting local country rock (Figure 4.2).

The modern glaciation of the area can be divided into two distinct types, related to the Southern Patagonian Icefield and high alpine glaciers of the Cordillera Paine (Marden 1993). The South Patagonian Icefield has a surface area of 13,500 km^2 which, when added to that of the North Patagonian Icefield, constitutes the largest ice body outside polar latitudes. The icefield is a transection complex in which local ice domes and plateaux coalesce and fill intermontane trenches to feed outlet glaciers, the largest of which, the Uppsala, is 60km long (Martinic, 1982). The mean elevation of the icefield is 1500-2000m, but many of the west flowing glaciers terminate at sea level in the west, where they calve into deep fjords (Naruse *et al.* 1987). In the east many of the outlet glaciers terminate into lakes, such as Lago Grey and Lago Dickson located within the Parque National Torres del Paine. Detailed glaciological data related to these outlet glaciers is sparse (Lliboutry. 1956, Naruse *et al.* 1987).

Within the Cordillera Paine the development of alpine glaciers is restricted by the near vertical nature of the potential accumulation areas (Marden 1993). The massif consists of precipitous rock towers and spires resulting from Late Miocene magmatic activity. Cerro Paine Grande (3246m) and Monte Almirrante Nieto (2668m) are complex peaks with a variety of steep faces, glaciers and ridges, whilst other peaks present precipitous rockwalls. Although there is frequent snow, there are few sites where ice can build up to nourish glaciers in the available accumulation areas. This, together with long term overdeepening of the troughs, means that even their headward reaches are marginal for present day glaciation.

Surrounding the massif the landscape is dominated by undulating and dissected basement, where long term glacial erosion has resulted in deep troughs and undulating basin areas, and remnant upland plateaux at an altitude of 200-600m (Marden 1993). Many of the troughs are presently occupied by lakes, or are infilled with glaciolacustrine and fluvioglacial sediments. Local differential erosion has resulted in a rugged landscape characterised by small troughs and basins, and whale-back and roche-moutonée landforms, some of which can exceed 200m in height.

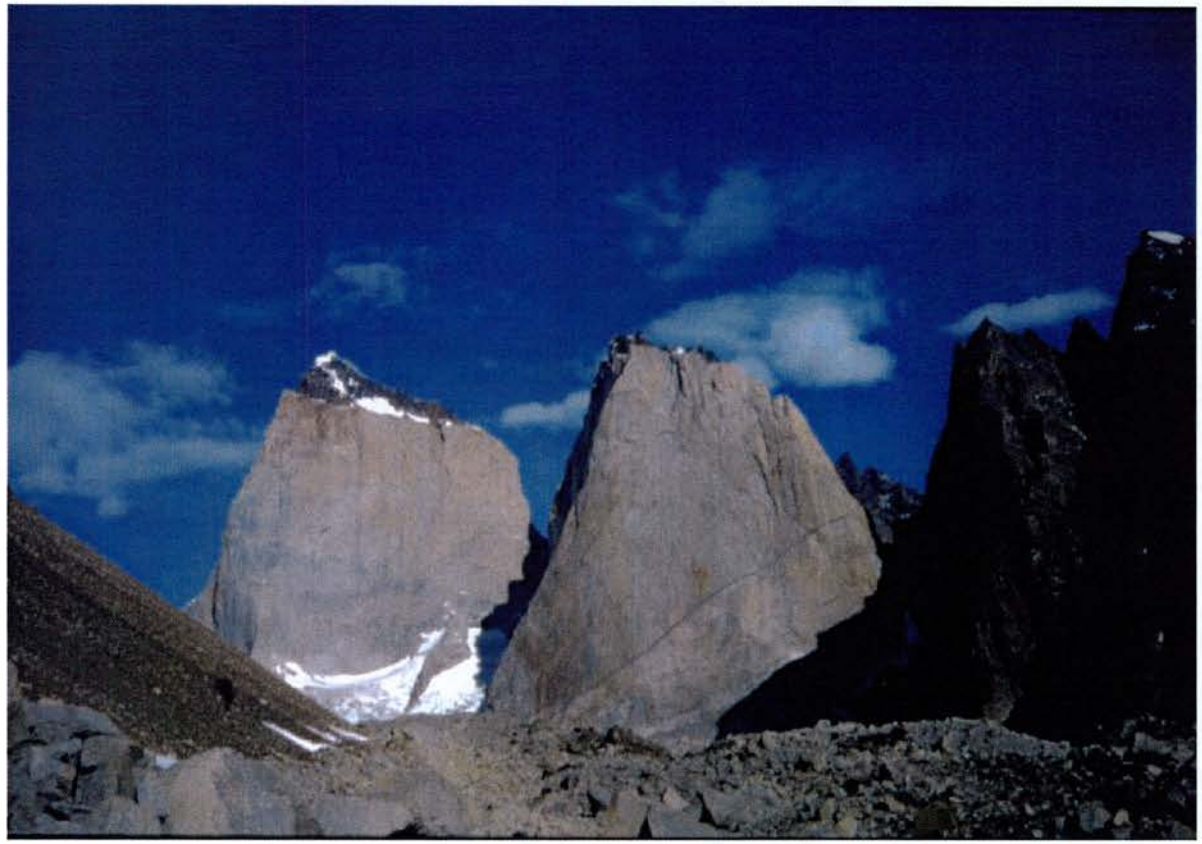

Figure 4.2. View up the Valle del Silecio, of Co. Fortaleza (2681m) and Co. Escudo (2240m), demonstrating the steep granite walls which typify the Paine Massif, and the Black shale roof pendant of the local country rock.

4.5 The climate

Torres del Paine lies under the influence of westerly atmospheric circulation. With the latitudinal extent and intensity of the southern westerlies being controlled by Antarctic sea ice, the position of the circum-Antarctic oceanic convergence, and the strength of the tropical anticyclonic cells over the Pacific and Atlantic Oceans (Clapperton *et al.*, 1995). Today the core of the westerlies and the related precipitation maximum lies south of 50° during the austral summer, migrating north in winter to nourish the glaciers and ice sheets of the western Andean sea board of Patagonia (McCulloch *et al.*, 2000). This relationship can be seen in Figure 4.3, which shows the resultant precipitation maximum between 49-50° and its seasonal migration north in the Austral Winter (inset).

This configuration brings year round precipitation to areas south of 38^0S, as the convergence of the south Pacific sub-tropical high and the polar front produces low pressure areas and storms throughout the year (McCulloch and Davies, 2001). The southernmost Patagonian Andes presents an abrupt and continuous barrier to the passage of westerly air masses, causing the moist maritime air to rise and cool and initiate the intense precipitation experienced on the western seaboard of Patagonia. Allied to this orographic effect, the Andes create a marked leeside precipitation shadow to the east of the icefield. Available climatic data for Torres del Paine indicates increasing continentality from west to east; thus the average annual precipitation at Rio Grey is 798mm, in comparison with 254.9mm at Cerro Guido, which is located only 60km to the east (Pisano, 1974).

4.6 Approach and Methodology

The absolute and relative chronology established by Marden (1993) was used as a framework for selecting glacial landforms and features from which to sample for cosmogenic radionuclide exposure dating. Marden (1993), identified 8 major moraine or drift stages, which he related to glacial advances from the Neo-glacial to the Last Glacial Maximum (see Table 4.1) on the basis

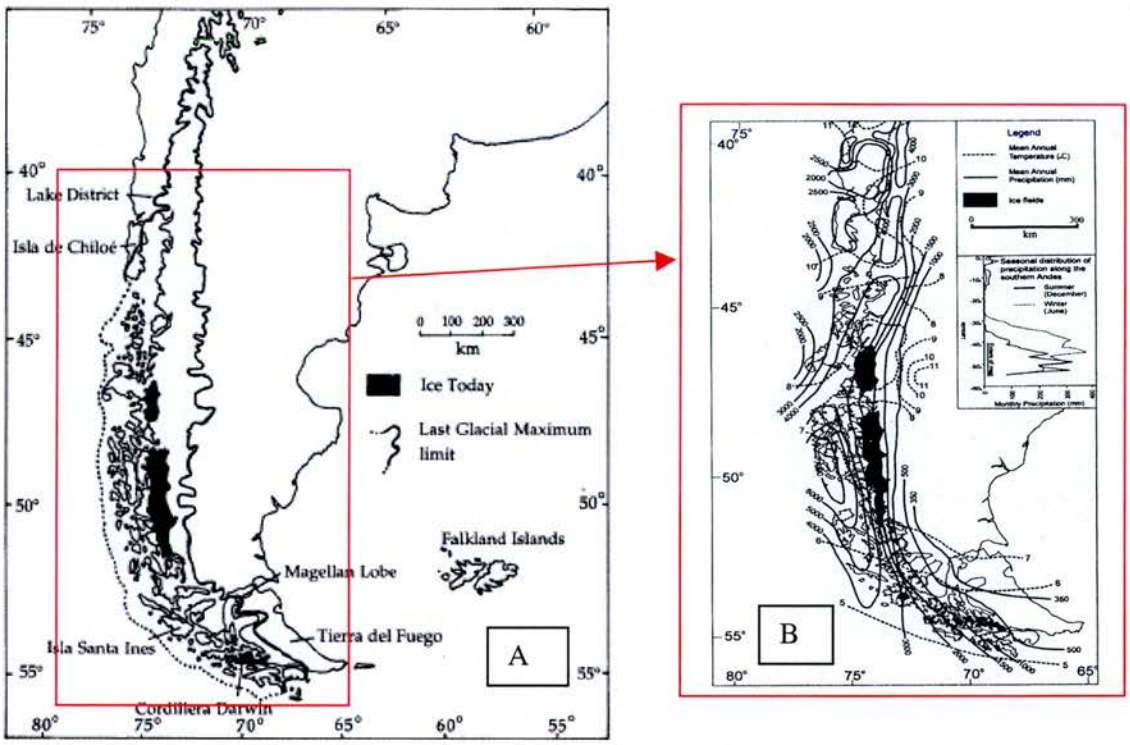

Figure 4.3. A. Southern South America, showing the extent of glacier ice at the present day and during the last glacial maximum (After Porter *et al.*, 1992 and Hulton *et al.*, 1994). B. Distribution of present glaciers and the main climatic features, from Romero (1985). The seasonal migration of the westerlies is also shown (inset), (After McCulloch *et al.*, 2000).

Glacial Stage	Geomophological charactristics description	Type of glaciation	Age model / chronolgy (Marden 1993)
1	The youngest moraine system outside modern limits, accute sharp crested moraines, notably fresher, in terms of its morphological preservation and degree of post depositional cover.	Limited glacial advance located 0.5-5km from modern limits	On the basis of both relative and absolute dating that these moraines were deposited between 1650-1900 AD, possibly correlate with Neoglacial advance 3 (Mercer. 1970). Age model from both historical records and dendrochronological studies
2	Occouring just outside stage 1 moraines, but which are however noticably less fresh, with subdued morphology and crests.	Located within tens of metres of those related to stage 1 limits, therefore limited valley glaciation	No absolute dates, however, speculative corelation with Neo-glacial advance 1 and 2 (Mercer 1970), therefore 4500-4000yrs BP and/or 2700-2000yrs BP.
3	Located 10-16km beyond modern ice sheet limits very close to limits of glacial stage 4, however can be differentiated both spatially and morphologically	Extensive valley glaciation.	Minimum radiocarbon dates of 4495 ^{14}C yrs Bp, from basal dates in peat bogs indicating time of organic development after ice retreat. However, other dat (Rosqvist un pub.) indicate that minimum could be 8360±100^{14}C years BP, therefore very close to stage 4 dates
4	Located 10-16km beyond modern ice sheet limits just outside stage 3 moraines. Ridge crest and related features of deglaciation suggest that this stage is not directly correlatable with stage 3.	Extensive valley glaciation.	Minimum basal dates of 9140^{14}C yrs BP, from kettle holes close to ice contact face. However, internal inconsistencies with radiocarbon dates from this stage suggest that these are not close limiting ages due to bog development and buried ice melt out from kettle holes. Stratigraphic relationship with the Recluse Tephra (12,050± yrs BP), provide an limiting age for this advance
5	Located 40-50km beyond modern ice limits, extensive evidence of lateral trimlines on valley sides, and lateral / terminal landforms at limit	Ice sheet stage	Stratigraphic relationship with Recluse Tephra suggest minimum age of >12,050±^{14}C yr BP, however minimum radiocarbon dates from peat bog cores indicate 10,560^{14}C yr BP. This indicates a significant time lapse between ice retreat and build up or preservation of organic material
6	Located beyond 50km from the modern ice margin, this limit can be identified from both erosive lateral trimlines high on the side f the Paine Massif and from terminal moraine ridges found at the end of the large lake systems of Lago Sarmiento and Toro	Ice sheet stage	There are no limiting radiocarbon dates for this advance. Marden (1993) speculated that this could be an advance related to the Last Glacial Maximum, where as Both Caldenius (1932) and Wenzen (1999) suggested that this advance was related to the Younger Dryas or a late glacial advance

7	Located immediately outside stage 6 moraines, and can be differentiated morphologically from this.	Ice sheet stage	There are no limiting radiocarbon dates for this advance. Marden (1993) speculated that this could be an advance related to the Last Glacial Maximum, where as Both Caldenius (1932) and Wenzens (1999) suggested that this advance was related to the Younger Dryas or a late glacial advance
8	Formed only outside stage 7 moraines at the end of Lago Sarmiento. Its morphology suggest there is a significant time lapse between this and the stage 7 moraines, they also differ in significantly in their components with the stage 8 moraine comprising mostly fine sands with well rounded clasts, suggesting a stage of basin clear out.	Ice sheet stage	There are no limiting radiocarbon dates for this advance. Marden (1993) speculated that this could be an advance related to the Last Glacial Maximum, where as Both Caldenius (1932) and Wenzens (1999) suggested that this advance was related to the Younger Dryas or a late glacial advance

Table 4.1. Major moraine or drift stages identified by Marden (1993). Describing the charctristics, the type of glaciation and any avaliable constraints on the chronology of glaciation in Torres del Paine. This outline was used as a guide in the field for sampling of boulders and erratics thought to be a product of the LGM and LGIT expansion of the South Patagonian Ice Sheet.

of both absolute and relative techniques. The available radiocarbon chronology was used as guide to identify suitable landforms to sample for this study, in order to constrain deglaciation over the LGIT. Sampling of the landforms and deposits related to glacial stages 5, 6 and 7 was undertaken in the austral summers of 1998 and 1999, with the aim of testing the proposed chronology of Marden (1993), and the recent controversy highlighted by the work of Wenzen (1999) and McCulloch *et al.* (2000). Reflecting problems with the interpretation of minimum radiocarbon dated sequences to date glacier retreat, leading some workers to infer significant glacial advance at a similar time to the Younger Dryas stadial, which directly contradict other interpretations of minimal late glacial expansion of the ice sheet in this central region (Marden and Clapperton, 1995; McCulloch and Bentley, 1998, Wezens, 1999). By attempting to date the actual emplacement of these limits through analysis of the TCN ^{10}Be build-up over time, it is hoped to shed further light on this debate.

4.7 Geomorphology

In an attempt to constrain the timing of the ice advance and retreat during the LGIT of the Sarrmiento Lobe of the Patagonian Ice Sheet, three type localities were chosen for sampling. These were identified and mapped by Marden (1993). The following section provides a description of their geomorphology and context of the landforms and the samples.

4.7.1 Glacial Stage 5: Type site Estancia Cerro Paine

The clearest evidence for this stage is located in the vicinity of Estancia Cerro Panie (Figure 4.4). A clear lateral moraine, conspicuous from afar because of the pattern of gullying in drift, descends obliquely across the southern flank of Monte Almirate Nieto towards the mouth of the Rio Ascensio. The moraine is an asymmetric ridge c. 5 m high with abundant boulders. East of the valley the ridge merges with a flat topped gently-sloping terrace (4° west to east), with a 30 m scarp face. The proximal part of the terrace is characterised by small moraine ridges, hummocks, boulders and kettle holes (Figure 4.5). The scarp face continues as an arc, 2 km east of the Estancia buildings. The terrace has been dissected by subsequent stream erosion in places. North of the Estancia building there is a lower secondary terrace. The distal parts of the

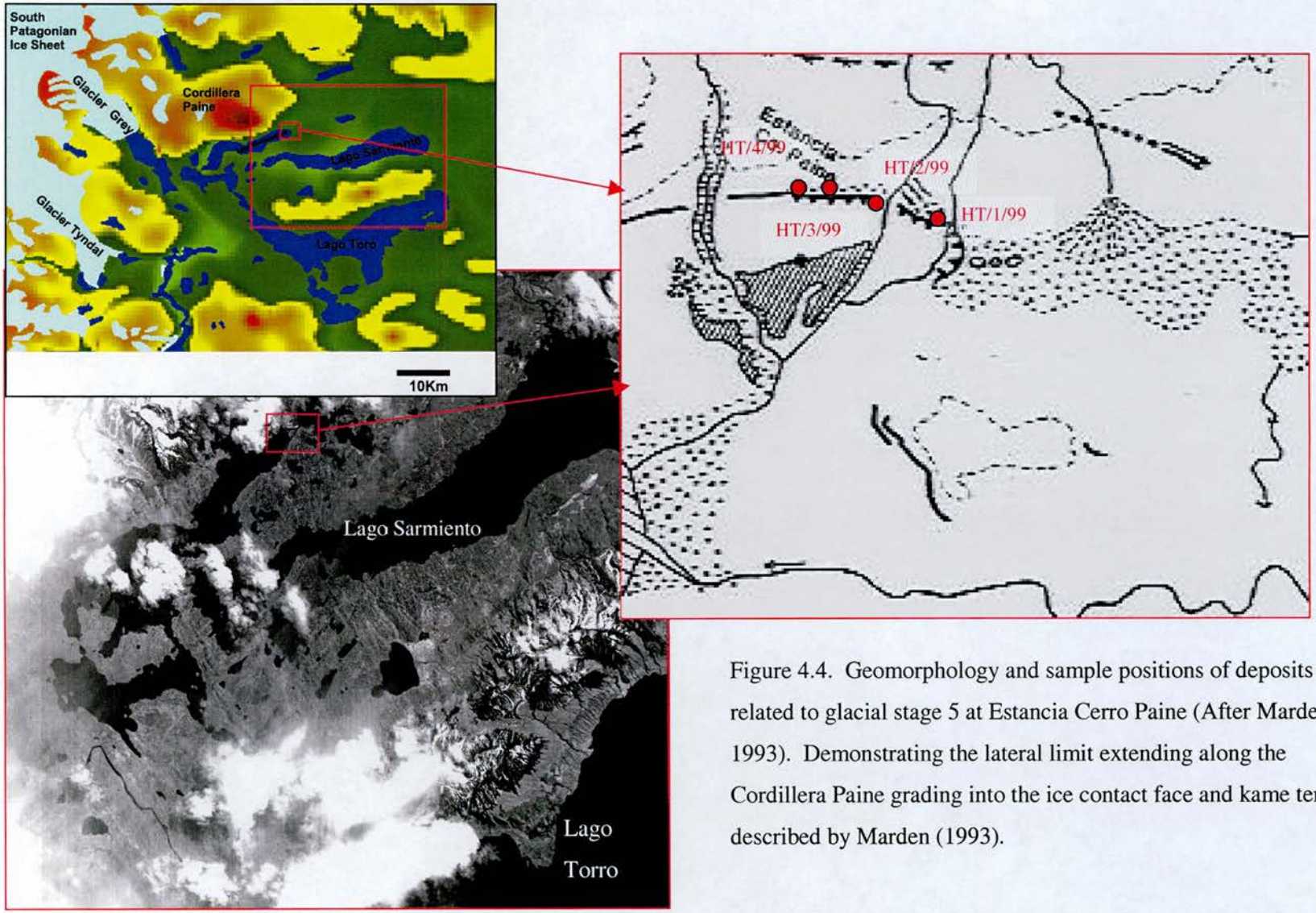

Figure 4.4. Geomorphology and sample positions of deposits related to glacial stage 5 at Estancia Cerro Paine (After Marden, 1993). Demonstrating the lateral limit extending along the Cordillera Paine grading into the ice contact face and kame terrace described by Marden (1993).

Figure 4.5. Typical samples from the lateral moraine and kame terrace at Estancia Paine. Photo A shows a typical large quartz monzonite boulder (4 by 3m) which was found on the upper surface of this landform, this photo is looking due west back to the Cordillera Paine, where the lateral moraine can be seen cutting diagonally down to this sample. Photo B shows a smaller ($1.5m^2$) quartz diorite boulder which is perched on a small thrust moraine at the edge of the kame terrace, a feature indicating a renewed period of advance prior to ice retreat from this landform.

landform comprise an extensive flat topped accumulation of sediments which leads into several gorges and channels cut through bedrock.

The landform assemblage indicates former ice marginal deposition. The sediments of the flat topped landforms are not exposed; however the planar morphology and association with meltwater channels suggests that they are water lain. The presence of kettle holes, hummocks and large boulders along the proximal parts indicates that the landforms are ice contact in origin. The sloping lateral deposit, characterised by a proximal ice contact face, is therefore interpreted as a kame terrace. The more extensive accumulation of sediments east of the road are interpreted as proglacial outwash deposits originating from a glacier terminating near the 30m scarp which marks its western margin. This body of sediment was therefore deposited as an outwash head, and this level was abandoned as the ice receded.

A total of four samples were obtained from the upper surface of the gently sloping kame terrace at this locality. Their positions can be seen on Figure 4.4, together with related field photographs in Figure 4.5. These samples are composed of quartz diorite and quartz monzonite, with signs of glacial plucking and striations indicating their glacial origin. The boulders have been deposited in close proximity and reflect a period of active formation of this landform and will therefore provide an age estimate of ice withdrawal from this limit.

4.7.2 Glacial Stage 6: Type site; eastern end of Largo Sarmiento

Moraines related to this advance are best preserved at the eastern end of Lago Sarmiento (Figure 4.6). On aerial photographs the innermost moraines are seen to be more continuous and better defined than the outer ridges related to earlier glaciation, but it is difficult to make such a distinction on the ground. On the north side of the lake there are three continuous ridges up to 10m high. These have a distinctive chevron or saw-tooth pattern. The individual chevrons, which may be irregular in form, display remarkable repetition between successive ridges. Moraines with saw-tooth plan form have been described beyond outlet glaciers of the Jostedlsbreen ice cap in Norway. Mattews *et al.* (1979) and Lien and Rye (1988) describe the formation of these moraines by push mechanisms at the margin of glaciers indented by heavy radial crevassing as a result of unconfinement. Since the pattern of successive Stage 6 moraines are remarkably similar, giving a nested appearance, it implies that the pattern of marginal

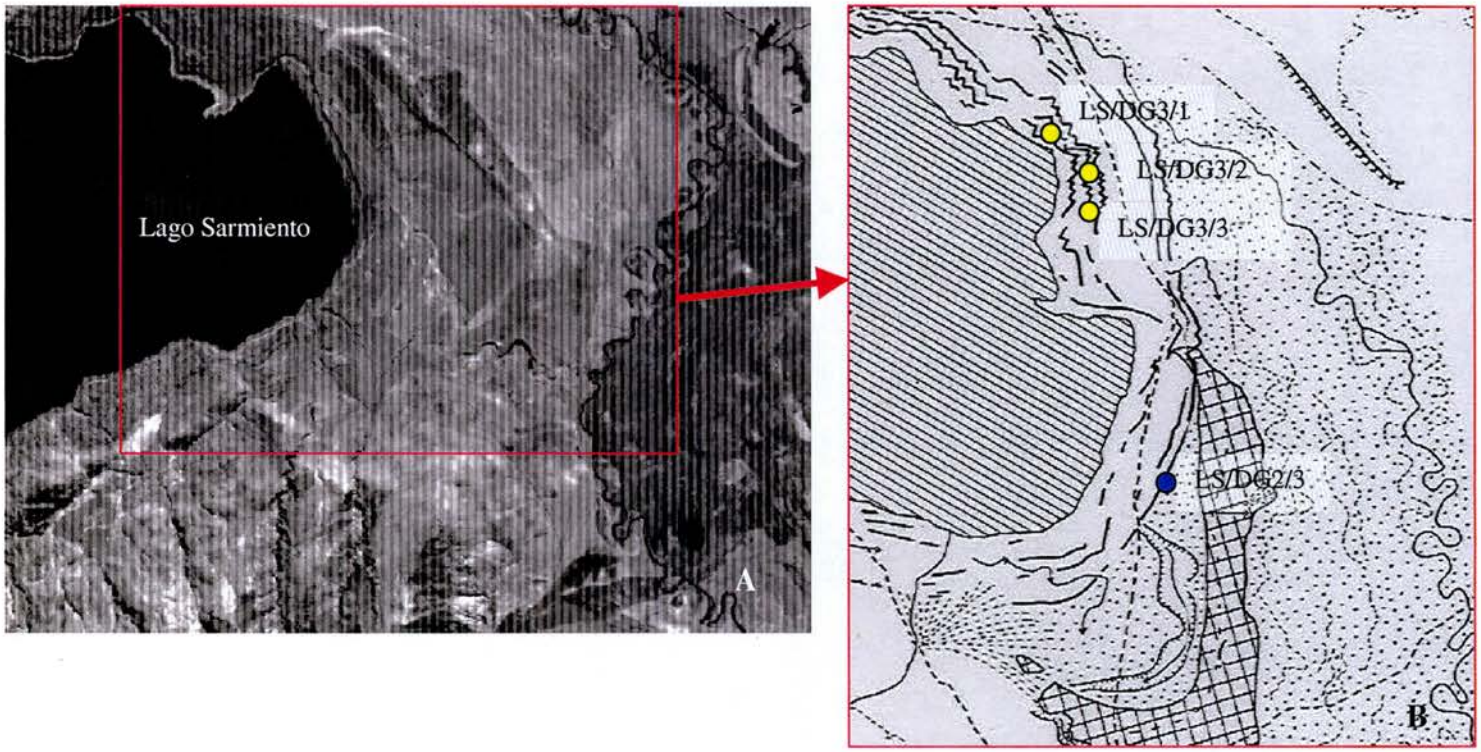

Figure 4.6. Geomorphology and sample positions at eastern end of Lago Sarmiento. Image A, is a composite satellite image of around 15m resolution from the NOAA GLIMS satellite. B, is a geomorphological map of this area, showing moraine ridges and channel systems, with sample locations. Yellow points represent samples from drift group 6, and blue drift group 7.

crevassing was likely to have been nearly identical during the formation of each moraine. The implication is that they may be very close in age.

The composition of the till forming these moraines is generally pebble to boulder sized clasts in a grey-brown sand, or a white silty clay matrix. Exposed sections at the lake shore are composed of white silt and clay, which is often laminated and with dropstones and evidence of local deformation. This suggests that these moraines were formed of reworked glaciolacustrine sediments. To provide an age estimate of the final deglaciation from this limit cosmogenic samples were taken from erratics related to the innermost ridge related to this stage. It was noted that the choice of suitable samples was limited from this moraine, but four suitable boulders were sampled (Figure 4.7), the details of which are included in Table 4.3.

4.7.3 Glacial Stage 7: Type site; eastern end of Largo Sarmiento

This moraine can be trace unbroken from Laguna Amarga north towards Lago Sarmiento, where it forms a part of a system of concentric ridges to the east of the lake (Figure 4.7). At the end of Lago Sarmiento moraines of this stage overlie an extremely large and subdued moraine related to earlier glaciation which has possibly been overridden at other localities.

The Stage 7 moraine system is up to 500m wide at this locality, and comprises several ridges, some of which are poorly preserved due to later erosion by meltwater. Moraines typically have a bouldery surface, with gullied section south of the lake revealing till which comprises clasts including large boulders in a white silt or clay, or darker sand. As with stage 6 this indicates that the till comprises much reworked glaciolacustrine sediment. Four samples were taken from this moraine for analysis of their TCN concentration, the details of which are included in Table 2.

4.8 Exposure dating

Exposure dating with *in situ* cosmogenic nuclides provides a means of dating glacial deposits directly, particularly those devoid of organic material suitable for radiocarbon dating. As a result of secondry cosmic-ray bombardment, ^{10}Be and other TCN nuclide are produced within the uppermost decimeters of a rock surface (Lal, 1991). The measured concentration of the

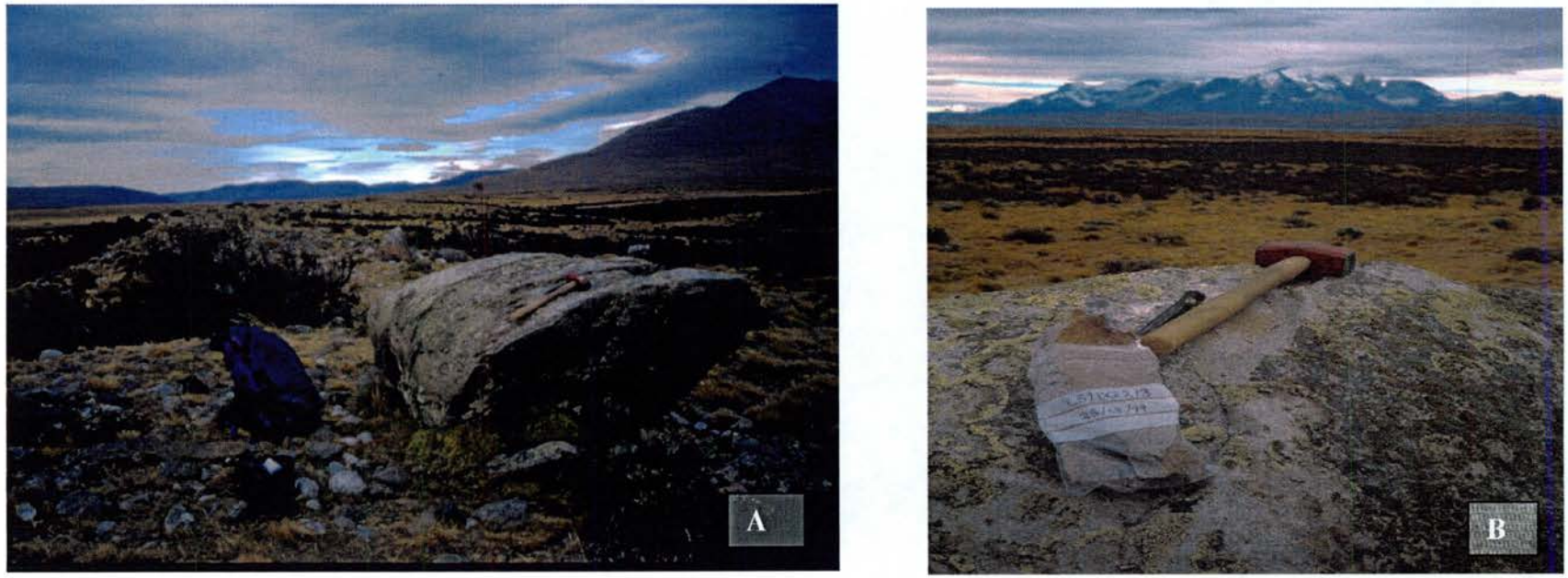

Figure 4.7. Typical sample from drift groups 6 and 7 at the eastern end of Lago Sarmiento. Photo A shows sample LS/DG2/3, a large (2 by 4m) boulder on top of a subdued moraine ridge. Photo B shows the upper surface of one of these samples looking east towards Lago Sarmiento and the Paine Massif. In both pictures the hammer length in approximately 30cm.

radioactive isotope can be used to calculate an exposure age of the surface providing the rate of production of the TCN in question is known (Cerling and Craig, 1994).

We measured the concentration of the TCN ^{10}Be in 9 boulders on top of the landforms described above. Samples were taken from suitably large boulders, by removing the uppermost centimeters of their top surfaces. By choosing the largest boulders from those available, any problems related to exhumation or significant coverage by snow or vegetation were minimised. Sampling was restricted to boulders in stable positions on top of landforms, to avoid any post-depositional movement. As quartz is the ideal mineral for the application of the technique of TCN when using the isotope ^{10}Be, only quartz-rich granites and granidiorites were sampled. The lithology and sample descriptions together with the ages ascribed by Marden (1993) are recorded in Table 4.2.

The isotope ^{10}Be was selectively extracted from the quartz component of the whole rock sample following the standard procedures described by Kohl and Nishizumi (1992) and Ivy-Ochs (1996). The isotopic ratios were measured at the ETH tandem AMS facility in Zurich, Switzerland. Tables 2 and 3 list the cosmogenic ^{10}Be radionuclide data, the location and type of sampling site and the conventional exposure ages of each sample. In this study the reference production rate used is that of Kubik *et al* (1998), which has been determined experimentally. *In situ* production of the cosmogenic nuclide ^{10}Be is a combination of three principle components, the most important being spallation, with fast and stopped muons making a less significant contribution to total production. There is strong evidence that the relative muon contribution to total production is much lower than the 16% originally assumed (Heisinger, 1997; Stone 2000). Therefore this study incorporates the modified values of Kubik *et al* (1998) to provide a more accurate representation of the stopped and fast muon components (Heisinger, 1997; Stone 2001). Therefore the reference production rate for ^{10}Be used is a spallation component of 5.22±0.22 atoms/g (qtz)/yr, together with a value of 0.12 atoms/g (qtz)/yr for stopped muons and 0.027 atoms/g (qtz)/yr for fast muons (Schaller *et al.*, 2000). Including muons, this results in a total surface production rate (P_0), at sea level and high latitude (SLHL) for ^{10}Be of 5.37±0.22 atoms/g (qtz)/yr. This value was chosen for three reasons; (1) it is referenced to the calibrated radiocarbon timescale, hence the exposure ages given here should be directly comparable to calibrated radiocarbon ages (2) all relevant data necessary for the calculations are available (3) due to the lack of a suitable calibration site in the southern hemisphere on this time scale.

The reference production rate was scaled to that of the site in question following the methods outlined by Stone (2000). The total production at the site, was corrected for attenuation of cosmic radiation due to the thickness of the sample itself, and any shielding due to the surrounding topography following the procedures of Dunne *et al.* (1999). These correction factors were applied to model the effect of the reduced incoming cosmogenic signal on the total production at the sample site. Errors related to the AMS, the production rate and a 5% sample reproducabilty are added quadratically, and calculated as a function of the eventual age. Corrections for unknown shielding events such as snow or tephra were not included, as in this environment they represent unknowns over the exposure period. Their effect would lead to a reduction in eventual age, but it was felt that a model of this would be unrealistic.

In order to provide a realistic age envelope, the ages have been calculated for the effect of surface erosion, at rates of 1mm, 3mm and 1cm per 1000 years. The rate of erosion will obviously vary with lithology and environmental conditions, therefore this is only offered as a guide to the possible upper and lower age limits of the surface in question. The surface of some samples provide evidence of the magnitude of erosion, such as striations and surface pitting, details are described in Table 4.3.

4.9 Results and discussion

Tables 4.2 and 4.3 list the cosmogenic ^{10}Be radionuclide data, the location and type of sampling site and the relative age of each sample derived from the work of Marden (1993). The following discussion interprets the specific numerical ages produced from this work in a sample specific and landform context.

Table 4.2 Cosmogenic radionuclide data

sample ID	Latitude (^{0}S)	Longditude (^{0}E)	Altitude (m)	Sample mass (g)	Depth shielding factor[1]	topographic shielding factor[2]	Be carrier (mg)[3]	measured $^{10}Be/^{9}Be$ ratio[4]	± % error[5]	measured laboratory blank $^{10}Be/^{9}Be$[6]	±% error[7]	Blank corrected ratio[8]	^{10}Be atoms /g in sample[9]	± % error[10]	± % error inc. 5% sample reproducability[11]
HT/1/99	51	72	200	70.22	0.947893	0.990887	0.507007	2E-13	7	2.48E-14	16.8	1.75E-13	84532	8.3	9.7
HT/2/99	51	72	200	47.94	0.95632	0.990887	0.507007	1.49E-13	7.3	2.48E-14	15.9	1.24E-13	87762	9.3	10.6
HT/3/99	51	72	200	84.92	0.95632	0.990887	0.507007	2.36E-13	8.3	2.48E-14	15.9	2.11E-13	84256	9.5	10.7
HT/4/99	51	72	200	79.39	0.947893	0.990887	0.507007	2.51E-13	7	2.48E-14	15.9	2.26E-13	96530	8.0	9.4
LS/DG3/1	51	72	140	45.47	0.964849	0.999996	0.35455	1.64E-13	7.6	2.8E-14	17.5	1.36E-13	88434	9.8	11.0
LS/DG3/2	51	72	140	31.02	0.964849	0.999996	0.35455	1.19E-13	10.4	2.8E-14	17.5	9.1E-14	69494	14.6	15.5
LS/DG3/3	51	72	140	19.67	0.964849	0.999996	0.35455	7.3E-14	7.2	2.8E-14	17.5	4.5E-14	34365	16.0	16.7
LS/DG2/3	51	72	130	50.25	0.964849	0.999996	0.35455	1.94E-13	5.9	3.4E-14	17.5	1.6E-13	75431	8.1	9.5

1. Calculated using "flat" dependency of Massirik and Reedy (1995)
2. Calculated using the relationship $\sin^{2.3}\theta$, for 360^0 around the sample, where θ is the angle of the topographic obstruction from the horizontal.
3. Carrier addition measured by calibrated pipette, and corrected for temperature and density.
4 & 5. Reported from AMS measurements, include errors related to "in-house" standard.
6 & 7. Removes possible effects of exposure and chemical loading of other samples, measured during same accelerator run.
8. Total blank corrected $^{10}Be/^{9}Be$ ratio.
9 & 10. Concentration of cosmogenic ^{10}Be in sample with errors propagated step-wise (atoms / gram).
11. Additional 5% error related to sample reproducability, based on multiple analyses on single samples by Ivy-Ochs (1996).

Table 4.3 Sample descriptions and cosmogenic radionuclide ages

Sample ID	Glacial stage[1]	Altitude(m)	Location[2]	Sample type[3]	Relitive Age[4]	10Be exposure age (yrs)[5]	±error (yrs)	Comments	Exposure age (yr) @E=1mm/ka	Exposure age (yr) @E=3mm/ka	Exposure age (yr) @E=1cm/ka	Mean landform age (yr)[6]
HT/1/99	5	200	***Estancia Cerro Paine***	Bm	>R	13,610	1,436	No striations, rough pitted appearance	13,780	14,138	15,618	
HT/2/99	5	200	***Estancia Cerro Paine***	Bm	>R	14,007	1,588	No striations, rough pitted appearance	14,187	14,567	16,146	
HT/3/99	5	200	***Estancia Cerro Paine***	Bm	>R	13,446	1,541	No striations, rough pitted appearance	13,612	13,960	15,400	**15,832±767**
HT/4/99	5	200	***Estancia Cerro Paine***	Bm	>R	15,549	1,594	Striations on sides of boulder	15,771	16,243	18,250	
LS/DG3/1	6	140	***Lago Sarmiento***	Bm	>R	11,760	1,385	Subdued moraine morphology indicates possible deflation	11,886	12,150	13,217	
LS/DG3/2	6	140	***Lago Sarmiento***	Bm	>R	11,532	1,844	Subdued moraine morphology indicates possible deflation	11,653	11,907	12,928	N/A[7]
LS/DG3/3	6	140	***Lago Sarmiento***	Bm	>R	5,695	981	Subdued moraine morphology indicates possible deflation	5,724	5,784	6,009	
LS/DG2/3	7	130	***Lago Sarmiento***	Bm	>R	12,642	1,306	Subdued moraine morphology indicates possible deflation	12,789	13,095	14,349	N/A[8]

1. Glacial stages based on this work, Clapperton et al.'s (1995) original glacial stage is shown in parenthesis where the relative ages of moraines have been reinterpreted.
2. See text for descriptions, and Figures 3 and 4.
3. Sample type; Bm=Boulder perched on moraine, E=Erratic, B=bedrock surface
4. Avaliable minimum constraints on landform; R=Reclus tephra (15,382 cal yr BP) (McCulloch and Davies, 2001), A=Minimum radiocarbon date of 20,834 cal yr BP above blue gray clays (McCulloch pers com), B=Minimum radiocarbon date of 16,591 cal yr BP at Estancia California (McCulloch pers com).
5. Calculated using a ^{10}Be production rate of 5.37±0.22 at/g/yr (Schaller et al., 2001), scaled following the methods outlined by Stone (2000), which are a reformulation of those of Lal (1991).
6. Error weighted mean of TCN ages from boulders off individual landforms

7 & 8. Spread of ages together with subdued morphology suggest that these samples have been affected by deflation by wind, causing the gradual exhumation of individual boulders from the fine grained sediment from which this moraine was comprised.

4.9.1 Glacial stage 5

The TCN ages of boulders from this the kame terrace demonstrate that ice recession from the landform was between 13,610 ka yrs and 15,549ka yrs. The spread of ages is most likely a product of differences in the erosion rate of the quartz diorite boulders in comparison to that of the quartz monzonite. To test this theory erosion corrections can be made to samples of the lithologies that are more easily eroded. This difference in weathering and its relationship to lithology was noted during sampling. Samples from the quartz diorite boulders were easily removed, whilst the quartz monozonite boulders were very hard, and could only be removed in the form of surface chips. It was also noted in the field that the quartz monozonite often displayed evidence of surface polish and striations, whereas the diorite boulders tended to have pitted outer surfaces with little or no signs of ice scouring (Figure 4.8). These observations suggest that erosion rates are dependent on lithology, with higher erosion rates on the more easily eroded diorites (Figure 4.8). Table 4.4 demonstrates the increased ages of the quartz diorite samples assuming an erosion rate of 1cm/ka, therefore substantially increasing the apparent exposure age of the boulders in question, providing an age envelope for the emplacement of these boulders by advancing ice.

Table 4.4 Lithology specific erosion corrections

Sample ID	Lithology	^{10}Be Age (E=0)	^{10}Be Age lithology specific erosion correction
HT/1/99	Quartz diorite	13,610	15,617 (E=1cm/ka)
HT/2/99	Quartz diorite	14,007	16,146 (E=1cm/ka)
HT/3/99	Quartz diorite	13,466	15,399 (E=1cm/ka)
HT/4/99	Quartz monzonite	15,549	15,549 (E=0mm/ka)

Table 4.4, is obviously only a guide, to help provide exposure estimates for the observations made in the field. It is likely that the rate of erosion has varied through time as environmental conditions varied. Also, it should also be noted that these exposure estimates do not allow for any temporary cover by snow, sediment, vegetation or volcanic tephra that could have reduced the incoming cosmogenic signal through time.

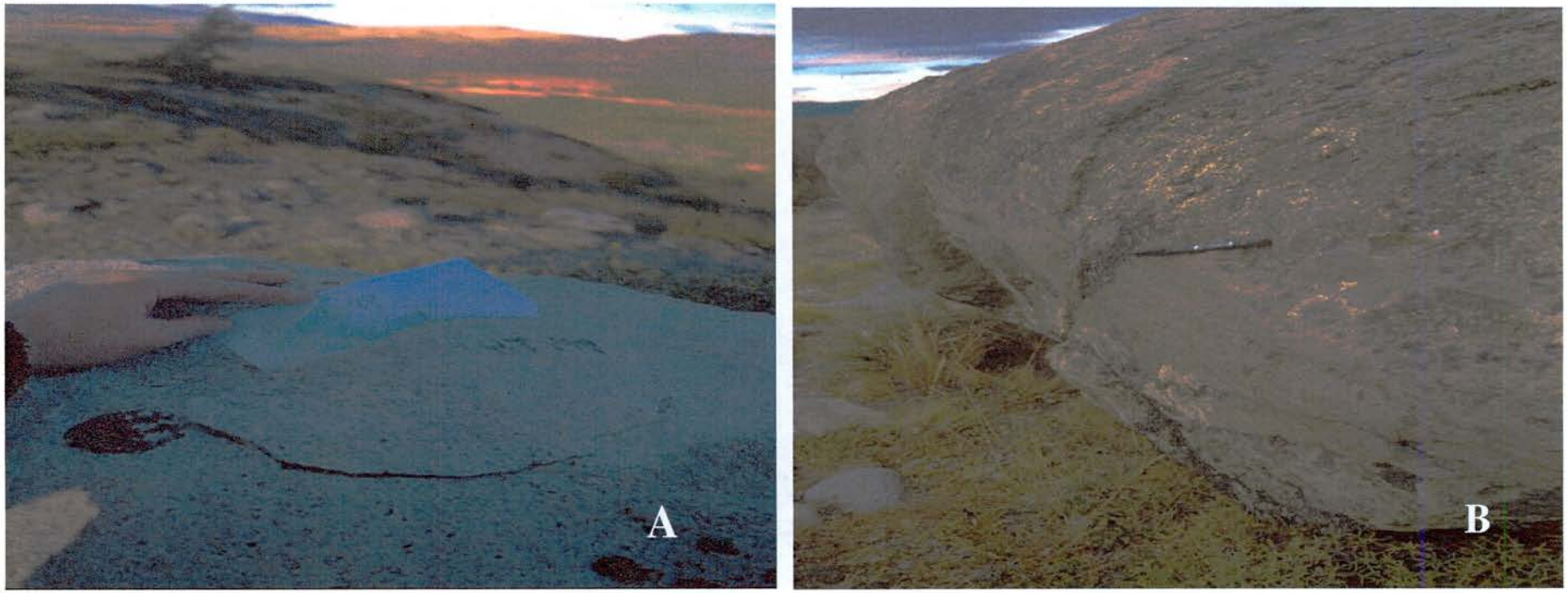

Figure 4.8. Images showing the differences in surface weathering between boulders of quartz diorite (A), and the quartz monzonite (B) lithologies, located on the Landform at Estancia Torres. Photo A demonstrates the rounded, pitted nature of the quartz diorite which showed no evidence of glacial transport, it is believed this results from high weathering due to wind action. Photo B shows sample HT/4/99, a quartz monzonite boulder which shows signs of striations on its sides and upper surface suggesting lower weathering rate.

Using the sample specific erosion correction outlined in Table 4, the mean landform age of this feature is found to be 15,832±767 ^{10}Be yr BP, thus suggesting a period of readvance, or positive mass balance at this time in the Sarmiento lobe of the Torres del Paine Ice Sheet.

4.9.2 Glacial Stages 6 and 7

The three boulders analysed from glacial stage 6 at the eastern end of Lago Sarmiento (Figure 4.7), indicate a wide spread of exposure ages between 5,622±968 to 14,496±1,708 ^{10}Be yr BP. This age range is clearly problematic with the available radiocarbon data, which imply much greater age of these landforms. Also these ages are inconsistant with those related to glacial stage 5, which is morphostratigraphically inside these limits as outlined above.

Therefore, following the concepts of Hallet and Putkonen (1994), it is suggested that these ages actually relate to the competing effects of moraine erosion and boulder weathering. Suggesting gradual exposure of these boulders by erosion of the fine glacilacusurine and glacifluvial sediments from which these moraines are composed. These landforms are subjected to extreme scouring by the prevailing westerly winds and dust storms. It may be that the exposure ages reflect the appearance of a boulder from a deflating surface.

This interpretation is backed up by the exposure ages on the moraines of glacial stage 7 just outside these limits, which provide an exposure age of 12,480 ±1,290 ^{10}Be yr BP. If this exposure date is interpreted as an age of emplacement, it suggests the moraine of stage 6 was deposited first, a hypothesis rejected on morphostratigraphic grounds.

Although it is recognised that these exposure ages do not represent emplacement of these landforms, the oldest age may be interpreted as a minimum age of the earliest period of exposure after ice withdrawal. Therefore the moraine of glacial stage 6 was emplaced before 14,496±1,708 ^{10}Be yr BP (E=0). Allowing for an erosion rate of 1cm/ka for quartz diorites of the Torres del Paine Massif this indicates a minimum age of 16,804±1,708 ^{10}Be yr BP for glacial stage 6. It is accepted that due to internal inconsistencies in the data sets related to glacial stages 6 and 7 that no climatic or chronological inferences can be made for the emplacement of these landforms. Rather the results demonstrate the limitations of the technique in its application to surface exposure dating of moraines on ageing landforms. Hallet and Putkonen (1994), offer models to attempt to model the gradual downwasting of moraines due to their slope angle and

length, thus providing a coefficient of topographic diffusivity (the volume of soil moving downslope through time). However the most important mechanism for sediment removal in the arid environment at the eastern end of Lago Sarmiento is deflation due to the prevailing westerly winds. This process is enhanced in the case of these moraines with the general fine-grained matrix with little protective vegetation. Thus it is not possible to apply downwasting models to obtain a correction with any degree of certainty.

4.10 Discussion

Due to the factors described above, it is difficult to relate the cosmogenic exposure ages of glacial stages 6 and 7 to climatic forcing. Therefore the discussion focuses on the interpretation of the formation of the landforms related to the glacial advance of stage 5. The fresh morphology of this landform and the internal consistency of the calculated exposure ages provides a significant fix on ice expansion at this time. The exposure ages confirm relative chronology of Marden (1993), which suggests this climatically forced advance was related to a late glacial event during general recession from Last Glacial Maximum limits.

Allowing for the lithologicaly specific erosion corrections, the cosmogenic exposure dating indicate deglaciation from this limit between 15,399±1521 and 16,242±1568 ^{10}Be yr BP, providing a mean landform age of 15,832±767 ^{10}Be yr BP. The presence of the Reclús tephra throughout glacilacusterine and glacifluvial sediments immediately within these limits suggests that withdraw from this expanded limit was then rapid to within 16km of modern ice sheet limits (Marden 1995). The age of this tephra has been ascertained from multiple analyses of it in relation to organic sediments immediately above and below, and has provided an age of 12,700^{14}C yr BP (15,382 cal. yr BP) (McCulloch and Davies, 2001). This retreat phase was only punctuated by a final stage of ice re-growth that has been identified between 12,700 and 9140 ^{14}C yr BP. This conclusion is based on the indistinguishable difference between the exposure age of this landform and the presence of the Reclús tephra right throughout the field area (Marden, 1993). This can be seen visually in Figure 4.9.

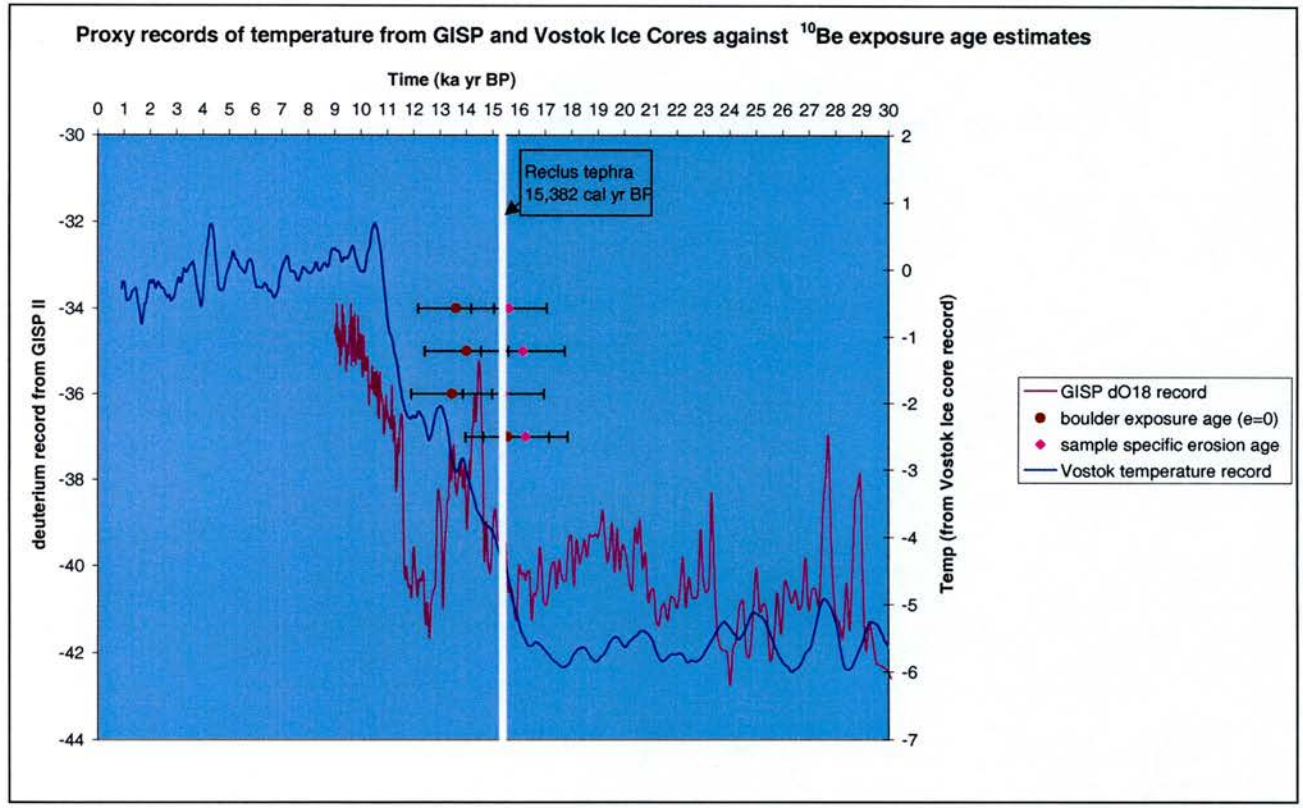

Figure 4.9. Exposure ages of boulders from glacial stage 5 at Estancia Cerro Paine, in Torres del Paine, seen against records of proxy atmospheric temperature from Greenland (GISP 2, delta O^{18} record) and VOSTOK, Antarctica. The calibrated age of the Reclus tephra is also marked to demonstrate the time of eruption of this constraining tephra.

4.11 Regional Correlations

The ^{10}Be exposure ages place the ice advance of glacial stage 5 of the Sarmiento lobe of the Patagonian Ice Sheet to the end of a period of cooling immediately prior to significant lateglacial warming. A late glacial readvance of the margins of the Patagonian Ice Sheet is recorded in well constrained records both to the north of this region in the Chilean Lake District (Denton *et al.*, 1999) and to the South in the Strait of Magellan (McCulloch *et al.*, 2000). These records suggest advance between 14,805-14,550 ^{14}C yr BP and 14,600-14,300 ^{14}C yr BP respectively. When calibrated these data indicate advance at between 17,500-17,150 cal yr BP, a date which seems difficult to reconcile with the exposure dating of the landform which has been ascribed to this stage in Sarmiento Lobe at Torres del Paine. This disparity is difficult to relate to climate due to the inherent errors in both the technique of cosmogenic exposure dating and the uncertainties related to the calibration of radiocarbon dated chronologies on this time scale. However, if it is accepted that the cosmogenic ages from the boulders related to the landforms of glacial advance 5 in Torres del Paine reflect a minimum age of ice decay from these limits at 15,832±767 ^{10}Be yr BP, with no correction for cover by snow, soil or tephra. Even without corrections for these unknown factors this age is within error of the radiocarbon dated sequences to the north and south of this site. This data provides the first directly dating of this advance outside the Chilean Lakes or Magellan Region to the north and south respectively.

The importance of this conclusion is that glacial advances 6 and 7, outside this limit are now constrained by their morphostratigraphic position, therefore, as Marden (1993) suggested are probably related to the LGM expansion in this region. Providing the first direct evidence, that these limits, which can be traced throughout the central latitudes of the Patagonian Region, are not contemporaneous with the Younger Dryas event in the Northern Hemisphere as suggested by Caldenius (1932)Mercer (1976) and Wenzens (1999).

4.12 Conclusions

Interpretation of the data presented in this study provides two significant conclusions for the glacial history Patagonian Ice Sheet draining through Torres del Paine at 51° South. The first is the identification of a retreat or re-advance stage during the general recession from the Last Glacial Maximum conditions, which actively formed glacial landforms at over 45km from the present ice margin. The field relationships between these landforms and a tephra occurring at 12,700^{14}C yr BP (15,382 cal. yr BP) indicate that recession was rapid from this limit, and ice was close to modern limits by the time the tephra was deposited (McCulloch and Davies, 2001). The direct dating of this event provides constraints on both the LGM and late glacial expansion of the south Patagonian Ice Sheet in this central region. As such it confirms the earlier work of Marden (1993), that places the LGM expansion in this region to the limit ascribed by Caldenius (1932) and Wenzen (1999) as the limit of Late Glacial or (Younger Dryas / Finiglacial) expansion in this area.

The second finding of this work is the application of surface exposure dating using TCN to samples of differing lithologies. It has been demonstrated that the effects of differential erosion can cause variation in the concentration of cosmogenic nuclides in samples related to the same event. To solve this problem a sound understanding of erosion of the lithologies in questition is critical, and it is suggested that only boulders displaying evidence of direct glacial transport be sampled in this context. This work has also highlighted problems with the application of the TCN technique in this environment, where processes such as deflation may lead to exhumation of boulders. This was only recorded in fine-grained moraines composed predominantly of glacifluvial and glacilacusterine silts and sands. These observations further emphasise the need for careful fieldwork and observation during sampling for the TCN technique.

4.13 References

Caldenius C. 1932. Las glaciations cuaternarias en la Patagonia y Tierra del Fuego. Geografiska Annaler 14. 1-64.

Cerling TE, Craig H. 1994. Geomophology and in situ cosmogenic isotopes. Annual Review of Earth and Planetary Sciences 22. 273-317.

Clapperton CM, Hall M, Mothers P, Hole MJ, Still JW, Helmens KF, Kuhry P, Gemmell AMD. 1997. A Younger Dryas ice cap in the equatorial Andes. Quaternary Research 47: 13-28.

Clapperton CM, Sugden DE, Kauffman D, McCulloch RD. 1995. The last glaciation in central Magellan Strait, southernmost Chile. Quaternary Research 44: 133-148.

Cockburn HAP. (1998) Landscape evolution in Namibia and Antarctica: Quantifying denudation rates using in-situ cosmogenic isotope analysis. Unpublished PhD thesis, The University of Edinburgh, 246pp.

De Geer G. 1927. Late glacial clay varves in Argentina, measured by Dr. Carl Caldenius, dated and connected with the solar curve through the Swedish time scale. Geografiska Annaler. 9.

De Geer G. 1929. Gotiglacial clay varves in southern Chile, measured by Dr. Carl Caldenius, identified with synchronous varves in Sweden, Finland and the USA. Geografiska Annaler. 11.

Denton GH, Heusser CJ, Lowell TV, Moreno PI, Anderson BG, Heusser LE, Schlüchter C, Marchant DR. 1999. Interhemispheric linkage of paleoclimate during the last glaciation. Geografiska. Annaler 81A(2): 107-153.

Dunne J, Elmore D, Muzikar P. 1999. Scaling factors for the rates of production of cosmogenic nuclides for geometric shielding and attenuation at depth on sloped surfaces. Geomorphology. 27. 3-11.

Ferugilio E. 1949-50. Descripcion geologica de la Patagonia. Buenos Aires, Direccion General Yacimientos Petroloiferos Fiscals. Vols. 1,2,3.

Gosse JC, Phillips FM. 2001. Terrestrial in situ cosmogenic nuclides: theory and application. Quaternary Science Reviews 20. 1475-1560.

Hallet B, Putkonen, J. 1994. Surface dating of dynamic landforms:young boulders on ageing moraines: Science. V.265. 937-940.

Heisinger B. 1997. In situ production of radionuclides at great depths. Nuclear Instruments and Methods. B. 123. 341-346.

Hofmann HJ. Beer J, Bonani G. von Gunten HR. Raman S, Suter S, Walker RL, Wölfli W, Zimmermann D. 1987. Half-life and AMS standards: Nuclear Instruments and Methods. B29. 32-36.

Hubbard AL. 1997. Modelling climate, topography and palaeoglacier fluctuations in the Chilean Andes. Earth Surf. Processes and Landforms. 22. 79-92.

Hulton N, Sugden DE, Payne A, Clapperton CM. 1994.Glacier modelling and the climate of Patagonia during the last glacial maximum. Quaternary Research. 42. 1-19.

Hulton N.R.J., Purves R.S. 2000. A climatic-scale precipitation model compared with the UKCIP baseline climate. International Journal of Climatology, 20(14) 1809-1821

Ivy –Ochs S. 1996. The dating of rock surfaces using the in situ produced ^{10}Be, ^{26}Al, and ^{36}Cl, with examples from Antarctica and the Swiss Alps. Ph. D. Thesis, Swiss Federal Institute of Technonology, Zurich. 196pp.

Kohl CP and Nishizumi K. 1992. Chemical isolation of quartz for measurement of *in situ* produced cosmogenic nuclides. Geochemica et Cosmochemica Acta. 56. 3583-3587.

Kubik PW, Ivy-Ochs S, Masarik J, Frank M, Schlüchter C. 1998. ^{10}Be and ^{26}Al production rates deduced from an instantaneous event within the dendro-calibration curve, the landslide of Köfels Ötz Valley, Austria, Earth and Planetary Science Letters 161. (1-4). 231-241.

Lal D. 1991. Cosmic ray labeling of erosion surfaces: in situ nuclide production rates and erosion rates. Earth and Planetary Science Letters 104, 424-439.

Lal D, Arnold JR. 1985. Tracing quartz through the environment. Proceedings of the Indian Academy of Science (Earth Planetary Science Section) 94. 1-5.

Lowell TV, Heusser CJ, Anderson BG, Moreno PI, Hauser A, Heusser LE, Schlüchter C, Marchant DR, Denton GH. 1995. Interhemispheric correlation of Late Pleistocene glacial events. Science 269, 1541-1549.

Lliboutry L. 1956. Nives y Glaciares de Chile. Santiago.

Lien R, Rye N. 1988. Formation ofsaw-toothed moraines in front of Bodalsbreen glacier, western Norway. Norsk Geologisk Tidsskrift. 68. 21-30.

Marden CJ. 1993. Late Quaternary glacial history of the South Patagonian Icefield, at Torres Del Paine, Chile. Ph. D Thesis, University of Aberdeen. 298pp.

Masarik J, Reedy RC. 1995. Terrestrial cosmogenic-nuclide production systematics calculated from numerical simulations. Earth and Planetary Science Letters. 136. 381-395.

Mattews JA, Cornish R. Shakesby RA 1979. "Saw-tooth" moraines in front of Bodalbreen, southern Norway. Journal of Glaciology. 22. 535-546.

McCulloch RD, Bentley MJ, Purves RS, Hulton NRJ, Sugden DE, Clapperton CM. 2000. Climatic inferencesfrom glacial and palaeoecological evidence at the last glacial termination, southern South America. Journal of Quaternary Science 15. 409-417.

McCulloch RD, Sugden DE. 2001. Climatic inferences from glacial and palaeoecological evidence at the last glacial termination, southern South America: a reply Journal of Quaternary Science. 16 (3) 291-294.

McCulloch RD, Bentley MJ. 1998. Late glacial ice advances in the Straight of Magellan, southern Chile. Quaternary Science Reviews. 17. 775-787.

McCulloch RD, Sugden DE. 2001. Climatic inferences from glacial and palaeoecological evidence at the last glacial termination, southern South America: a reply Journal of Quaternary Science. 16 (3) 291-294.

McCulloch RD, Davies SJ. 2001. Late-glacial and Holocene palaeoenvironmental change in the central Strait of Magellan, southern Patagonia. Palaeogeography, Palaeoclimatology, Palaeoecology. 173. 143-173.

Martinic M. 1982. Hielo Patagonia Sur. Publicationes del Instituto de la Patagonia. Serie Monografias, Punta Arenas. pp 117.

Mercer JH. 1976. Glacial history of southernmost South America. Quaternary Research. 6. 125-166.

Michael PJ. 1983. Emplacement and differentiation of Miocne plutons in the foothills of the southernmost Andes. Unpublished PhD thesis, unnamed University (copy at Torres del Paine National Park).

Naruse R, Pena H, Aniya M and Inoue J. 1987. Flow and surface structure of the Tyndall Glacier, the Southern Patagonian Icefield. Bulletin of Glacier Research. 4. 133-140.

Nishiizumi K, Finkle RC, Klein J, Kohl CP. 1996. Cosmogenic production of ^{7}Be and ^{10}Be in water targets. Journal of Geophysical Research 101. 22,225-22,232.

Nishiizumi K, Winterer EL, Kohl CP, Lal D, Arnold JR, Klein J, Middleton R. 1989. Cosmic ray production rates of ^{10}Be and ^{26}Al in quartz from glacilly polished rocks. Journal of Geophysical Research 94 (B12). 17,907-17,915.

Porter SC, Clapperton CM, Sugden DE. 1992. Chronology and dynamics of deglaciation along and near the Strait of Magellan. Southernmost South America. Sveriges Geologiska Undersokning. Ser. Ca 81. 233-239.

Pisano E. 1974. Estudio ecologico de la region continental sur del area andino Patagonico. Annales del Instituto de la Patagonia. 5. 59-104.

Romero H. 1985. Geografiça de Chile: geografia de los climas. Instituto Geografico Militar: Santiago.

Schaller M, von Blanckenburg F, Hovius N, Kubik PW. 2001. Large-scale erosion rates from in situ produced cosmogenic nuclides in European river sediments. Earth and Planetary Science Letters 188. 441-458.

Steig *et al.*, 1998. Synchronous climate changes in Antarctica and the North Atlantic. Science. 282. 92-95.

Stone JO. 2000. Air pressure and cosmogenic isotope production. Journal of Geophysical Research. 105. B10. 23,753-23,759.

Wenzens G. 1999. Fluctuations of outlet glaciers in the southern Andes (Argentina) during the past 13,000years. Quaternary Research. 51. 238-247.

Wenzens G. 2001. Climatic inferences from glacial and palaeoecological evidence at the last glacial termination, southern South America: comment. Journal of Quaternary Science. 16 (3) 291-294.

White JWC, Ciais P, Figge P, Kenny R, Markgraf V. 1994. A high-resolution record of atmospheric CO_2 content from carbon isotopes in peat. Nature. 376. 153-156.

CHAPTER 5

A Preliminary Chronology of George V1 Sound, Graham Land, and Southern Palmer Land Antarctica: from the measurement of *in situ* cosmogenic nuclides ^{10}Be and ^{26}Al.

5.1 Abstract

This paper presents the first systematic attempt to constrain the timing of deglaciation of the Antarctic Peninsula Ice Sheet from its configuration at the Last Glacial Maximum (LGM), through the measurement of the cosmogenic radionuclides ^{10}Be and ^{26}Al within erratics deposited on glacial landforms. At the LGM the ice sheet expanded to form two ice domes in Palmer Land and merged with an expanded and thicker West Antarctic Ice Sheet in the Weddell Sea. Ice from the Peninsula merged with ice from Alexander Island in George VI Sound.

The pattern of deglaciation is very complex. Two distinct phases of ice sheet lowering are recorded in George VI Sound. Initial ice sheet lowering between 18.3 and 15 ka was followed by final outlet glacier or local ice cap retreat between 8.7 to 6.4 ka. In the central portion of the Antarctic Peninsula, exposure ages from the Behrendt Mountains suggest deglaciation at 11.8ka. which probably reflects a delayed response to retreat of grounded ice in the Weddell Sea. The wide range of ages and evidence of complex exposure histories from many of the available erratics, provides the first terrestrial evidence that there has been repeated glaciation of the Antarctic Peninsula, over several glacial cycles.

5.2 Background

One of the critical questions in the subject of global change is the past history and future stability of the West Antarctic Ice Sheet (WAIS). In its modern configuration the WAIS is the only existing marine ice sheet where much of the bed is grounded below sea level, making it extremely sensitive to sea level and environmental change. Both today and in the past it has been a significant, and at present unquantified, sink and source of global seawater during the last glacial interglacial cycle (Bentley and Anderson, 1998). Arguably the lack in our understanding of the past dynamics of this ice sheet impedes the prediction of response of the WAIS to future environmental change.

This lack of knowledge has lead to numerous interpretations of how the WAIS will react to future climate change. The review of Oppenheimer (1998) has attempted to draw together the results of recent work concerning the response of the WAIS to global warming. These hypotheses range from suggestions that rising global temperatures relating to increasing levels of CO_2 and other greenhouse gases may cause a sudden collapse of the WAIS. This could instigate a rise in global sea level of 4-6m within the coming century and a substantial change in the climate patterns of the Southern Hemisphere. Alternative models predict slow ice sheet disintegration and thinning, that has been occurring throughout the Holocene and is continuing today, causing the bulk of the WAIS to be discharged over the next few hundred years. In this scenario the rate of discharge is dependant on the reaction of ice streams to the changing configuration of the WAIS. These hypotheses contrast with other predictions, which suggest that as a result of internal ice sheet readjustments there could be a reduction in the discharge of grounded ice. Leading to "the Antarctic contribution to sea-level rise to turn increasingly negative", in other words causing an overall reduction in the net balance (Oppenheimer, 1998: p. 330) . In commenting on this suite of scenarios Oppenheimer (1998: p. 330) states "it is not possible to place high confidence in any specific prediction about the future of the WAIS." Given such uncertainty this work aims to improve knowledge of the spatial and temporal record of deglaciation of the Antarctic Peninsula Ice Sheet (APIS). The knowledge of which may well help indicate the mechanisms by which this sector of the WAIS responds to changes in forcing, such as temperature, precipitation and sea level.

5.3 Introduction

Attempts to elucidate the spatial and temporal extent of glaciation in different sectors of the WAIS from the Last Glacial Maximum (LGM) to its modern configuration have proved difficult due to the lack of direct chronological control. Geomorphological studies of the ice free areas of the Antarctic Peninsula have identified a rich Quaternary record of glacial fluctuations producing erosional surfaces, trimlines and erratics by ice at much higher elevations than present (Clapperton and Sugden 1982). However, direct dating of these landforms has proved difficult. This is mainly due to the scarcity of organic and carbonate material suitable for radiocarbon dating (Bentley and Anderson, 1998). Also it reflects the lack of raised beach deposits such as those found and dated in areas like the Dry Valleys and the Scott Coast of Victoria Land (Denton *et al.* 1989). Raised beaches are limited due to the persistent presence of ice shelves surrounding much of the coastline of the Antarctic Peninsula throughout the Last Glacial Cycle (Bentley and Anderson, 1998).

In order to provide constraints on the former ice sheet configuration, erratic samples were taken from two principal areas of the southern Antarctic Peninsula. The first area is an 800 by 200 km swathe of Southern Palmer Land (Figure 5.1). This region is important because it not only records the behaviour of the Antarctic Peninsula Ice Sheet, but also provides a record of the interaction between Peninsula ice and an expanded WAIS in the Weddell Sea. The second study region consists of the ice-free areas along the west and east sides of George VI Sound. This area was highlighted by Clapperton and Sugden (1982) as recording the interaction between Peninsula Ice and a separate ice dome centred on Alexander Island. This research aims to quantify the deglacial history of this region, using the technique of terrestrial *in situ* cosmogenic nuclide exposure dating (TCN) using the radionuclides ^{10}Be and ^{26}Al in glacial erratics (Gosse and Phillips, 2001).

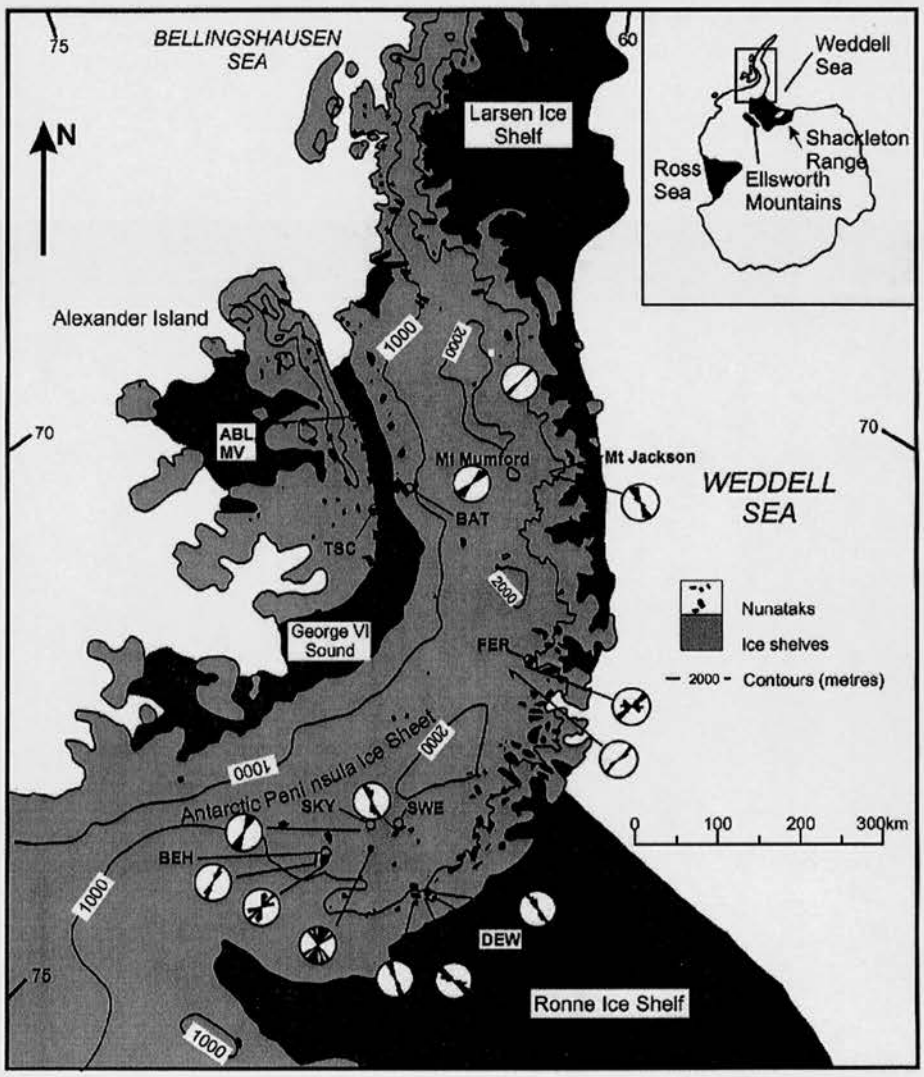

Figure 5.1. Location map of Antarctic Peninsula, with principle field localities marked, principle ice flow directions are also marked as recorded by striations on summit nunataks (Figure from Bentley and Anderson, 1998). Localities, DEW=Mt Dewe, SWE=Sweeny Mountains, BEH=Berhants Mounatins, SKY=Sky-Hi Nunataks, FER=Ferguson Nunataks, BAT=Batterbee Mountains, TSC=Two Steps Cliff, ABL=Ablation Point and MV=Moutonee Valley.

5.4 Physical setting

At present this region lies at the transition zone between the cyclonic pressure systems moving from west to east, and occasional northwards extensions of the anticyclonic system from West Antarctica. The latter, inducing clear stable weather with air temperatures well below freezing even at the height of summer. In general the more dominant and persistent system is that of the cyclonic depressions, drawing relatively mild weather with heavy cloud cover to the peninsula. The mean annual temperature range in he vicinity of GeorgeVI Sound is between –20°C in winter to 8°C in summer, with a mean annual temperature of between –8°C to –10°C. This is in comparison with further south on the Peninsula where temperatures of –20°C are recorded year round on ground above 1500-2000 m (Clapperton and Sugden, 1982).

George VI Sound is a deep tectonic trench between Palmer Land on the Antarctic Penisnsula and Alexander Island. Under modern conditions the sound is filled by an ice shelf, which is up to 500 km long, 20-60 km wide and 100-500 m thick. The ice shelf is fed from outlet glaciers from one of the three main domes that comprising the WAIS. Ice from Alexander Island also contributes to the ice shelf, but to a much lesser degree that that from the mainland. This is clearly seen from the air, where ice from the largest of the Alexander Island glaciers is rapidly engulfed by ice emitted from Palmer Land. The ice shelf calves to the north and south and into Marguerite Bay and the Bellingshausen Sea. Much of the ice flow is westwards across the sound, where there is surface melting along the Alexander Island margin (Clapperton and Sugden, 1982).

Both Alexander Island and Palmer Land have areas of ice-free land surrounding the sound. Previous workers have described both the solid geology and the glacial geomorphology of such areas (Elliot 1974; Bell 1975; Sugden and Clapperton, 1980; Clapperton and Sugden 1982). This work demonstrated the existence of suitable sites and lithologies for application of the TCN technique using the isotopes ^{10}Be and ^{26}Al, and also suggested possible glacial histories through the interpretation of a number of radiocarbon and amino acid racemisation dates.

5.5 Evidence of past glaciation

Evidence of past glacial maximum conditions from geomophological mapping, points towards increased ice thickness on both Alexander Island and the Antarctic Peninsula (Sugden and Clapperton, 1980). This work described both features of glacial erosion and deposition by separate ice domes centred on the mainland of the Antarctic Peninsula and Alexander Island itself. Good indicators of the extent and direction of former ice cover include fresh striations and ice-scoured surfaces on the flanks of George VI Sound and in the Batterbee Mountains together with concentrations of erratics at localities related to these erosional landforms. Fresh striations are also seen on high altitude summits and nunataks exposed today in the interior of the ice sheet of the peninsula itself. Fresh striations and roches moutonnee have been identified in many areas of hard volcanic rocks typical of this region (Clapperton and Sugden, 1982; Sugden and Clapperton, 1983; Bentley, 2000). Striations are also found in areas where more easily eroded lithologies such as shale outcrop, but only where a protective veneer of regolith exists. Through analysis of these erosive glacial features Clapperton and Sugden (1982), were able to reconstruct the Late Quaternary ice-flow configuration of George VI Sound. This pattern, together with the absence of erratics derived from the mainland above an altitude of 85m on Alexander Island, suggested that both Palmer Land and Alexander Island acted as independent centres of outflow for ice domes during the Late Quaternary (Sugden and Clapperton, 1980). This represented less ice than indicated by previous models of maximum conditions in the late Wisconsin for this part of the Antarctica, with ice flowing across Alexander Island out to the edge of the continental shelf to the west (Hughes, 1975; Denton and Hughes, 1981). This was an important conclusion, as it indicates a significantly less substantial build-up of ice on the Antarctic Peninsula than predicted on theoretical grounds by the CLIMAP reconstruction. However the timing of this expansion was unconstrained by the available chronology, due to inconsistencies between the radiocarbon and amino acid analyses of shell samples found within till deposits at around 100m altitude on the flanks of George VI Sound (Clapperton and Sugden, 1982).

Modelling studies of the growth and decay of the Peninsula Ice sheet backs up this field evidence indicating that George VI Sound acted as a major conduit that allowed the ice to flow radially away from the two separate ice centres (Payne *et al.*, 1989). Using sea level as the

principal forcing mechanism, this work concluded that ice growth and decay of the peninsula ice sheet is characterised by thresholds which separate periods of steady state from periods of rapid transition. Eustatic sea level was found to be the primary control, with small fluctuations resulting in rapid variations in calving and thereby ice sheet morphology. The implication is that changes in eustatic sea level can change the topographic configuration of the periphery of the ice sheet, even triggering switching between periods of growth and decay (Payne *et al.*, 1989).

5.6 Approach and Methodology

Using the framework chronology established by Clapperton and Sugden (1982) and the recent field mapping of Bentley (2000), sites were selected from which to collect rock samples from landforms to reveal the time that glaciers last occupied the ice free areas of George VI Sound and Palmer Land. Figure 5.2 and 5.3 demonstrate sample locations and some examples of the erratics sampled. The exposure histories of the rock surfaces in question were estimated by the measurement of the concentration of the terrestrial *in situ* cosmogenic nuclides (TCN) ^{10}Be and ^{26}Al. These radionuclides are produced in the upper decimeters of rock surfaces exposed to cosmic ray bombardment where these rare isotopes are formed within the lattices of certain minerals (Lal, 1991; Gosse and Phillips 2001). The measured concentration of the radioactive isotope can be used to calculate an exposure age of the surface provided that the rate of production of the TCN in question is known (Cerling and Craig, 1994).

5.7 Samples and analytical methods

Dr M.J. Bentley, supported in the field by the British Antarctic Survey undertook sampling in the Austral summers of 1999 and 2000. In total twelve samples were analysed for their TCN concentrations of the isotopes ^{10}Be and ^{26}Al, together with a total of 4 chemistry blanks. These have been combined with data from 16 samples analysed for their isotopes ^{10}Be and ^{26}Al concentrations in this region by Dr M.J. Bentley.

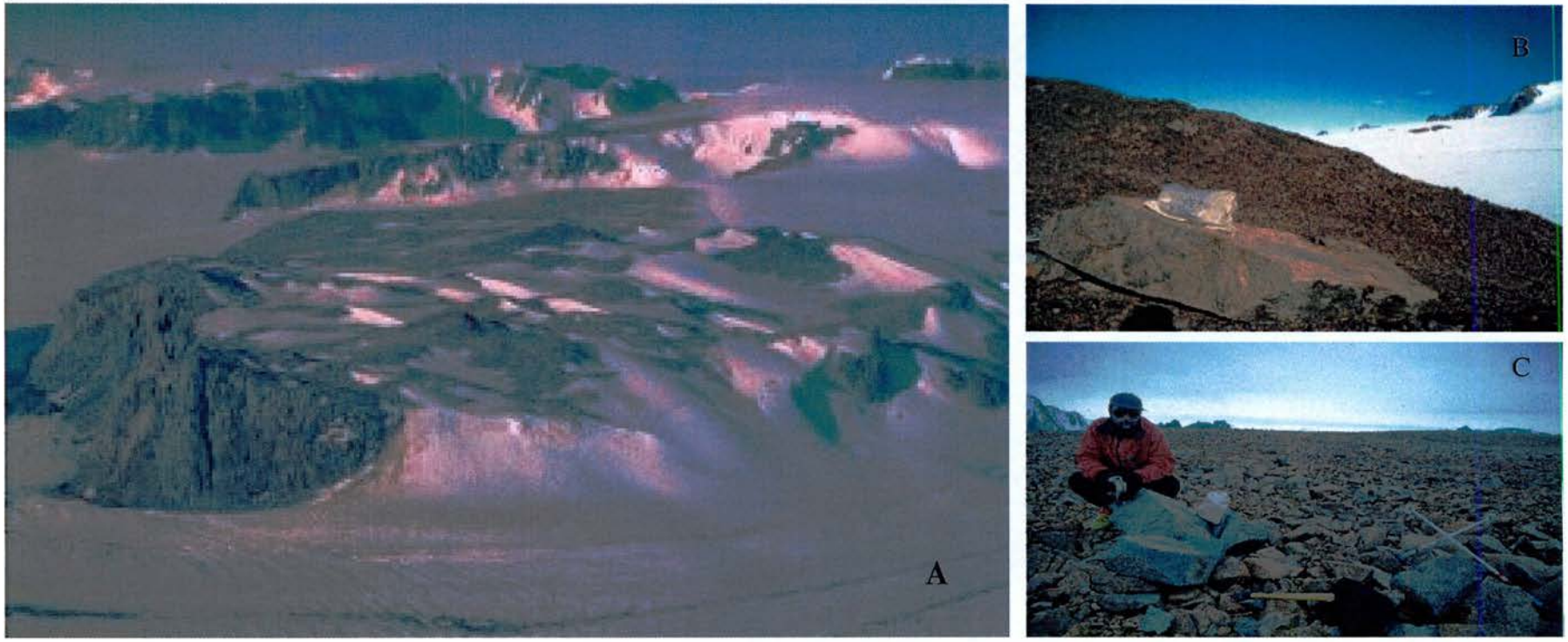

Figure 5.2. The Batterbee Mountains. A. A general view when flying from the south, with a large outlet glacier of the Peninsula Ice Sheet flowing west into George VI Sound. B. A large (1 by 3m) granite glacial erratic located at 860m altitude with an error weighted mean exposure age of 25,589±3,019 yr BP. C A small (1 by 1m) granidiorite boulder located at 426m with a mean age of 17,881±1,504 yr BP.

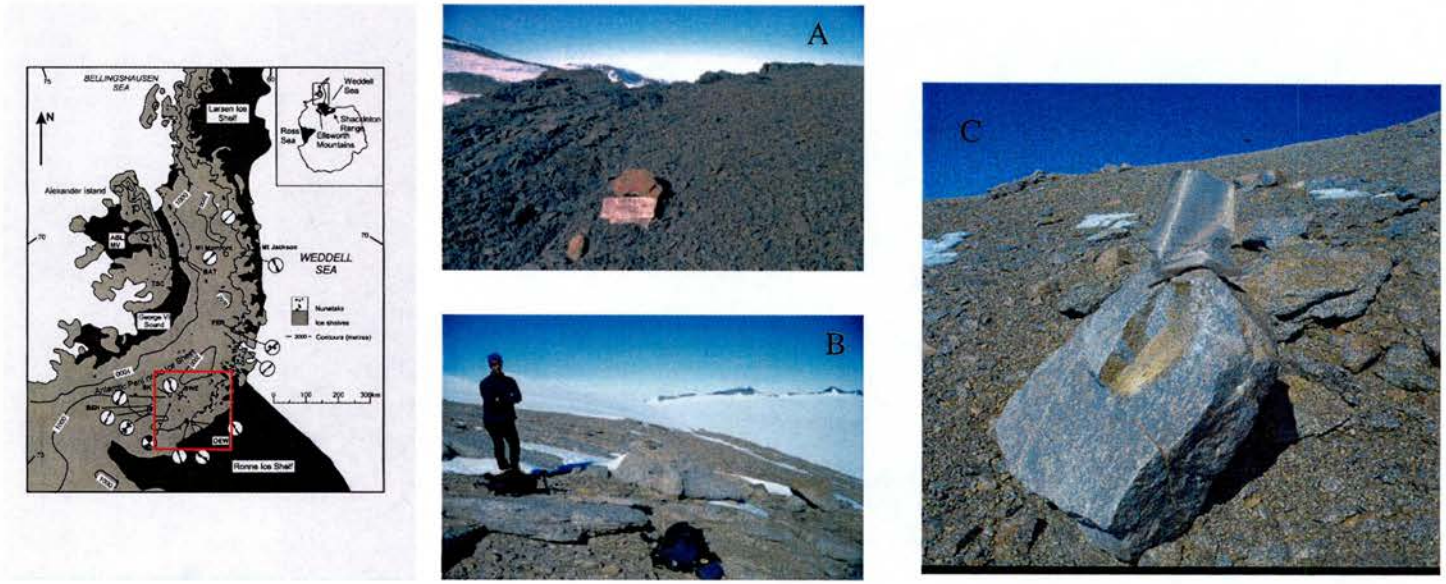

Figure 5.3. Typical samples from the nunataks located in the ice dome centred on the more continental portion of Antarctic Peninsula. This is highlighted on the Antarctic Peninsula map of Bentley and Anderson (1998). A. Small (50cm) granite erratic lying on sedimentary rocks on Mt Dewe. B & C. Typical erratics found on Nunataks in the Behrent Mountains giving exposure ages of around 11ka BP.

The analysis of two independent radionuclides with different production rates and decay constants, provides a indication of possible complex exposure histories or sample processing problems. This approach was first proposed by Lal and Arnold (1985), and is based on fact that the half-lives differ markedly and ratio between the production rates of the isotopes is known. Therefore any significant periods of exposure or burial of the sample will cause the eventual ratios of different nuclides to vary.

The isotopes ^{10}Be and ^{26}Al were selectively extracted from the quartz component of the whole rock sample following the standard procedures described by Kohl and Nishizumi (1992) and Ivy-Ochs (1996). The isotopic ratios were measured at the ETH tandem accelerator mass spectrometry (AMS) facility in Zurich, Switzerland. In this study the reference production rate used is that of Kubik *et al* (1998), which has been determined experimentally. *In situ* production of the cosmogenic nuclide ^{10}Be is a combination of three principle components, the most important being spallation, with fast and stopped muons making a less significant contribution to total production. There is strong evidence that the relative muon contribution to total production is much lower than the 16% originally assumed (see Heisinger, 1997 and Stone 2000 for discussion). Therefore this study incorporates the modified values of Kubik *et al* (1998) to provide a more accurate representation of the stopped and fast muon components (Heisinger, 1997; Stone 2000). Therefore the reference production rate for ^{10}Be used is a spallation component of 5.22±0.22 atoms/g (qtz)/yr, together with a value of 0.12 atoms/g (qtz)/yr for stopped muons and 0.027 atoms/g (qtz)/yr for fast muons (Schaller *et al.*, 2001). Including muons, this results in a total surface production rate (P_0), at sea level and high latitude (SLHL) for ^{10}Be of 5.37±0.22 atoms/g (qtz)/yr, with a ^{26}Al /^{10}Be ratio of 6.5±0.43 (Kubik *et al.*, 1998). This value was chosen for three reasons; (1) it is referenced to the calibrated radiocarbon timescale; hence the exposure ages given here should be directly comparable to calibrated radiocarbon ages, (2) all relevant data necessary for the calculations are available, (3) due to the lack of a suitable calibration site in the southern hemisphere on this time scale.

The reference production rate was scaled to that of the site in question following the methods outlined by Stone (2000). The total production at the sample site, was corrected for attenuation of cosmic radiation due to the thickness of the sample itself, and any shielding due to the surrounding topography following the procedures of Dunne *et al.* (1999). These correction factors were applied to model the effect of the reduced incoming cosmogenic signal on the total

production at the sample site. No correction has been made for the possible effect of changing eustatic sea level on atmospheric pressure, and thereby the production rate of the sample in question. It is acknowledged that this could make a significant difference to the age of the samples, but modelling this accurately through time would be very difficult due to the frequency of sea level variation through the Quaternary. To provide a maximum constraint ages were recalculated assuming atmospheric pressure at the time of maximum eustatic sea level lowering at the LGM (-120 m) throughout the exposure period. Recalculating the production rates would cause an 11% increase in exposure age. Although significant this represents an absolute maximum, and any real variation would be much less than this.

Errors related to the AMS, the production rate and 5% sample reproducibility are added quadratically, and calculated as a function of the eventual age. In order to provide a realistic age envelope, the ages have been calculated for the effect of surface erosion, at rates of 1mm, 3mm and 1cm per 1000 years. The rate of erosion will obviously vary with lithology and environmental conditions. Therefore, this is only offered as a guide to the possible upper and lower age limits of the surface in question. Erosion is not thought to be a problem as most of the samples retained signs of active glacial transport, such as striations or plucking.

5.8 Results

The cosmogenic radionuclide data related to the AMS data and field and procedural elements are summarised in Table 5.1. Table 5.2 presents the sample descriptions and cosmogenic radionuclide ages calculated as described above. As might be expected from the first attempt to constrain the glacial chronology of such a large area, a complex picture emerges from the TCN analysis. There is no clear relationship between age and altitude, as might be expected from a simple decline in ice surface altitude over time. This suggests that some of the erratic boulders have been reworked.

Following the approach of Owen *et al.* (2001), we have analysed the ^{26}Al /^{10}Be age ratio to aid interpretation of each sample's history. Ratios close to 1 represent concordant ^{26}Al and ^{10}Be ages and imply both a simple sample history and analytical integrity. Low ^{26}Al /^{10}Be ratios can

Table 5.1. Cosmogenic radionuclide data

Sample Id	Location	Latitude (°S)	Altitude	shielding and depth correction [1]	sample mass (g)	Carrier Be (mg) [2]	Al (ppm) [3]	Measured $^{10}Be/^{9}Be$ ratio [4]	± % error	^{10}Be (at/g) blank corrected [5]	± % error [7]	Measured $^{26}Al/^{27}Al$ ratio [6]	±% error	^{26}Al (at/g)blank corrected [5]	± % error [7]
9.2/3	BEH 1	75	1.22	0.947678	20.6781	0.5	123	9.70E-14	6.9	131520.9	12.57038	4.01E-13	11	1065150	13.6
9.2/1	BEH 2	75	1.18	0.955151	47.7424	0.499	240	3.89E-13	5.9	223210.2	7.672032	2.72E-13	7.6	1387347	9.3
9.2/2	BEH 3	75	1.20	0.956219	33.05227	0.50397	115	2.28E-13	16.6	195621	5.471729	6.32E-13	5.1	1588776	8.4
13.4/1	DEW 1	75	0.96	0.981193	25.9531	0.5	138	1.063E-12	5.7	1348355	9.075853	2.35E-12	6	7204160	11.2
13.4/2	DEW 2	75	1.00	0.954889	32.76641	0.50397	186	7.15E-13	14.6	697841	9.464036	1.17E-12	4.2	4803086	12.6
15.2/2	DEW 3	75	0.99	0.95632	16.3755	0.50397	N/A	2.80E-13	9.8	501777.1	6.744027	7.23E-13	6.3	0	9.2
13.4/5	DEW 4	75	0.92	0.955443	23.929	0.49408	21	7.19E-13	4.0	957923.4	12.68486	1.35E-12	5.3	5576439	10.3
13.4/6	DEW 5	75	0.91	0.953014	51.132	0.49408	10	1.05E-12	4.0	661237.9	6.475659	1.03E-12	6.6	3380050	8.4
20.3/1	BAT 1	71	0.86	0.956303	26.1364	0.499	319	4.3E-13	6.5	460545.9	0	3.32E-13	9.6	2271200	8.2
19.2/1	BAT 2	71	0.35	0.955939	21.61503	0.499	241	2.1E-13	6.9	217662	27.31842	3.14E-13	6.6	1619040	9.9
20.1/1	BAT 3	71	0.86	0.956319	28.8585	0.501293	166	1.00E-12	25.0	1084232	35.37425	6.33E-13	6.6	2297068	9.8
19.2/2	BAT 4	71	0.426	0.956142	50.348	0.49408	10	2.89E-13	5.6	173244.2	25.94503	4.55E-13	8.3	1062961	10.9
2000-01	BAT 5	71	0.35	0.947826	19.034	0.5021	26	6.77E-14	7.5	75618.55	7.846808	3.76E-13	6.5	726029.2	8.3
2000-02	BAT 6	71	0.33	0.956253	31.32849	0.502164	16	1.60E-13	7.3	127135.8	21.41589	4.5E-13	5.7	822040.8	8.9
2000-04	BAT 7	71	0.27	0.939344	41.18	0.5021	12	5.88E-13	4.0	458775.6	16.27775	1.18E-12	3.7	2495317	8.3
2000-05	BAT 8	71	0.23	0.956303	20.31041	0.502164	25	1.23E-13	6.7	135968.3	13.39289	5.28E-13	6.2	1077849	9.6
17.3/1	FER 1	73	1.59	0.95632	30.15318	0.499	269	1.15E-12	4.2	1194379	0	1.26E-12	5.8	7474733	8.4
18.2/2	FER 2	73	1.36	0.96255	35.905	0.499	257	7.59E-12	2.2	6983427	8.04682	5.77E-12	4.5	33022002	11.0
18.2/3	FER 3	73	1.33	0.914252	35.01984	N/A	N/A	N/A	N/A	0	6.518128	9.9E-12	4.5	0	8.8
4.1/2	SKY 1	75	1.70	0.955785	27.33519	0.499	704	2.71E-12	4.0	3216740	6.475536	9.21E-13	4.3	14266997	9.7
4.1/1	SKY 2	75	1.70	0.955785	21.3793	0.50397	517	1.96E-12	5.9	3032165	15.79774	1.53E-12	4.3	17539135	9.7
2.4/1	SWE 1	76	1.28	0.955487	35.01984	0.501293	100	N/A	N/A	0	12.45531	2.12E-12	4.2	4698142	11.4
30.1/1	ABL 1	71	0.69	0.931247	38.69155	0.501293	95	5.38E-13	30.5	406117.6	6.552156	5.02E-13	6.3	1036828	8.0
30.1/2	ABL 2	71	0.69	0.956229	20.56044	0.501293	164	3.55E-13	20.4	466109.5	13.99299	7.04E-13	8	2529274	11.1
2000-09	TSC 1	72	0.376	0.939492	27.79316	0.502164	18	8.79E-14	13.3	56622.81	29.36058	3.44E-13	6	515456.3	13.0
2000-10	TSC 2	72	0.365	0.956246	29.0154	0.502164	17	9.74E-14	8.2	65223.94	19.35679	2.33E-13	7.6	450388.4	17.4
MV1	MV1	71	0.6	0.955775	10.9054	0.50239	46	8.40E-14	6.4	182235.1	12.32203	4.69E-13	7.8	1311357	10.6
MV2	MV2	71	0.65	0.955775	22.70545	0.50239	22	2.66E-13	6.4	332662.8	9.571807	1.53E-12	5.6	1954967	9.1
MV5	MV5	71	0.5	0.931303	6.8341	0.50239	74	5.60E-14	11.6	73682.07	63.31756	1.82E-13	8.7	809761	12.4

Continues on next page.

Table 5.1 continued. Cosmogenic radionuclide data (Samples in bold were processed by MJB, samples in plain text by CJF. All samples re-interpreted, by CJF).

1. Depth shielding calculated using "flat" dependency of Massirik and Reedy (1995); topographic shielding calculated using the relationship $\sin^{2.3}\theta$, for 360^0 around the sample, where θ is the angle of the topographic obstruction from the horizontal.
2. Carrier addition measured by calibrated pipette, and corrected for temperature and density.
3. Measured from aliquot of whole sample by ICP-AES.
4. Reported $^{10}Be/^{9}Be$ ratio from AMS measurements, include errors & corrections related to "in-house" standard.
5. Removes possible effects of exposure and chemical loading of samples measured during same accelerator run.
6. Reported $^{26}Al/^{27}Al$ ratio from AMS measurements, include errors & corrections related to "in-house" standard.

Table 5.2. Sample details and TCN ages

Sample ID	Location[1]	Altitude (km)	Sample description[2]	^{10}Be age[3]	± Error	^{26}Al age[4]	± Error	Error weighted mean[5]	± error	Al/Be age ratio[6]	±Error	Comments[7]
9.2/3	BEH 1	1.22	E	6,761	1,115	8,445	1,434	7,395	880	1.25	0.24	
9.2/1	BEH 2	1.18	E	11,789	1,483	11,304	1,585	11,562	1,083	0.96	0.15	
9.2/2	BEH 3	1.20	E	10,143	2,759	12,722	1,415	12,185	1,259	1.25	0.21	
13.4/1	DEW 1	0.96	E	85,314	9,219	71,154	8,258	77,458	6,151	0.83	0.11	Possible burrial history
13.4/2	DEW 2	1.00	E	43,379	9,040	46,505	4,801	45,818	4,240	1.07	0.15	low Al/Be ratio in zone in forbidden zone due to blank correction
15.2/2	DEW 3	0.99	E	31,334	5,442					0.00		
13.4/5	DEW 4	0.92	E	64,189	6,123	58,252	6,409	61,356	4,427	0.91	0.11	
13.4/6	DEW 5	0.91	E	44,621	4,230	35,327	4,243	39,989	2,996	0.79	0.10	Possible burrial history
20.3/1	BAT 1	0.86	E	32,305	4,110	24,618	3,824	28,185	2,800	0.76	0.13	Possible burrial history
19.2/1	BAT 2	0.35	E	24,857	3,977	28,676	3,563	26,976	2,654	1.15	0.17	low Al/Be ratio in zone in forbidden zone due to blank correction
20.1/1	BAT 3	0.86	E	76,830	26,245	24,902	3,039	25,589	3,019	0.32	0.16	Possible metoric contamination
19.2/2	BAT 4	0.426	E	18,290	1,991	17,337	2,294	17,881	1,504	0.95	0.14	
2000-01	BAT 5	0.35	E	8,677	1,699	12,871	1,495	11,040	1,122	1.48	0.21	Small sample size
2000-02	BAT 6	0.33	E	14,781	2,322	14,758	2,013	14,767	1,521	1.00	0.16	
2000-04	BAT 7	0.27	E	58,365	5,395	49,344	4,728	53,263	3,556	0.85	0.09	Possible burrial history
2000-05	BAT 8	0.23	E	17,559	3,049	21,550	2,850	19,689	2,082	1.23	0.19	
17.3/1	FER 1	1.59	E	45,455	4,521	44,240	5,154	44,927	3,399	0.97	0.12	low Al/Be ratio in zone in forbidden zone due to blank correction
18.2/2	FER 2	1.36	E	339,256	29,647	258,114	28,088	296,495	20,390	0.76	0.09	Possible burrial history
18.2/3	FER 3	1.33	E									
4.1/2	SKY 1	1.70	E	114,267	11,095	78,881	8,397	91,768	6,696	0.69	0.08	High Al from Aliquot
4.1/1	SKY 2	1.70	E	107,546	12,058	97,849	10,377	101,975	7,866	0.91	0.11	High Al from Aliquot
2.4/1	SWE 1	1.28	E			35,595	3,687					
30.1/1	ABL 1	0.69	E	34,225	14,917	13,424	1,605	13,662	1,595	0.39	0.24	Possible metoric contamination
30.1/2	ABL 2	0.69	E	38,291	12,313	32,180	4,291	32,842	4,052	0.84	0.22	Possible burrial history
2000-09	TSC 1	0.376	E	6,381	2,272	8,962	1,396	8,254	1,190	1.40	0.35	
2000-10	TSC 2	0.365	E	7,304	1,735	7,775	1,621	7,555	1,185	1.06	0.28	
MV1	MV1	0.6	E	16,228	2,565	18,055	2,329	17,229	1,724	1.11	0.17	
MV2	MV2	0.65	E	28,326	3,601	25,761	2,853	26,750	2,236	0.91	0.12	
MV5	MV5	0.5	E	6,719	5,684	11,405	1,890	10,939	1,793	1.70	1.00	Small sample size

Continues on next page.

Table 5.2 continued. Sample details and TCN ages (Samples in bold were processed by MJB, samples in plain text by CJF. All samples re-interpreted, by CJF).

1. Locations; BEH=Behrents Mountains, DEW=Mt Dew, BAT=Batterbee Mounatins, FER=Fergurson Nunataks, SKY=Sky Hi Nunataks, SWE=Sweeny Mountains, ABL=Ablation Point, TSC=Two-Steps Cliff, MV=Moutonee Valley.
2. Sample description; E=Erratic on bedrock surface.
3. Calculated using a ^{10}Be production rate of 5.37±0.22 at/g/yr (Schaller et al., 2001), scaled following the methods outlined by Stone (2000), which are a reformulation of those of Lal (1991).
4. Calculated using a ^{26}Al/^{10}Be ratio of 6.5 (Kubik 1998).
5. Error weighed mean of Al and Be exposure ages.
6. Ratio of Al age to Be age, Ratios close to one signify a simple exposure history, with no anylitical problems.
7. Comments on possible sample processing or analyltical problems.

indicate a complex exposure or burial history, reflecting the more rapid decay of ^{26}Al than ^{10}Be, when there is no isotopic production. These criteria have been used to reject samples from Mt Dewe, which have generally low ratio values, and show a large spread of ages from 85.3 to 31.3 ka. On this basis we have identified 11 samples from Mt Dewe, the Batterbee Mountains, Sky-Hi and other locations as being probably reworked.

Alternatively very low or high ^{26}Al /^{10}Be ratios could indicate contamination of a sample may have occurred. Very low ratios indicate that contamination may have occurred during sample processing. This has been identified in two samples from one laboratory batch, with ratios as low as 0.4. On the basis we reject the results from this laboratory batch from further discussion (ABL1, ABL3, BAT3). It is noted that the inclusion of these samples would not change the overall interpretation.

A further criteria that could indicate possible reworking or complex exposure history was when samples in close proximity (<100m) record widely diverging ^{10}Be ages. In this case we have made the assumption that the youngest of the adjacent samples represents a reasonable age for deglaciation. This rationale has been followed in the Batterbee Mountains where we have assumed that a cluster of dates (i.e. those within error) are more likely to record the timing of glaciation than an older outlier which may well have survived from earlier phases of glaciation. The apparent outlier sample (BAT 2) has a exposure age of 24.9 ka, but sits closely adjacent to a boulder dated to 18.3ka. It is suggested that the 18.3ka erratic is part of a cluster of ages that provide a more reliable age for deglaciation than the single 24.9ka age.

Due to its higher analytical precision, we believe the best approach is to treat the ^{10}Be age as the most reliable age estimate, so all subsequent discussion will focus on the ^{10}Be ages only. On the basis outlined above we can identify those samples that have a complex or reworked exposure history. After excluding these samples a number of inferences can be made from the cosmogenic data.

5.9 Discussion of Results

The exposure age estimates from this study indicate that the pattern of deglaciation of this area is complex. This may well be a function of multiple stages of deglaciation and re-growth of the ice centres located on the Antarctic Peninsula and Alexander Island, which may have reincorporated previously exposed erratics during the Quaternary. However, it is possible to recognise patterns of deglaciation and suggest possible causal mechanisms for deglaciation. It is important to note that we found no moraines or other depositional landforms of deglaciation that can be directly dated. All of the ages reported here are assumed to record the withdrawal of ice from the bedrock surface on which the erratic samples now lie.

From analysis of the sample data it can be seen that there are three clusters of ages, separated by age and altitude relationships in the last 30,000yrs. These can be seen in Figure 5.4, where the sample exposure ages are seen plotted against the record of eustatic sea level over the past 35,000yrs. The implications of these data are discussed below.

The oldest sample ages for deglaciation occurred between 18.3 and 14.8 ka, and come from the Batterbee Mountains on the eastern flank of George VI Sound. The age of 18.3 ka comes from a sample (BAT4) lying on a bedrock ridge on a plateau in the Maclaughlin Cliffs area of the Batterbee Mountains, west side of George VI Sound. ^{26}Al and ^{10}Be ages for this sample are concordant. Another date for deglaciation of 17.6 ka comes from an erratic (BAT 8) a few hundred metres away on the same plateau, as does a sample (BAT 6) with highly concordant ^{10}Be and ^{26}Al ages of c. 14.8 ka. Further north, an erratic (MV1) at 600m altitude in Moutonnee Valley implies deglaciation was underway here by at least 16.3 ka. Other, older ages at these sites are assumed to represent reworking.

The youngest sample ages come from the west side of George VI Sound. Erratics at Two Step Cliffs, directly across George VI Sound from the Batterbee Mountains, yield ages for deglaciation of 7.3 ka and 6.4 ka. Further north, an erratic (MV5) at 500m altitude above

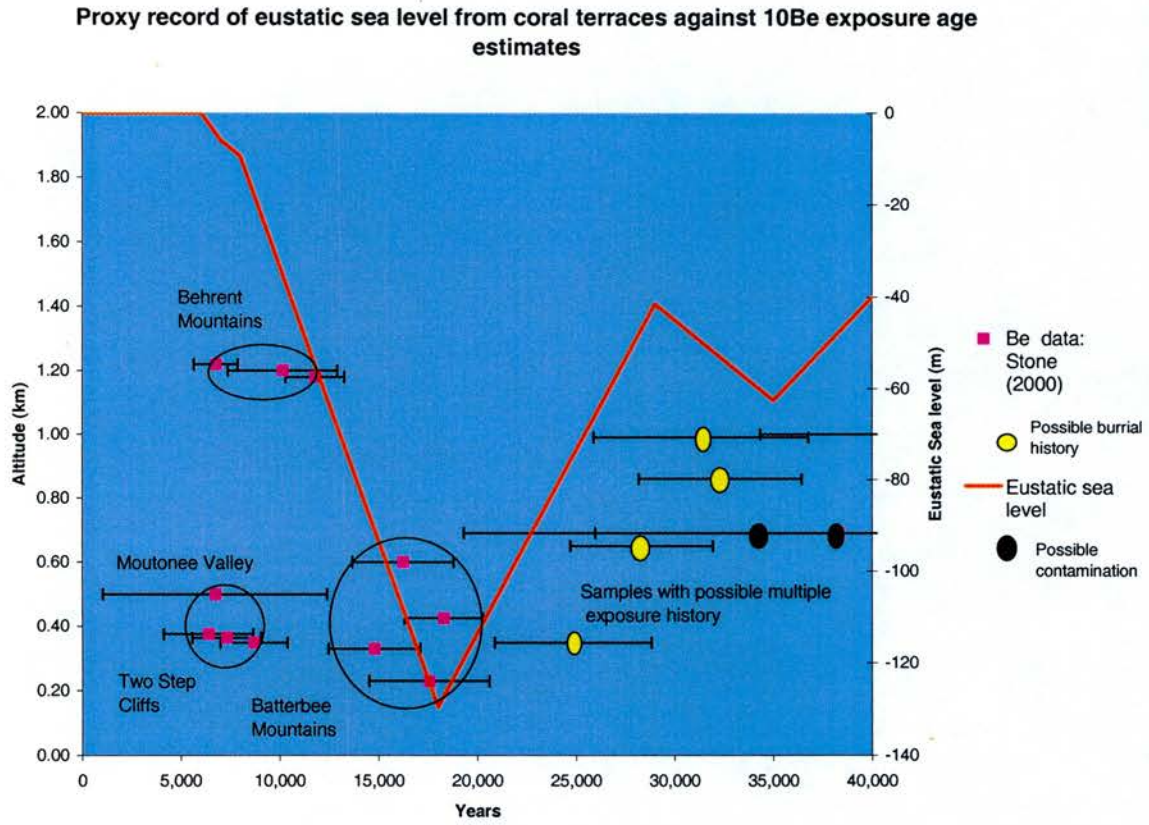

Figure 5.4. Erratic exposure ages plotted against the eustatic sea level record as recorded by the Paupa New Guinea sea level terraces over the past 40,000yr (From Shackleton, 1987).

Moutonnee Valley implies deglaciation of this level by 6.7 ka. An erratic (BAT5) on the Maclaughlin Cliffs plateau yields an exposure age of 8.7 ka.

Three erratics from a nunatak in the Behrendt Mountains, east of the Peninsula ice divide, yield ages of 11.8-6.1 ka. The dates are from erratics of the same grantitic lithology on the same nunatak, and imply thinning in this area by 11.8 ka.

5.10 Interpretation

The dates from George VI Sound suggest that there was a two-step deglaciation of this area. The first step saw ice thinning at 18.3 - 14.8 ka. This represents a thinning from the LGM. The second step of deglaciation is shown by dates from both sides of George VI Sound, with ice retreat underway on the east side of the sound by 8.7 ka, and on the west side by at least 7.3 ka.

The dates from the Behrendt Mountains reflect thinning of the Weddell Sea side of the Peninsula ice sheet, close to the ice divide. This thinning was most likely linked to retreat of grounded ice in the Weddell Sea to the east. The response at the ice divide would be delayed relative to the retreat of the grounded margin and so the date of 11.8 ka is unlikely to be a close minimum for deglaciation of the Weddell Sea. We attempted to more closely constrain the deglaciation of the Weddell Sea by dating seven samples from the Mt Dewe and Ferguson nunataks areas. Almost all of the samples analysed have complex exposure histories and so we are unable to use these to provide a close date for retreat of the south-eastern sector of the Antarctic Peninsula ice sheet.

The samples from the Sky-Hi nunataks also lie close to the ice divide. The ^{10}Be dates of 114 and 108 ka are intriguing as they fall within the last interglacial and if interpreted alone might suggest continuous exposure of this part of the ice divide since the penultimate glaciation. However, the ^{26}Al ages suggest that one, or perhaps both, of the samples may have had a burial history. In such a case they are much older than the apparent ages. This is something that should be tested by further analyses from this region of the ice divide.

Finally, the presence of numerous reworked boulders scattered across nunataks in the southern Antarctic Peninsula provide the first direct terrestrial evidence that there has been repeated glaciation of the Peninsula, over several glacial cycles.

5.11 Wider Implications

It is acknowledged that this interpretation is dependent on both the robust measurement and analysis of the TCNs, and the arguments regarding the acceptance or rejection of exposure ages. These data indicate that sea level would have been the primary control on behaviour of the Peninsula ice sheet, particularly given the minimal surface melting (Payne *et al.*, 1989). Initial ice sheet lowering in George VI Sound closely followed the onset of post-LGM eustatic sea level rise at c. 19 ka (Figure 5.4). We speculate that such a rapid response may have been linked to the presence of an ice stream in the George VI Sound trough extending to the shelf in Marguerite Bay (Kennedy and Anderson, 1989). Such an ice stream would have been sensitive to initial sea level rise and may have led to downdraw at the southern end of the ice stream. In such a case it is likely that thinning would lag the sea level rise by 1-4 ka.

Threre are two possible mechanisms for the second phase of deglaciation. The first is that the George VI Sound outlet glacier saw a second, rapid decline after 8.7 ka. There is no obvious rapid rise in sea level at this time but it may represent an internal threshold of stability for the outlet glacier responding to progressive sea level rise. The second mechanism requires a one-step decline of the George VI Sound outlet was followed by *local* ice advance and subsequent retreat, perhaps related to increased moisture supply after the LGM. For example, the 8.7 ka date is close to the present local ice cap margin and so it is possible that this date reflects retreat of this local ice mass rather than the main outlet in George VI Sound. Similarly, the dates on the west side of the Sound could reflect withdrawal of Alexander Island ice, rather than the main outlet glacier. The complexity of the pattern of dates means that we are currently unable to distinguish between these two alternative explanations. The retreat of a George VI Sound outlet glacier or ice stream would be closely linked to behaviour of the grounded ice margin on the continental shelf in Marguerite Bay to the north. However, at present there are no reliable dates for deglaciation of this region. It is interesting to note that Pudsey *et al.* (1994) suggested that

there was a two-step deglaciation recorded on the shelf north of Marguerite Bay from the analysis of marine cores.

The onset of ice sheet decline at c. 18.3 ka was relatively early, compared to other areas of the WAIS, and could imply a rapid response to sea level rise following the LGM. The Ross Sea sector of the WAIS did not undergo significant decline until sometime after 12,700 ^{14}C yrs BP (15,400 cal yr BP) with major grounding line retreat not occurring past Ross Island until 8340 14C yr BP (c.9400 cal yr BP) (Conway *et al.*, 1999). One explanation of the contrast is that the relatively small ice mass, and relatively high accumulation and ablation rates of the Antarctic Peninsula Ice Sheet (and particularly the Pacific margin), make it the most sensitive part of the Antarctic ice sheet.

5.12 Conclusions

Cosmogenic exposure dating of glacial erratics on ice free areas of the Antarctic Peninsula indicate a very complex pattern of deglaciation. In part this can be seen as the result of attempting to constrain deglaciation over such a large area with limited control points, but it also reflects the complex controls of glaciation of this region. Through careful analysis of the available data this work draws the following conclusions:

- Deglaciation of George VI Sound occurred as a two-step process, with ice cap thinning after the LGM between 18.3 - 14.8 ka. This was followed by a second step of more comprehensive deglaciation, with ice retreat on the eastern side of the Sound at 8.7ka, and on the western side at 7.3ka.
- In the central portion of the APIS, exposure ages from the Behrendt Mountains suggest deglaciation at 11.8ka. The age and location of these samples probably reflect a delayed response to retreat of grounded ice in the Weddell Sea.
- The wide range of ages and indication of complex exposure histories from all of the available erratics provides the first terrestrial evidence that there has been repeated glaciation of the Antarctic Peninsula, over several glacial cycles.

5.13 References

Bell CM. 1975. Structural geology of parts of Alexander Island. British Antarctic Survey Bulletin 41 and 42, 43-48.

Bentley MJ. 2000. Glacier and ice shelf history, George VI Sound. Un-published BAS field report. R/1999/GL3.

Bentley MJ, Anderson JB. 1998. Glacial and marine geological evidence for the ice sheet configuration in the Weddell Sea-Antarctic Peninsula region during the Last Glacial Maximum. Antarctic Science 10. 3. 309-325.

Blunier T, Chappellaz J, Schwander J, Dällenbach A, Stauffer B, Stocker TF, Raynaud D, Jouzel J, Clausen HB, Hammer CV, Johnsen SJ. 1998. Asynchrony of Antarctic and Greenland climate during the last glacial period. Nature 394: 739-743.

Cerling TE, Craig H. 1994. Geomorphology and *in situ* cosmogenic isotopes. Annual Reviews of Earth and Planetary Sciences 22. 373-317.

Clapperton CM, Sugden DE. 1982. Late Quaternary glacial history of George VI Sound area, West Antarctica. Quaternary Research 18. 243-267.

Conway H, Hall BL, Denton GH, Gades AM, Waddington ED. 1999. Past and future grounding-line retreat of the West Antarctic Ice Sheet. Science 286 (5438). 280-283.

Denton GH, Hughes TJ (eds). 1981. The last great ice sheets. Wiley-Interscience.

Denton GH, Anderson BG, Rutford RH, Anderson BG. 1992. Glacial history of the Ellsworth Mountains, West Antarctica. Geological Society of America Memoir. 170. 403-432.

Dunne J, Elmore D, Muzikar P. 1999. Scaling factors for the rates of production of cosmogenic nuclides for geometric shielding and attenuation at depth on sloped surfaces. Geomorphology. 27(1-2)3-12.

Elliot MH. 1974. Stratigraphy and sedimentary petrology of the Ablation Point area, Alexander Island. British Antarctic Survey Bulletin 39. 87-113.

Gosse JC, Phillips FM. 2001. Terrestrial in situ cosmogenic nuclides: theory and application. Quaternary Science Reviews 20. 1475-1560.

Hallet B, Putkonen, J. 1994. Surface dating of dynamic landforms:young boulders on ageing moraines: Science. V.265. 937-940.

Heisinger B. 1997. *In situ* production of radionuclides at great depths. Nuclear Instruments and Methods. B. 123. 341-346.

Hughes T. 1975. The West Antarctic Ice Sheet: Instability, disintegration, and initiation of ice ages. Reviews of Geophysics and Space Physics 13. 502-526.

Ivy –Ochs S. 1996. The dating of rock surfaces using the in situ produced ^{10}Be, ^{26}Al, and ^{36}Cl, with examples from Antarctica and the Swiss Alps. Ph. D. Thesis, Swiss Federal Institute of Technology, Zurich. 196pp.

Kennedy DS, Anderson JB. (1989). Glacial-marine sedimentation and Quaternary glacial history of the Marguerite Bay, Antarctic Peninsula. Quaternary Research **31.** 255-276.

Kohl CP, Nishizumi K. 1992. Chemical isolation of quartz for measurement of *in situ* produced cosmogenic nuclides. Geochemica et Cosmochemica Acta. 56. 3583-3587.

Kubik PW, Ivy-Ochs S, Masarik J, Frank M, Schlüchter C. 1998. ^{10}Be and ^{26}Al production rates deduced from an instantaneous event within the dendro-calibration curve, the landslide of Köfels Ötz Valley, Austria. Earth and Planetary Science Letters 161. (1-4). 231-241.

Lal D, Arnold JR. 1985. Tracing quartz through the environment. Proceedings of the Indian Academy of Science (Earth Planetary Science Section) 94. 1-5.

Lal D. 1991. Cosmic ray labelling of erosion surfaces: in situ nuclide production rates and erosion rates. Earth and Planetary Science Letters 104, 424-439.

Masarik J, Reedy RC. 1995. Terrestrial cosmogenic-nuclide production systematics calculated from numerical simulations. Earth and Planetary Science Letters. 136. 381-395.

Mercer JH. 1978. West Antarctic ice sheet and CO_2 greenhouse effect: a threat of disaster. Nature 271. 321-325.

Oppenheimer M. 1998. Global warming and the stability of the West Antarctic Ice Sheet. Nature 393. 325-332.

Payne AJ, Sugden DE, Clapperton CM. 1989. Modelling the growth and decay of the Antarctic Peninsula Ice Sheet. Quaternary Research 31. 119-134.

Pudsey CJ, Barker PF, Larter RD. 1994. Ice sheet retreat from the Antarctic Peninsula Shelf. Continental Shelf Research 14(15). 1647-1675.

Schaller M, von Blanckenburg F, Hovius N, Kubik PW. 2001. Large-scale erosion rates from in situ produced cosmogenic nuclides in European river sediments. Earth and Planetary Science Letters 188. 441-458.

Shackleton NJ. 1987. Oxygen isotopes, ice volume and sea level. Quaternary Science Reviews 6. 183-190.

Steig EJ, Brook EJ, White JWC, Sucher CM, Bender ML, Lehman SJ, Morse DL, Waddington ED, Clow GD. 1998. Synchronous climate changes in Antarctica and the North Atlantic. Science. 282. 92-95.

Stone JO. 2000. Air pressure and cosmogenic isotope production. Journal of Geophysical Research. 105. B10. 23,753-23,759.

Sugden DE, Clapperton CM. 1980. West Antarctic ice sheet fluctuations in the Antarctic Peninsula area. Nature 286. 378-381.

Sugden DE, Clapperton CM. 1983. Geomorphology of the Ablation Point massif, Alexander Island, Antarctica. Boreas. 12. 125-135.

Yokoyama Y, Lambeck K, De Deckker P, Johnstone P, Fifield LK. 2000. Timing of the Last Glacial Maximum from observed sea-level minima. Nature 406. 713-716.

CHAPTER 6

Preliminary constraints on age, erosion and uplift of the Shackleton Range, Antarctica: determined from the *in situ* cosmogenic nuclides ^{10}Be and ^{26}Al.

6.1 Abstract

The concentrations of the cosmogenic nuclides ^{10}Be and ^{26}Al in glaciated rock surfaces from the Shackleton Range, Antarctica provide minimum exposure ages and maximum rates of erosion for several landscape elements. Summits and plateau areas indicate minimum exposure ages of 1.6±0.1Ma to 3.0±0.3Ma, with maximum long-term erosion rates of between 10-35 cm/Ma. The high concentrations of the isotope ^{10}Be indicate little or no uplift of the massif during the exposure period.

These data point towards two major conclusions for the landscape and glacial evolution of this region. First the exceptionally low erosion rates indicate that the modern cold arid climatic conditions have persisted since at least Pliocene time. Second, the high concentrations of radionuclides suggest the glacial landscapes are millions of years old, and similar to relict glacial landscapes in the McMurdo sector of the Transantarctic Mountains. These dates provide firm constraints on the Quaternary expansion of the East Antarctic Ice Sheet during periods of maximum sea-level lowering in the Quaternary, including the Filchner-Ronne Ice Shelf, which marine evidence indicates was significantly expanded during the Last Glacial Maximum, did not thicken by more than 200-300m at the landward margin of the East Antarctic Ice Sheet.

6.2 Background

The evolution of presently ice-free areas such as the Shackleton Range can provide a unique insight into the history and therefore the past and present health of the Antarctic Ice Sheet. The Shackleton Range lies at the junction of the East Antarctic Ice Sheet (EAIS) and the Ronne-Filchner Ice Shelf (RFIS) (Figure 6.1). The history of past glaciation and landscape evolution could provide critical evidence on two major debates in Antarctic evolution and glaciology (Kerr and Hermichen, 1998).

The first debate concerns the uncertainty in the former extent of grounded ice in the area of the Weddell Sea embayment at the Last Glacial Maximum, for which only a few constraints exist (Denton et al., 1992; Elverhoi, 1981; Cararra, 1981; Kerr and Hermichen, 1998; Bentley and Anderson, 1998). The Weddell Sea is an area of substantial ice volume change in Antarctica at the LGM. Knowledge of the past behaviour of the ice draining into the Weddell Sea could contribute to two important questions (Bentley and Anderson, 1998). First, quantifying the extent of grounded ice within the embayment would help constrain the contribution of the WAIS to the global water balance during and after the LGM. Second, improved spatial and temporal control on the changing volumes of the ice masses of the WAIS, EAIS and the Antarctic Peninsula Region, could inform debate on the response of these ice masses to changes in climate forcing, such as temperature and sea level. At present our understanding is based mainly on glaciological modelling studies, that are poorly constrained by empirical knowledge.

Reconstructions based on field observations have been made by numerous workers, but still await the firm chronologies that have been obtained for LGM expansion in the Ross Sea Sector. At present the most comprehensive reconstruction of the LGM in the Weddell Sea is that of Bentley and Anderson (1998) (Figure 6.2). The comparison of this with numerically-derived glaciological models such as that of Huybrects (1992), demonstrates a generally good match, but there are some differences. These may be a function of several factors, including the spatial resolution of the data in question, gaps in the onshore field data, and the disparity between field evidence of glacial trimlines surrounding the Weddell Sea and ice core evidence. This last issue reflects the assumption that erosional trimlines, which have been mapped surrounding the embayment were cut by ice at the LGM. If so, the implied thickening disagrees with estimates

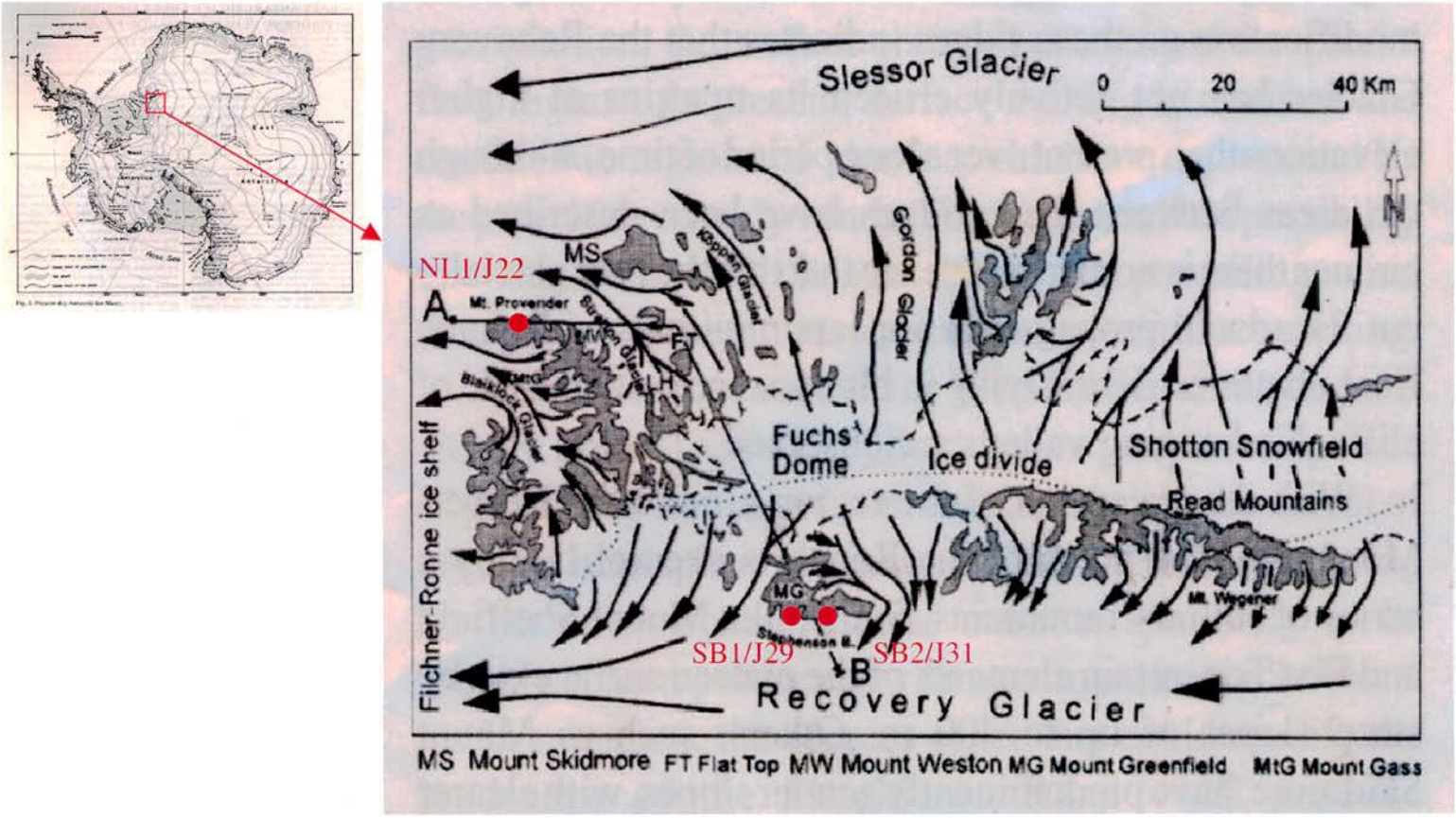

Figure 6.1. Location of the Shackleton Range within Antarctica, with detailed map, showing summits and principle ice-flow directions, after Kerr and Hermichen (1999). The positions of the sample sites are also shown and labeled.

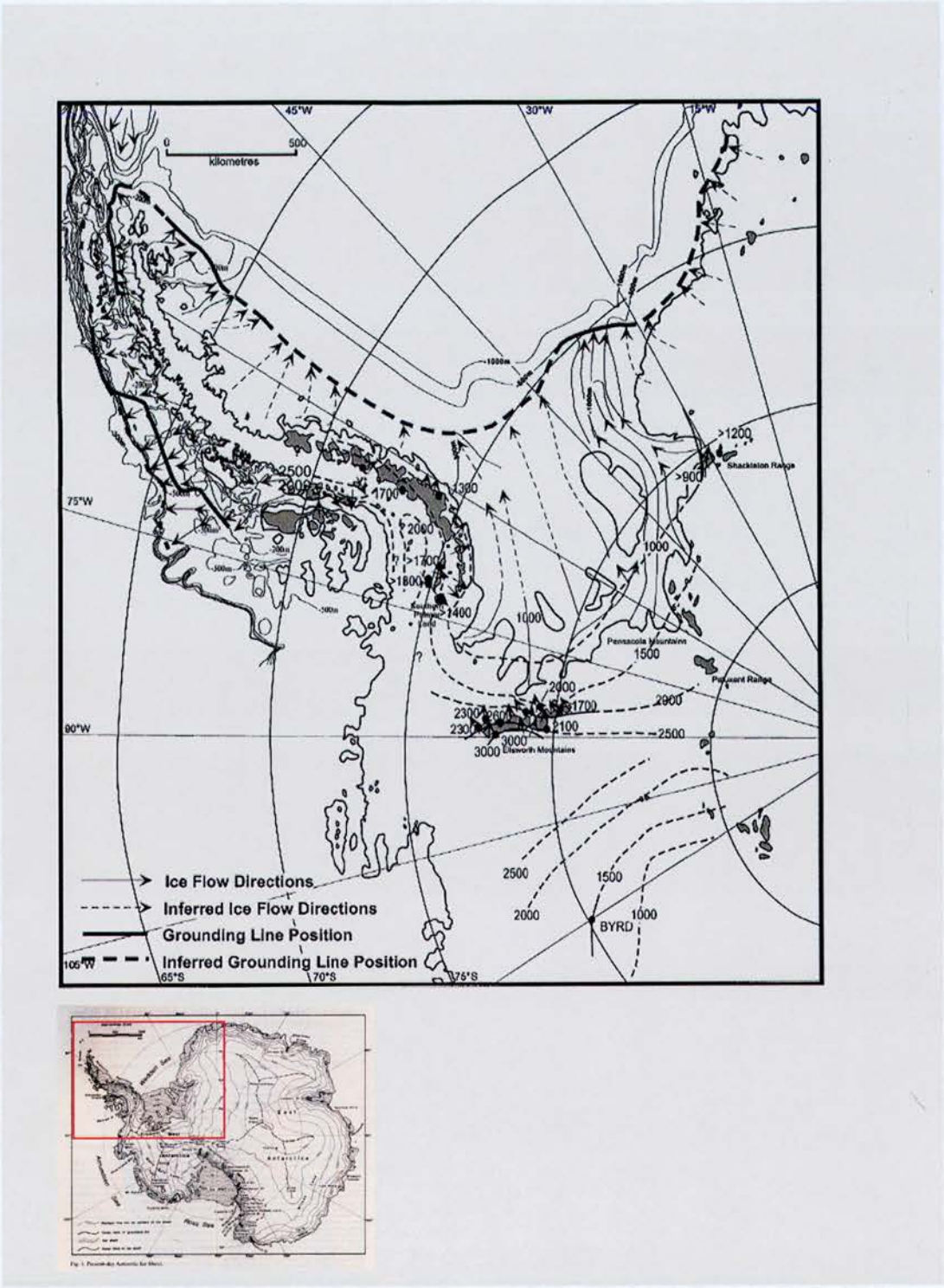

Figure 6.2. Field based reconstruction of ice thickness on land surrounding the Weddell Sea Embayment, from Bentley and Anderson (1999). This reconstruction indicates that ice thickening in the Shackelton Range was greater than 900m in the north west and greater than 1200m in the south east of the range, suggesting that all summits were covered.

from the analysis of gases trapped within ice, which suggest little or no change in altitude for the interior of Antarctica. With this in mind, the application of surface exposure dating provides the opportunity to date striated surfaces directly, providing a test of the age models for former ice expansion in the embayment.

This region may also shed light onto the Pliocene-Pleistocene evolution of the East Antarctic Ice Sheet, on which no direct chronology currently exists in this region. The question of whether the East Antarctic Ice Sheet has been a stable feature of Antarctica since achieving its modern configuration, or whether its size can vary significantly within a short period of time is critical to our understanding of both Antarctica and its global climatic significance (Sugden *et al.*, 1993). Debate on this question is divided into two hypotheses concerning the stability of the EAIS. One view, relying predominately on the interpretation of the Sirius Group glacial deposits in the Transantarctic Mountains, suggests that the EAIS has been fluctuating dramatically throughout its existence, and that it last disappeared during the Pliocene around 3Ma ago (Webb and Harwood, 1987). By analogy, acceptance of this hypothesis states that the modern ice sheet is susceptible to global warming. The alternative hypotheses, based on marine core and terrestrial evidence suggests that the EAIS has remained stable for at least 14Ma, and that the climate has remained cold and polar, similar to present throughout this period (Denton *et al.*, 1984; Sugden *et al.*, 1993; Kennett, 1993). These contrasting scenarios have profound implications with the EAIS locking up a mass of water equivalent to a 60m rise in global sea level (Drewry, 1982). The Shackleton Range remains an unknown with respect to these hypotheses, but may well hold evidence to contribute to this debate.

6.3 Introduction

As described by Kerr and Hermichen (1998), the Shackleton Range is well placed "to allow examination of the fluctuations of both East Antarctic and Filchner-Ronne ice." It is bounded to the north and south by outlet glaciers of the East Antarctic Ice Sheet, which drain westwards to the Filchner-Ronne Ice Shelf in the Weddell Sea (Figure 6.1). Therefore, the exposed landforms in this region provide a record of ice expansion from both the interior ice sheet and the ice shelf in the Weddell Sea embayment.

This area was visited in 1994/5 by the International EUROSHAK expedition, which aimed to build upon previous work to forward the understanding of both the geology and glacial history (Kerr and Hermichen, 1998). The glacial project was to assess the relationship of the present landscape to the past glaciation of this area. From this a relative chronology was developed based on the existence and preservation of different landscape elements within the range. Samples of bedrock were taken to constrain the age, erosion and uplift history of the Shackleton Range through the measurement of the concentrations of the *in situ* cosmogenic nuclides ^{10}Be and ^{26}Al within bedrock surfaces.

Kerr and Hermichen (1998), described three sources of ice which could modify the Shackleton Range. These are the East Antarctic Ice Sheet, the local ice caps, and the Filchner-Ronnie Ice Shelf. Expansion of any one of these glacial systems would leave a different signal of landscape evolution, which as indicated by other studies, would have been unlikely to have waxed and waned contemporaneously (Denton *et al.*, 1992). This is due to the differing controls on the net mass balance of these systems in the Antarctic environment. The controlling mechanisms and feedback loops involved in these systems are described by Kerr and Hermichen (1998), and are outlined in Table 6.1.

6.4 Geomorphic evidence of past glacial activity

The Shackleton Range is composed of a narrow, undulating plateau rising above two outlet glaciers draining the EAIS, the Slessor Glacier to the north and the Recovery Glacier to the south (Figure 6.1). Past studies of its glacial history have described the geomorphological evolution of this mountain range (Stephenson, 1966; Skidmore and Clarkson, 1972; Höfle and Buggisch, 1993; Kerr and Hermichen, 1998). This evidence allowed Kerr and Hermichen (1998), to divide the range into two distinct sectors, differentiated on geomorphological grounds.

The North West is characterised by dissected alpine topography, comprising sinuous ridges and arêtes, which grades into the less dissected plateau areas typical of the central and eastern portion of the Shackleton Range. Höfle and Buggisch (1993) ascribe the modification of this area to the Last Glacial Maximum, due to the fresh appearanceof tills which cover the valley

Ice source	Effects on Shackleton Range	Controls on ice expansion
East Antarctic Ice Sheet	Expansion of Recovery and Slessor Glaciers draining the EAIS. Causing overriding of the northern and southern margin of the range	Net mass balance, and plasticity of ice (temp dependent). In brief, lower temperatures equals lower precipitation on the polar plateau. However, colder temperatures lead to increased plasticity and results in net thickening. These systems work on different time scales, therefore require modelling studies to distinguish controls
Filchner Ronnie Ice Shelf	Ice shelf thickening, likely to cause overriding from the west of the range, with the ice flowing predominately from south to north.	The surface elevation of the ice shelf is closely linked to sea level fluctuations, due to grounding line migration. Therefore, high stands are most likely to correspond to global sea level minima.
Local ice caps	Cause enhanced modification of the outlet valleys radiating from the Fuchs Dome and Shotton Snowfield	Linked to precipitation, surface energy balance and glacial flow regime. By analogy with present conditions increased activity of these local systems is unlikely without changing direction of prevailing wind, or rising local temperature causing enhanced surface melting.

Table 6.1. Descriptions of the sources of ice in the Shackleton Range, and their likely effects and controls as described by Kerr and Hermichen (1998).

floors and steep surrounding slopes. Erosive and depositional forms were also noted, including roches moutonnées and tenuous bouldery moraines marking former ice limits related to this stage. From detailed mapping of the nature and orientation of the glacial features such as striae and roche moutonnées, the final modification of this northwestern landscape was from ice from the Filchner-Ronnie Ice Shelf. Kerr and Hermichen (1998) suggest expansion of warm-based ice from this source can be tightly quantified from this work, with the lack of glacial modification by warm based ice noted at Flat Top (1380m) just 15 km south-east of Mt Provender (1109m).

To the south the high undulating plateau of Stephenson Bastion and Mount Greenfield are bounded by steep cliffs of up to 400m overlooking the Recovery Glacier (Figure 3). Work by Höfle and Buggisch (1993) has identified erratics and tills on lower parts of this plateau, comprising sub-angular to sub-rounded limestones and sandstones overlying the quartzite bedrock. Petrographic analysis of these erratics indicated a source area to the southwest. This evidence is backed up by roche moutonnées which are orientated SE-NW. These forms are cross cut by striations, which indicate later flow in a SW-NE direction. The presence of these erosional and depositional forms suggests the overriding of these areas by basal ice at the pressure melting point on lower parts of the plateau. The flow direction indicates expansion of the Recovery Glacier, which overtopped the lower parts of the Plateau. Subsequently the plateau was crosscut by flow from the southwest, possibly from an expanded Filchner-Ronne Ice Shelf. The expansion of these two systems could have been contemporaneous, with the expansion of the Filchner-Ronne Ice Shelf causing the buttressing and thickening of the Recovery Glacier (Kerr and Hermichen, 1998).

6.5 Samples and analytical methods

To test these hypotheses and attempt to constrain the age of the formation of these landscape elements the concentration of the *in situ* cosmogenic nuclides ^{10}Be and ^{26}Al were measured in bedrock surfaces. Initially a total of three samples were analysed, comprising bedrock surfaces which will provide evidence of the last major periods of erosive glaciation of the higher areas of the Southern Plateau and the North West portion of the range. Table 6.2 outlines the details of

Sample ID	Alt. (m)	Lat.	Long	Depth (cm)	Geology	General description: Including sample details and
SB1/J29	1600	$80^0$46 '39	$27^0$03'14	7	Grey / Green Low grade Quartzite, predominately Quartzites and some slates	Stephenson Bastion Col: Sample of glacially smoothed slab of quartzite, surrounded by evidence of deposition and erosion by warm based ice (i.e. till, roches mountonees). Evidence points to pre-quaternary, as ice unlikely to be sufficiently thick during Quaternary at this altitude to cause warm basal conditions required.
SB2/J31	1785	$80^0$46 '	$26^0$58'	5	Grey / Green Low grade Quartzite, predominately Quartzite's and some slates	Stephenson Bastion Top: On eastern edge of summit plateau and dropping to glaciers 100-440m below. Over higher surfaces of Stephenson Bastion, there is very weathered surface of shattered local quartzite with no glacial erratics visible. The bedrock outcrop lie on the edge of the plateau where any frost shattered blocks fall over the cliff, whereas in the centre of the summit plateau there is a layer of debris on all bedrock. Some snow cover is likely though unlikely to be heavy build up due to proximity of the cliff. Not known if cold-based glaciers overtopped this point but see sample. Most likely Pre-Quaternary though might have been covered by cold ice in the Quaternary (ie: not eroded but lacking in cosmogenic signal)
NL1	950	$80^0$22 '94	$29^0$57'47	10	Gneiss of the Metamorphic complex.	Mt Provender: Top of Mt Provender. Three ridges rising to sharp summit of mountain, with sinuous ridge dropping to east and connecting with other lower hills. The ridges crosscut geology of the Shackleton Metamorphic Complex, but erosion of softer rock to west (Blaciklock Glacier Group) and elsewhere has left the upstanding Mt. Provender which is composed primarily of Gneiss. Weathered gneiss around and other bedrock exposures. Jointing heavily weathered to depth of >10cm in places. Jointing dips to north and strike east-west. Variable weathering rind on surrounding rocks, deep to light weathering on sample. Blocky fragments of outcrop lying around though predominately below the sampling site. The Slessor Glacier flows to the north of Mt Provender and currently ice reaches an altitude of 370m to the north below a steep slope. However, general sub-glacial erosion forms on surrounding (lower) peaks, indicates flow from the south-east, and this is likely to have affected Mt. Provender.

Table 2. Sample details and descriptions based on the field descriptions of Dr A. Kerr.

the samples analysed, as recorded in the field by Dr. A Kerr, Figures 6.3 and 6.4 show photographs of the samples in the field.

The TCN nuclides ^{10}Be and ^{26}Al are produced within the uppermost decimeters of a rock surface as a result of secondary cosmic-ray bombardment (Lal, 1991). The measured concentration of the radioactive isotope can be used to calculate an exposure age of the surface providing the rate of production of the TCN in question is known (Cerling and Craig, 1994).

The isotopes ^{10}Be and ^{26}Al were selectively extracted from the quartz component of the whole rock sample following the standard procedures described by Kohl and Nishizumi (1992) and Ivy-Ochs (1996). The isotopic ratios were measured at the ETH tandem AMS facility in Zurich, Switzerland. Tables 2 and 3 list the cosmogenic ^{10}Be radionuclide data, the location and type of sampling site and the conventional exposure ages of each sample. In this study the reference production rate used is that of Kubik *et al* (1998). *In situ* production of cosmogenic ^{10}Be is a combination of three principle components, the most important being spallation, with fast and stopped muons making a less significant contribution to total production. There is strong evidence that the relative muon contribution to total production is much lower than the 16% originally assumed (see Heisinger, 1997 and Stone 2000 for discussion). This study incorporates the modified values of Kubik *et al* (1998) to provide a more accurate representation of the stopped and fast muon components (Heisinger, 1998; Stone 2000). The reference production rate for ^{10}Be used is a spallation component of 5.22±0.22 atoms/g (qtz)/yr, together with a value of 0.12 atoms/g (qtz)/yr for stopped muons and 0.027 atoms/g (qtz)/yr for fast muons (Schaller *et al.*, 2001). This results in a total surface production rate (P_0), at sea level and high latitude (SLHL) for ^{10}Be of 5.37±0.22 atoms/g (qtz)/yr, with a ^{26}Al /^{10}Be ratio of 6.5±0.43 (Kubik *et al.*, 1989). This value was chosen for three reasons; (1) it is referenced to the calibrated radiocarbon timescale: hence the exposure ages given here should be directly comparable to calibrated radiocarbon ages (2) all relevant data necessary for the calculations are available (3) due to the lack of a suitable calibration site in the southern hemisphere on this time scale.

The reference production rate was scaled to that of the site in question following the methods outlined by Stone (2000). The total production at the site, was corrected for attenuation of cosmic radiation due to the thickness of the sample itself and any shielding due to the

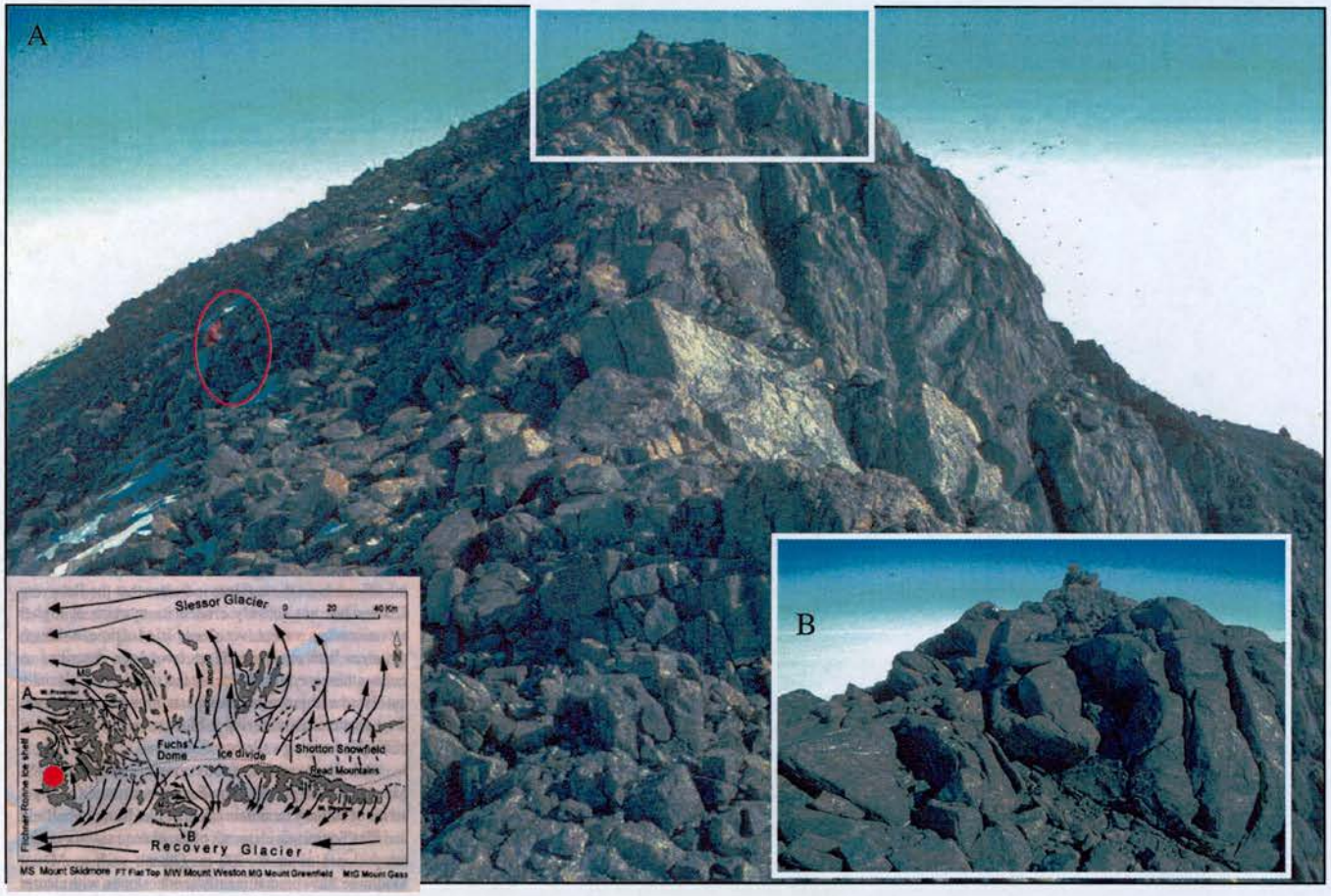

Figure 6.3. Summit of Mount Provender, location of sample NL1, from summit. Photo A shows a general view of the summit which is composed of gniess, and weathered up to a depth of 10cm. A figure on the left of this image provides scale. Photo B is a closer view of the summit of the mountain itself. The inset location map shows the position of the sample locality.

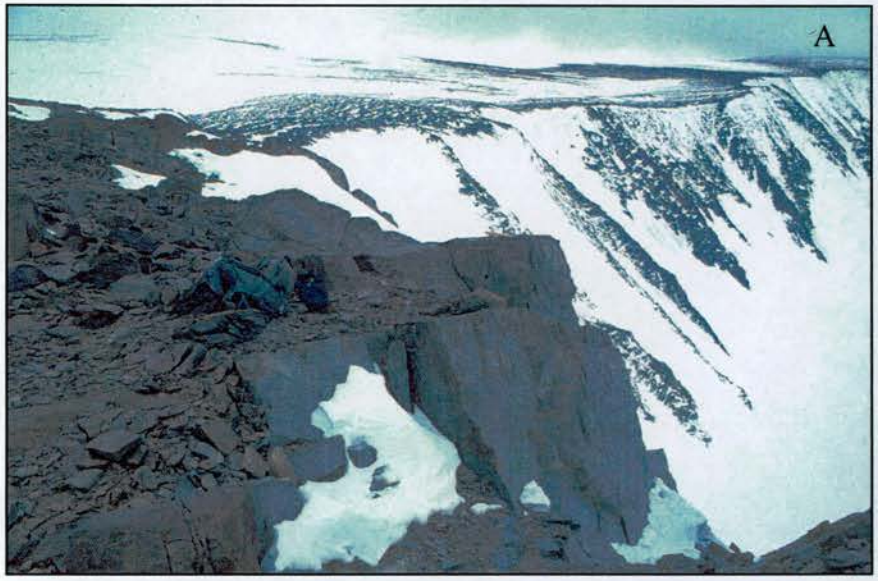

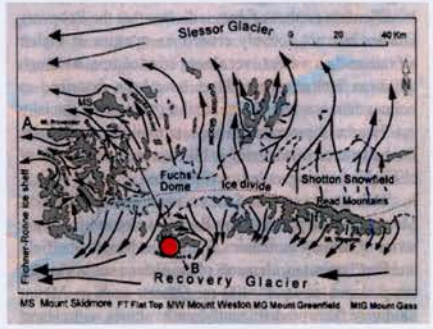

Figure 6.4. Photo A: shows the site of sample SB1/J29, on the edge of Stephenson Bastion overlooking the Recovery Glacier. This sample is a glacially smoothed slab, surrounded by evidence of deposition and erosion by warm based ice (Backpack for scale: approx 90cm long). Photo B: Shows the site of sample SB2/J31, which is located amongst deeply weathered local quartzite, with no glacial erratics. . The inset location map shows the position of the sample locality (Hammer for scale approx. 30cm long).

surrounding topography, following the procedures of Dunne *et al.* (1999). These correction factors were applied to model the effect of the reduced incoming cosmogenic signal on the total production at the sample site. Errors related to the AMS measurement, the production rate and a 5% sample reproducibilty are added quadratically, and calculated as a function of the eventual age.

6.6 Analysis of Results

The cosmogenic radionuclide data are summarised in Table 6.3. This provides an uncorrected record of the original data allowing recalculation of the data independently of the age models used in this study and exposure ages calculated according to the atmospheric scaling models as described earlier. Table 6.2 presents the sample descriptions and Table 6.4 presents the exposure age estimates for these surfaces. As well as providing exposure age estimates for these surfaces further analysis can provide some of the first estimates of erosion, denudation and uplift in this region of Antarctica.

6.6.1 Exposure ages

The exposure age estimates for these samples range from 1.16±0.1Ma (SB1/J29) to 1.74±0.16Ma (SB2/J31) on the Plateau area of Stephenson Bastion, to 3±0.3Ma (NL1/J22) in the far north-west of the range on the summit of Mt Provender (Table 6.4). These ages reflect minimum ages for the exposure of these surfaces after ice, till or soil was removed assuming no erosion. The assumption of no erosion is conservative, because it is likely that these surfaces will have experienced some erosion and weathering. If any erosion is included, the actual exposure age of the surface will always be older. As one cannot know the actual erosion rate during the whole exposure period, the ages must be interpreted as minimum ages. By measuring both ^{10}Be and ^{26}Al and analysing their ratios it can be seen that both of the samples from the Plateau area of Stephenson Bastion have a simple exposure history plotting very close to the line of continuous exposure (or zero erosion) on Figure 6.5. This approach was first proposed by Lal and Arnold (1985), and is based on fact that the half-lives differ markedly, therefore causing the concentration of different nuclides to vary depending upon periods of exposure and burial. A complex or simple exposure history can be identified

Table 6.3 Sample details and TCN ages

Sample Id	Location	Latitude (^{0}S)	Altitude	shielding and depth correction[1]	sample mass (g)	Carrier Be (mg)[2]	Al (ppm)[3]	Measured ^{10}Be/^{9}Be ratio[4]	± % error	^{10}Be (at/g) blank corrected[5]	± % error	Measured ^{26}Al/^{27}Al ratio[6]	± % error	^{26}Al (at/g)blank corrected[5]	± % error[7]
NL1/J22	Mt Provendure	80	0.95	0.915165492	2.7127	0.3569695	N/A	N/A	N/A	24277649.89	2.333405813	0	0	0	0.0
SB1/J29	Stephenson Bastion	80	1.6	0.956320164	3.69035	0.502164	136	2.71E-12	2.5	24177269.35	2.559816641	1.9967E-11	2.7	103207530.1	2.7
SB2/J31	Stephenson Bastion	80	1.785	0.956320164	9.05714	0.50239	55	1.00E-11	1.1	36973176.58	1.103443035	2.2314E-11	2.1	139510620.2	2.1

1. Depth shielding calculated using "flat" dependency of Massirik and Reedy (1995); topographic shielding calculated using the relationship $\sin^{2.3}\theta$, for 360^0 around the sample, where θ is the angle of the topographic obstruction from the horizontal.
2. Carrier addition measured by calibrated pipette, and corrected for temperature and density.
3. Measured from aliquot of whole sample by ICP-AES.
4. Reported ^{10}Be/^{9}Be ratio from AMS measurements, include errors & corrections related to "in-house" standard.
5. Removes possible effects of exposure and chemical loading of samples measured during same accelerator run.
6. Reported ^{26}Al/^{27}Al ratio from AMS measurements, include errors & corrections related to "in-house" standard.
7. Total error, including 5% for sample reproducibility and an extra 5% relating just to the Al sample for estimation of total Al by ICP-AES.

Table 6.4 Cosmogenic radio nuclide data

Sample ID	Altitude	Location[1]	Sample description[2]	^{10}Be age(yr)[3]	± Error (yr)	^{26}Al age[4]	± Error (yr)	Error weighted mean(yr)[5]	± error (yr)	Comments[6]
NL1/J22	0.95	MP	B	3,002,686	387,020					
SB1/J29	1.6	SB	B	1,167,018	111,594	879,654	99,616	1,007,091	74,315	In concordance on banana gram therefore constant exposure with little erosion
SB2/J31	1.785	SB	B	1,741,040	168,675	1,151,547	142,304	1,396,660	108,767	In concordance on banana gram therefore constant exposure with little erosion

1. Locations;SB=Stephenson Bastion, MP=Mount Provendure.
2. Sample description;B=Bedrock surface.
3. Calculated using a ^{10}Be production rate of 5.37±0.22 at/g/yr (Schaller et al., 2001), scaled following the methods outlined by Stone (2000), which are a reformulation of those of Lal (1991).
4. Calculated using a ^{26}Al/^{10}Be ratio of 6.5 (Kubik 1998).
5. Error weighed mean of Al and Be exposure ages.

Comments on possible sample processing or analytical problems.

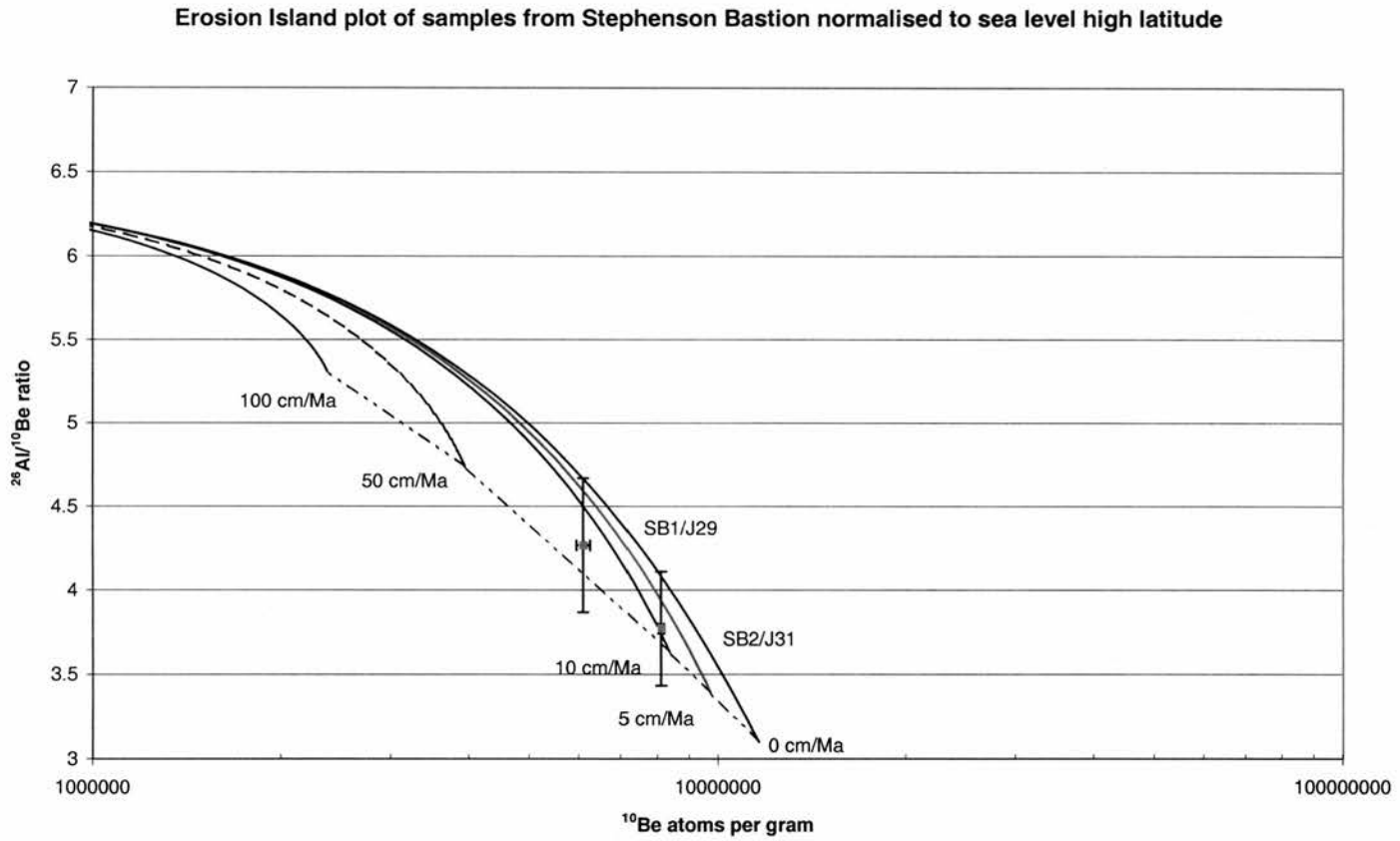

Figure 6.5. Erosion Island plot of $^{26}Al/^{10}Be$ against ^{10}Be, all concentrations have been normalised to sea level high latitude. The position of these samples plotting on the upper most line of this curve indicate two significant findings. The first is extremely low erosion over the exposure period, and second that the samples have had a simple erosion history since initial exposure with no substantial periods of coverage or erosion.

through the analysis of the ratio of the $^{10}Be/^{26}Al$ plotted against the log of measured ^{10}Be concentration (scaled to production at sea level and high latitude). This is termed an erosion island graph (Lal 1991). Figure 6.5, shows the curve produced when these variables are plotted for the samples from this study, eventually reaching an end point when both nuclides have reached saturation. The point of saturation gradually decreases as the erosion rate increases. By plotting this relationship for a number of erosion rates the "steady-state erosion island" (Lal, 1991) is produced. The steady-state term is used to describe samples plotting within this area as having a simple history just affected by erosion (Klein *et al.*., 1986; Lal, 1991). This is an important result as it precludes significant coverage or erosion by even cold-based ice during the coldest periods of the Quaternary. This evidence is supported by the discovery of an *in situ* meterorite located 350m above the Recovery Glacier in the Reed Mountains and dated to 415 ka by Höfle and Buggisch (1993). Together these results suggest little or no glacial expansion of the EAIS or the Recovery Glacier during the Quaternary.

The ^{10}Be exposure age estimate from Mount Provender in the more alpine landscape of the north west portion of the range is of particular interest. Having an exposure age of 3±0.3Ma, it suggests that this topographyhas not been significantly modified for millions of years. However, the absence of analysis of the ^{26}Al nuclide concentration for this sample, prevents this hypothesis being truly tested. It could be that this portion of the range is covered intermittently by ice from the warm based Filchner-Ronnie Ice Shelf, but this seems unlikely given the ^{10}Be concentration is close to saturation.

6.6.2 Erosion rates

It is also possible to use these data to provide estimates of the rates of erosion through the exposure period. This has been approached in two ways. The first method simply uses the concentration of ^{10}Be, and the second approach is based on analysis of the position of the sample on the erosion island plot.

The first approach following the work of Ivy-Ochs (1996), makes the assumption that the measured ^{10}Be concentration has reached secular equilibrium. This has the effect of making the exponential term from the equation for radionuclide build up to be zero. Therefore this allows the calculation of the maximum possible erosion rate for the measured ^{10}Be concentration in a sample (Equation 6.1):

$$\varepsilon = \frac{\Lambda}{\rho}\left(\frac{P}{N} - \lambda\right) \qquad \text{Eq 6.1}$$

where ε is erosion, Λ is the cosmic ray attenuation length in g/cm^2, ρ is the rock density in g/cm^3 and λ decay constant of the radionuclide in question.

This approach only provides an estimate of maximum erosion rate. A more realistic approach can be achieved through the analysis of the concentrations of ^{10}Be and ^{26}Al in the surfaces with the erosion island diagram (Figure 6.5). The concentrations of the isotopes within these samples provide some very interesting conclusions regarding the erosion in this region. The results of this can be seen in Table 6.5. The maximum erosion rates are extremely low. For instance sample NL1/J22 the oldest sample, has a maximum value of 8.7cm/Ma, while samples SB1/J29 and SB2/J31 are an order of magnitude larger being between 20-35cm/Ma. Since these latter samples are not close to saturation this provides an upper limit on erosion. A fact reflected by the preservation of striations on the upper surface of sample SB1/J29. The erosion island diagram provides further evidence of the extremely low erosion rates here with the two samples plotting between 10 to 20 cm/Ma, close to that of sample NL1/J22.

These rates are similar to those recorded in cosmogenic studies and field interpretations in other regions of Antarctica including the Dry Valleys area of the Transantarctic Mountains (Nishiizumi *et al.*, 1991; Brown *et al.*, 1991; Brook and Kurz. 1993, Brook *et al.*,1995; Marchant *et al.*, 1993a; Ivy-Ochs, 1996). Such extremely low rates of erosion indicate that the persistent cold dry conditions experienced in this region have been maintained throughout the exposure period (Ivy-Ochs, 1996). Erosion rates in more temperate regions are orders of magnitude greater than those reflected from the build up of cosmogenic radionuclides in this and other Antarctic environments (Saunders and Young, 1983; Summerfield, 1991; Ivy-Ochs, 1996). However, these low values contradict other studies based on physical measurements of erosion rates due to wind (15-2000cm/Ma), and weathering due to salt crystallisation (2000cm/Ma) in other regions of Antarctica (Malin, 1985, 1988; Spate *et al.*, 1995; Gore and Colhoun, 1995). Ivy-Ochs (1996) concluded that this disparity could be due to these records representing extremely localised effects, such as katabatic winds flowing off the polar plateau, suggesting that

areas of high erosion are localised with the continental portions of Antarctica being modified at extremely slow rates.

These conclusions of low *in situ* weathering rates agree with observations from marine cores from the oceans surrounding Antarctica, which indicate minimal chemical weathering since the Oligocene / Miocene boundary. This conclusion is based on the dominance of smectite from the analysis of the clay mineral composition in ocean cores surrounding Antarctica (Robert and Maillot, 1990). Taken together with data from other proxy records and locations in Antarctica, these data suggests there has been little or no chemical weathering for 36Ma in Antarctica (Robert and Maillot, 1990; Marchant *et al.*, 1993 a; Ivy-Ochs, 1996).

6.6.3 Uplift constraints

As described earlier, the production rate of a cosmogenic radionuclide increases exponentially with decreasing atmospheric pressure (Lal, 1991; Brook *et al.*, 1995). Therefore the isotopic concentration of a radionuclide can be used to set limits on the amount and rate of uplift which has taken place over the exposure period. Cosmogenic radionuclides are especially useful for this purpose, as the final saturation concentration is altitude dependent. Using cosmogenic radionuclides to constrain uplift has distinct advantages over other techniques such as fission track dating or ^{40}Ar-^{39}Ar thermochronology, as it allows uplift to be described relative to sea level (or atmospheric shielding), as opposed to denudation and inferred tectonic uplift (Brook *et al.*, 1995).

This approach was first explored and developed by Brown *et al.*, (1991), and Brook *et al.*, (1993, 1995). In brief it allows the differentiation between long periods of exposure at lower elevations and shorter periods of exposure at higher elevations, or a combination of these two. The model is descibed in Equation 6.2, which shows the altitudinal dependence of the radionuclide production rate. The amount of ^{10}Be accumulated during uplift is based on the following altitudinal dependence of cosmogenic radionuclide production

$$N = \left(\frac{Ps}{\left(\frac{U}{\Lambda_a}\right) + \left(\lambda + \frac{E}{\Lambda_a}\right)} \right) \left(e^{\left(U/\Lambda_a\right)t} \right) - \left(e^{-\left(\lambda + E/\Lambda_a\right)} \right) + N_0 e^{-\lambda t} \qquad \text{Eq 6.2}$$

where, N is the number of atoms/gram in SiO_2, P_s is the sea level production rate (at/g SiO_2.yr), t is the exposure time (yr), λ is the decay constant, ρ is the atmospheric density in g/cm^3, Λa is the cosmic ray attenuation length in the atmosphere (142 g/cm^2). This relationship allows the calculation of the concentration of ^{10}Be accumulated assuming different uplift trajectories from sea level to its present altitude. The model requires the derivation of the change in atmospheric shielding throughout the period of uplift. This is an important factor, as it significantly affects the rate of build up. As described earlier, for this study the atmospheric scaling model described by Stone (2000) was used.

Figures 6.6 and 6.7 demonstrate the uplift model results for each of the three samples and provides estimates of maximum uplift rates to raise the surface to their present altitudes from sea level over the exposure period. The important conclusion is that none of the surfaces demonstrate any evidence of being uplifted over their calculated exposure periods. None of the uplift scenarios can produce more than seventy percent of the measured ^{10}Be concentration over the sample exposure time. As noted by Brook *et al.* (1995), "Our approach only provides a "one way" test. High concentrations of radionuclides are inconsistent with high uplift rates, but low concentrations do not indicate high uplift rates due to the possible effects of erosion." As noted in the previous section erosion is not thought to be a significant problem with these samples.

This model also allows an estimate of the minimum age from uplift to be calculated, as described by Ivy-Ochs (1996). By taking the maximum uplift rate, which is limited by the current altitude of the surface in question it is possible to suggest the maximum exposure time required to uplift the surface from sea level to its present altitude. In each case this was found to be substantially more than indicated from the exposure age estimate (Table 6.5). These results, together with the direct evidence of minimal erosion back the conclusion that these surfaces have been exposed at their present altitude, with little or no uplift during the exposure period.

6.7 Implications for palaeoclimate and evolution of the Shackleton Range

The results from these analyses provide the first constraints on the evolution of the landscape, ice and climate for the Shackleton Range of Antarctica. The measurement of the *in situ*

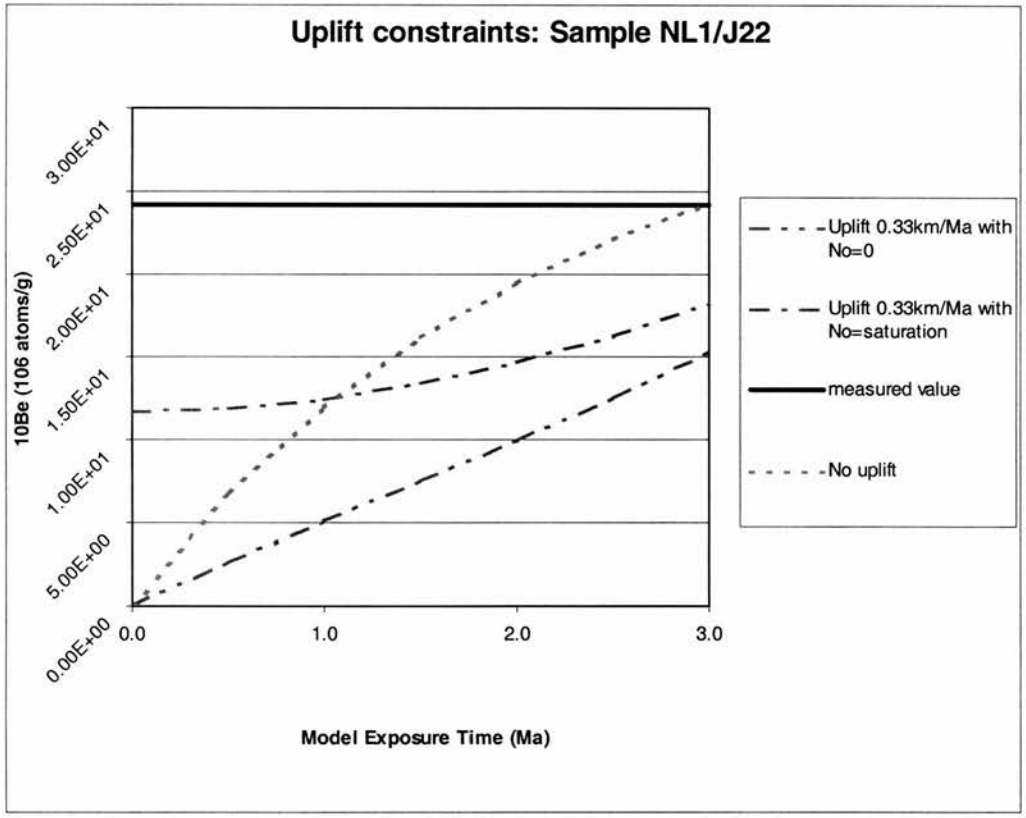

Figure 6.6. Uplift constraints on sample NL1/J22, from the summit of Mt. Provendure. This plot demonstrates that over the exposure time measured for this sample that no other uplift scenario could enplace this sample at this altitude. The maximum rate of uplift is constrained by the present sample altitude and the calculated exposure age, therefore this only provides a one way test. However the additional effect of erosion to this model would only cause further separation between the different scenarios.

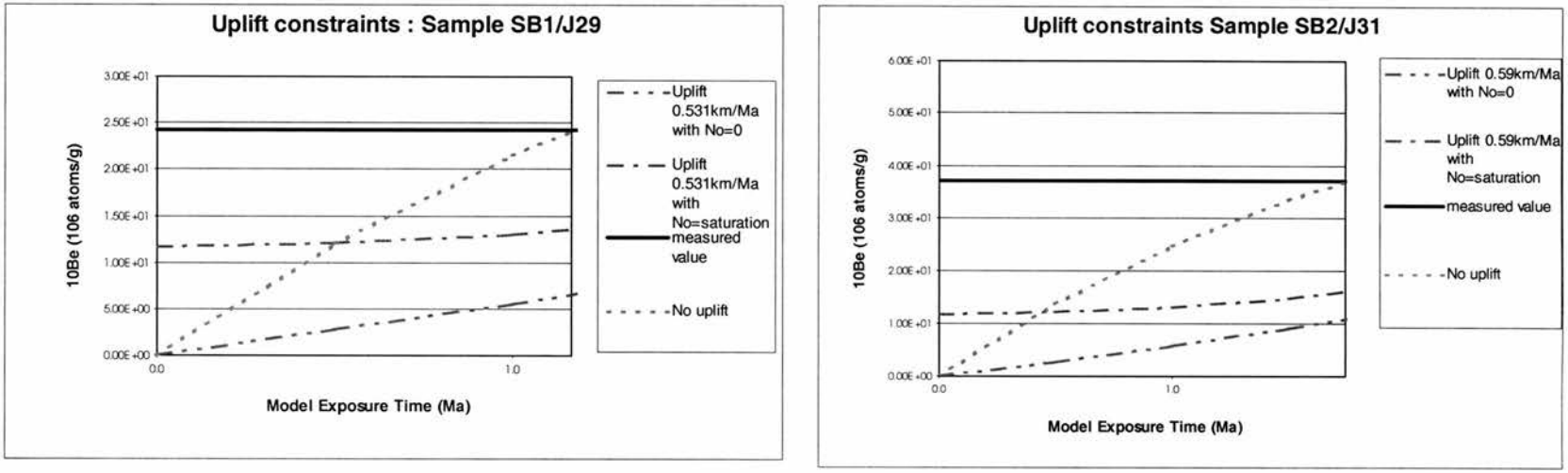

Figure 6.7. Uplift constraints for samples SB1/J29 and SB2/J31, from the Plateau area of Stephenson Bastion. This plot demonstrates that over the exposure time measured for thee samples that no other uplift scenario could enplace this sample at this altitude. The maximum rate of uplift is constrained by the present sample altitude and the calculated exposure age, therefore this only provides a one way test. However the additional effect of erosion to this model would only cause further separation between the different scenarios.

Sample	Max erosion rate, from ^{10}Be concentration [1]	Maximum erosion rate from erosion island plot[2]	Exposure age (^{10}Be)[3] (E=0)	Max uplift rate (U) (km/Ma)[4]	Minimum time at U to uplift surface to present altitude[5]
NL1/J29	8.7 cm/Ma	N/A	3.0 Ma	0.531	4 Ma
SB1/J29	20cm/Ma	10 cm/Ma	1.16 Ma	0.59	2.5 Ma
SB2/J31	35cm/Ma	25 cm/Ma	1.74 Ma	0.33	4 Ma

Table 6.5. Constraints on erosion rate and sample uplift from this study. 1) Maximum rate of erosion based on assumption that ^{10}Be is in saturation. 2). Erosion rate for ^{26}Al/^{10}Be isotope pair, when plotted on erosion island diagram. 3). Exposure estimate from 10Be, used to constrain uplift models. 4). Maximum rate of uplift possible over exposure period[4] from 0m to present altitude. 5). Theoretical time required to obtain measured isotope concentration at max uplift rate (U). These data only provide constraints, in a sample specific context, using the theoretical models and assumptions outlined in the text.

cosmogenic radionuclides ^{10}Be and ^{26}Al provide evidence of long term exposure of these surfaces, and indicate that the exposure periods have been characterised by very low rates of denudation and little or no uplift. This indicates that the landscape elements described by Kerr and Hermichen (1998) are essentially relict, relating to periods of pre-Quaternary glaciation. The timing of these events is impossible to infer from these analyses. Therefore the exposure ages calculated from this study reflect minimum ages for the exposure of these surfaces, if one allows for delayed exposure due to the removal of overlying sediments or tills or any erosion.

Similar conclusions have been drawn from cosmogenic isotope analyses in other portions of the Antarctic continent, most notably for the Sirius Group in the Dry Valleys region (Ivy-Ochs, 1996). The results of both cosmogenic isotope and tephra studies in this latter region indicate that the climate has not significantly altered in the past 5.8 Ma based on *in situ* ^{10}Be, or 15.2 Ma based on $^{40}Ar/^{39}Ar$ ash dating (Denton *et al.*, 1993; Marchant *et al.*, 1993a, 1993b; Ivy-Ochs 1996; Sugden *et al.*, 1995a). By using these extensive data sets as an analogy, the glacial features described in the Shackleton Range by Kerr and Hermichen (1998), were probably cut during early stages of Antarctic glaciation, possibly during the coalescence of alpine ice into extensive ice sheets. No direct dating relating to this exists on terrestrial Antarctica, but it is recorded in the variations within the oxygen isotope records from ocean cores at 36Ma (Kennett and Shackleton, 1976). Evidence for this process comes from areas such as the Dry Valleys, which were being modified by wet-based or polythermal ice at around 15.2Ma (Marchant *et al.*, 1993a). Tills deposited at this time were overridden as ice reached it maximum thickness. After which point it is hypothesised that the atmosphere became cooler and drier, through negative feedback effects, eventually leading to the EAIS shrinking to a size similar to its present extent.

Much further work would be required to thoroughly investigate these relationships hypotheses within the Shackleton Range. It would require extensive analyses of multiple stable (eg.^{3}He or ^{21}Ne) and radiogenic nuclides to provide more evidence of exposure histories for different altitudes and localities within the range. However these preliminary results do suggest there has been little or no modification of the highest summits of this region during the Quaternary. From the detailed mapping of Hoffle and Buggisch (1993), and the work of Kerr and Hermichen (1998) it seems likely that maximum expansion of ice during the Quaternary is recorded in the north west of the range. Here there are moraines east of Mount Skidmore that indicate a maximum thickening of 200-400 metres close to the edge of the Filchner-Ronne Ice Shelf. If

correct, this suggests that when the Filchner-Ronne Ice Shelf was grounded well offshore from its present position it did not cause substantial buttressing of the EAIS. A fact reflected in data from the analysis of ice cores from the interior of the EAIS, which suggest the interior of the ice sheet remained the same or even thinned relative to present (Jouzel *et al.*, 1989; Raynaud and Whillans, 1982).

6.9 Conclusions

New ^{10}Be and ^{26}Al data indicate that the landscape of the Shackleton Range has not been significantly modified throughout the Quaternary. Minimum exposure ages are between 1.16±0.1Ma and 3±0.3Ma, calibrated for Antarctic air pressure (Stone 2000). No evidence of significant periods of burial or substantial rates of erosion throughout this period are indicated from analysis of the concentrations of the radionuclides. The measurement of the concentrations of cosmogenic isotopes in these samples indicates maximum erosion rates of 10-35cm/Ma. Constraints on uplift suggest tectonic stability of this range which, together with low erosion rates, preclude the existence of a much more wet or temperate climate throughout this time. The main conclusion is that the different landscapes are essentially relict and probably reflect extensive glaciation during the early evolution of Antarctica, when much thicker ice was present.

6.10 References

Bentley MJ, Anderson JB. 1998. Glacial and marine geological evidence for the ice sheet configuration in the Weddell Sea-Antarctic Peninsula region during the Last Glacial Maximum. Antarctic Science 10. 3. 309-325.

Brook EJ, Kurz MD. 1993. Surface-exposure chronology using in situ cosmogenic ^{3}He in Antarctic quartz sandstone boulders. Quaternary Research 39. 1-10.

Brook EJ, Brown ET, Kurz MD, Ackert RP, Raisbeck GM, Yiou F. 1995. Constraints on age, erosion and uplift of Neogene glacial deposits in the Transantarctic Mountains using *in situ* cosmogenic ^{10}Be and ^{26}Al. Geology, V. 23. P 1063-1066.

Brown ET, Edmond JM, Raisbeck GM, Yiou F, Kurz MD, Brook EJ. 1991. Examination of surface exposure ages of Antarctic moraines using *in situ* produced ^{10}Be and ^{26}Al.. Geochimica et Cosmochemica Acta. V. 55. 2269-2283.

Cararra P. 1981. Evidence for a former largeice sheet in the Orville Coast- Ronnie Ice Shelf Area, Antarctica. Journal of Glaciology. 27. 487-491.

Cerling TE, Craig H. 1994. Geomophology and in situ cosmogenic isotopes. Annual Review of Earth and Planetary Sciences 22. 273-317.

Cockburn, HAP. 1998. Landscape evolution in Namibia and Antarctica: Quantifying denudation rates using in-situ cosmogenic isotope analysis. Unpublished PhD thesis, The University of Edinburgh, 246pp.

Denton GH, Anderson BG, Rutford RH, Anderson BG. 1992. Glacial history of the Ellswoth Mountains, West Antarctica. Geological Society of America Memoir. 170. 403-432.

Denton GH, Sugden DR, Marchant DR, Hall BL, Wilch TI. 1993. East Antarctic Ice Sheet sensitivity to Pliocene climate change from a Dry Valleys perspective. Geografiska Annaler. V. 75A. 155-204.

Drewry DJ. 1982. Ice flow, bedrock and geothermal studies from radio echo sounding inland of McMurdo Sound, Antarctica. In Craddock C (ed). Antarctic Geoscience. University of Wisconsin Press. 977-983.

Dunai TJ. 2000. Scaling factors for production rates of *in situ* produced cosmogenic nuclides: a critical reevaluation. Earth and Planetary Science Letters. 176. 157-169.

Dunne J, Elmore D, Muzikar P. 1999. Scaling factors for the rates of production of cosmogenic nuclides for geometric shielding and attenuation at depth on sloped surfaces. Geomorphology. 27(1-2). 3-12.

Elverhøi A. 1981. Evidence for a late Wisconsin glaciation of the Weddell Sea. Nature. 293. 641-642.

Gore DB, Calhoun EA. 1995. Regional contrasts in terrain and glacial sediments, Vestfold Hills, East Antarctica. VII International Symposium on Antarctic Earth Sciences. Siena (abstracts). p. 163.

Gosse JC, Phillips FM. 2001. Terrestrial in situ cosmogenic nuclides: theory and application. Quaternary Science Reviews 20. 1475-1560.

Heisinger B. 1997. In situ production of radionuclides at great depths. Nuclear Instruments and Methods. B. 123. 341-346.

Höfle HC, BuggischW. 1993. Glacial geology and petrography of erratics in the Shackleton Range, Antarctica. Polarorschung. 6.(2/3). 183-201.

Huybrechts P. 1992. The Antarctic ice sheet and environmental change: a three dimensional modeling study. Ph.D. Thesis, Bremerhaven. 241pp.

Ivy –Ochs S. 1996. The dating of rock surfaces using the in situ produced ^{10}Be, ^{26}Al, and ^{36}Cl, with examples from Antarctica and the Swiss Alps. Ph. D. Thesis, Swiss Federal Institute of Technonology, Zurich. 196pp.

Jouzel J, Raiseck G, Benoist JP, Yiou F, Lorius C, Raynauld D, Patit JR, Barkov NI, Korotkevitch YS, Kotlyakov VM. 1989. A comparison of deep Arntarctic ice cores and their implications for climate between 65,000 and 15,000 years ago. Quaternary Research, 31. 135-150.

Kennett JP, Hodell DA. 1993. Evidence for relative climatic stability of Antarctica during the early Pliocene: a marine perspective: Geografiska Annaler. 75A. 205-220.

Kennett JP, Shackelton NJ. 1976. Oxygen isotopic evidence for the development of the psychryosphere 38m.y. ago. Nature. 260. 513-515.

Kerr A, Hermichen WD. 1998. Glacial modification of the Shackleton Range, Antarctica. Terra Antarctica. 6(3) 353-360.

Klein J, Giegengack R, Middleton R, Sharma P, underwood JR, Weeks WA. 1986. Revealing histories of exposure using in situ produced ^{10}Be and ^{26}Al in Libyan desert glass. Radiocarbon 28. 547-555.

Kubik PW, Ivy-Ochs S, Masarik J, Frank M, Schlüchter C. 1998. ^{10}Be and ^{26}Al production rates deduced from an instantaneous event within the dendro-calibration curve, the landslide of Köfels Ötz Valley, Austria, Earth and Planetary Science Letters 161. (1-4). 231-241.

Lal D, Arnold JR. 1985. Tracing quartz through the environment. Proceedings of the Indian Academy of Science (Earth Planetary Science Section) 94. 1-5.

Lal D. 1991. Cosmic ray labelling of erosion surfaces: in situ nuclide production rates and erosion rates. Earth and Planetary Science Letters 104, 424-439.

Malin MC. 1985. Rates of geomorphic modification in ice-free areas, southern Victoria Land, Antarctica. Antarctic Journal of the United States. 20. 18-20.

Marchant DR, Denton GH, Swisher CC. 1993a. Miocene-Pliocene-Pleistocene glacial history of Arena Valley, Quatermain Mountains, Antarctica. Geografiska Annaler. 75A. 269-302.

Marchant DR, Denton GH, Sugden D, Swisher CC. 1993b. Miocene glacial stratigraphy and landscape evolution of the western Asgard Range, Antarctica. Geografiska Annaler. 75A. 303-330.

Masarik J, Reedy RC. 1995. Terrestrial cosmogenic-nuclide production systematics calculated from numerical simulations. Earth and Planetary Science Letters. 136. 381-395.

Nishiizumi K, Arnold JR, Klein J, Fink D, Middleton R, Kubik PW, Sharma P, Elmore D, Reedy RC. 1991. Exposure histories of lunar meterorites: ALHA 81005, MAC88104, MAC88105, and yamato 791197. Geochimica et Cosmochemica Acta. 55. 3149-3155.

Raynaud D, Whillans IM. 1982. Air content of the Byrd Ice Core and past changes in the West Antarctic Ice Sheet. Annals of Glaciology. 3. 269-273.

Robert C, Maillot H. 1990. Evolution and significance of clay associations and inorganic geochemical data in the Weddell Sea (southern ocean). Ocean Drilling Program Leg 113. In Barker PF, Kennett JP, *et al.*. Proc. ODP. Sci. Results 113, Ocean Drilling Program, College Station, Texas, USA.

Saunders I, Young A. 1983. Rates of surface processes on slopes, slope retreat and denudation. Earth Surface Processes and Landforms. 8. 473-501.

Schaller *et al.* 2001 Schaller M, von Blanckenburg F, Hovius N, Kubik PW. 2001. Large-scale erosion rates from in situ produced cosmogenic nuclides in European river sediments. Earth and Planetary Science Letters 188. 441-458.

Shackleton N J. 1987. Oxygen isotopes, ice volume and sea level. Quaternary Science Reviews 6: 183-90.

Skidmore MJ, Clarkson PD. 1972. Physiography and glacial geomorphology of the Shackleton Range. British Antarctic Survey Bullitin. 30. 69-80.

Spate AP, Burgees JS, Shevlin J. 1995. Rates of rock surface lowering, Princess Elizabeth Land, eastern Antarctica. Earth Surface Processes and Landforms. 20. 567-573.

Stephenson PJ. 1966. Geology. 1. Theron Mountains, Shackleton Range and Whichway Nunataks. Scientific Report: Transantarctic Expedition. 8. London. 79pp.

Stone JO. 2000. Air pressure and cosmogenic isotope production. Journal of Geophysical Research. 105. B10. 23,753-23,759.

Sugden DE, Marchant DR, Denton GH. 1993. The case for the stable East Antarctic Ice Sheet: The background. Geografiska Annaler. 75A(4). 151-154.

Sugden DE, Denton GH, Marchant DR. 1995. Landscape evolution of the Dry Valleys, Transantarctic Mountains: implications. Journal of Geophysical Research. 100. 9949-9967.

Summerfield M. 1991. Global geomorphology: John Wiley and Sons, New York, USA. P 371-402.

Webb PN, Harwood DM. 1987. The Sirius formation of the Beardmore Glacier region. Antarctic Journal of the U.S. 22. 8-12.

CHAPTER 7

Conclusions

7.1 Introduction

The preceding chapters give evidence for the timing of past glaciation in four localities affected by glaciers and ice sheets surrounding the Drake Passage. Through constructing chronologies of glacial expansion of these ice sheets we are able provide evidence to answer questions regarding the nature and timing of local and global environmental change, thus improving our understanding of how the ocean-atmosphere system of the two hemispheres interacts. To explain how the data from the analyses of the TCN's, ^{10}Be and ^{26}Al, has advanced our understanding of these problems, each area will be discussed individually. These local, site specific chronologies can then be used to describe possible regional responses to climate forcing during the last glacial cycle.

7.2 The Strait of Magellan

These data represent the first direct dating of the deglaciation of the Patagonian Ice Sheet from the Last Glacial Maximum in this region. The results fit well with the available radiocarbon chronology constraining ice withdrawal from these limits. Maximum expansion was achieved before 26 ka yr, with gradual decay from these limits being punctuated by readvances marked by small reticulate moraines and prominent meltwater channels. Two of these later events have been constrained to around 20.8 and 18.7 ka yr.

The major conclusion from this region is the culmination of LGM ice expansion prior to 26 ka yr, which strengthens inferences from other sectors of Patagonia that maximum ice extent was synchronous between the mid-latitude southern hemisphere and the northern hemisphere. The similarity of moraine chronologies at mid-latitudes in both hemispheres implies that the global atmosphere could be a major forcing mechanism of climatic change. Recession from these limits was punctuated by several periods of stabilisation or advance, two of these stages have been identified at 20.8 and 18.7 ka yr BP. These may well correspond with multiple glacial advances recorded further north in the Lakes Region of Chile, although any direct correlation would require more precise dating.

7.3 Torres del Paine

Interpretation of the data presented in this study provides two significant conclusions, the first is the identification of a retreat or re-advance stage before 15.8 ka yr BP, during recession from the LGM. This actively formed glacial landforms at over 45km from the present ice margin. The field relationships between these landforms and a tephra occurring at 12,700^{14}C yr BP (15,382 cal. yr BP) suggest that recession from this limit was rapid, and ice was close to modern limits by the time the tephra was deposited. The direct dating of this event provides relative constraints on both the LGM and late glacial expansion of the south Patagonian Ice Sheet in this central region. As such it confirms the conclusions work of Marden (1994), that places the LGM expansion in this region to the limit ascribed by Caldenius (1932) and Wenzens (1999) as the limit of Late Glacial expansion (Younger Dryas / Finiglacial).

If this advance reflects a minimum exposure time due to effects such as soil, snow cover, or higher erosion, this advance may correlate with expansion of the Patagonian Ice Sheet at around 17 ka. This has been recorded to both the north and south of this region and suggests that deglaciation was synchronous over 16° of latitude. This correlation strengthens inferences that maximum ice extent was synchronous between the mid-latitude southern hemisphere and the northern hemisphere. The similarity of moraine chronologies at mid-latitudes in both hemispheres implies that the global atmosphere could be a major forcing mechanism of climatic change.

The second finding of this work is the application of surface exposure dating to samples of differing lithologies. It has been demonstrated that the effects of differential erosion can cause variation in the concentration of cosmogenic nuclides in samples related to the same event. To solve this problem a sound understanding of erosion of the lithologies in question is critical, and it is suggested that only boulders displaying evidence of direct glacial transport be sampled in this context. This work has also highlighted problems with the application of the TCN technique in this environment, where processes such as deflation may lead to exhumation of boulders. This was only recorded in fine-grained moraines composed predominantly of glacifluvial and glacilacusterine silts and sands. These observations further emphasise the need for careful fieldwork and observation during sampling for the TCN technique.

7.4 The Antarctic Peninsula and George VI Sound

This paper presents the first systematic attempt to constrain the timing of deglaciation of the Antarctic Peninsula Ice Sheet from its configuration at the Last Glacial Maximum (LGM), through the measurement of the cosmogenic radionuclides ^{10}Be and ^{26}Al within erratics deposited on glacial landforms. At the LGM the ice sheet expanded to form two ice domes in Palmer Land and merged with an expanded and thicker West Antarctic Ice Sheet in the Weddell Sea. Ice from the Peninsula merged with Ice from Alexander Island in George VI Sound.

The pattern of deglaciation is very complex. Two distinct phases of ice sheet lowering are recorded in George VI Sound, with initial ice sheet lowering between 18.3 and 15 ka, followed by final outlet glacier or local ice cap retreat between 8.7 to 6.4 ka. The onset of ice sheet decline at c. 18.3 ka was relatively early, compared to other areas of the WAIS, and could imply a rapid response to sea level rise following the LGM. One explanation is that the relatively small ice mass, and relatively high accumulation and ablation rates of the Antarctic Peninsula Ice Sheet (and particularly the Pacific margin), make it the most sensitive part of the Antarctic ice sheet.

In the central portion of the Antarctic Peninsula, exposure ages from the Behrendt Mountains suggest deglaciation at 11.8ka. which probably reflects delayed thinning in response to retreat of

grounded ice in the Weddell Sea. The wide range of ages and evidence of complex exposure histories from many of the available erratics, provides the first terrestrial evidence that there has been repeated glaciation of the Antarctic Peninsula, over several glacial cycles.

7.5 The Shackleton Range, Antarctica

The concentrations of the cosmogenic nuclides ^{10}Be and ^{26}Al on glaciated rock surfaces from the Shackleton Range, Antarctica provide minimum exposure ages and maximum rates of erosion for several landscape elements. Summits and plateau areas indicate minimum exposure ages of 1.6±0.1Ma to 3.0±0.3Ma, with maximum long-term erosion rates of between 10-35 cm/Ma. The high concentrations of the isotope ^{10}Be indicate little or no uplift of the massif during the exposure period.

These data point towards two major conclusions for the landscape and glacial evolution of this region. First the exceptionally low erosion rates indicate that the modern cold arid climatic conditions have persisted since at least Pliocene time. Second, the high concentrations of radionuclides suggest the glacial landscapes are millions of years old, and similar to relict glacial landscapes in the McMurdo sector of the Transantarctic Mountains. These dates provide firm constraints on the Quaternary expansion of the East Antarctic Ice Sheet during periods of maximum sea-level lowering in the Quaternary. Including the Filchner-Ronne Ice Shelf, which marine evidence indicates was significantly expanded during the Last Glacial Maximum, did not thicken by more than 200-300m at the landward margin of the East Antarctic Ice Sheet.

7.6 Wider Implications

Through the measurement of the TCN's ^{10}Be and ^{26}Al, this thesis has attempted to solve previously unresolved problems regarding the timing and magnitude of glaciation during the last glacial Interglacial transition (LGIT) in terrestrial environments surrounding the Drake Passage.

The conclusions drawn provide sound numerical age models of the exposure history of these samples.

We have been able to demonstrate the timing of two major advances of the formerly expanded Patagonian Ice Sheet during the LGIT. In the past been these have been in question due to the paucity of radiocarbon dates, in the arid conditions prevailing to the east of the crest of the southern-most Andes. The timing of glaciation and initiation of deglaciation over 16° of latitude appears to be synchronous, although the magnitude of glaciation differed markedly from place to place. This asymmetry, in terms of size of expansion, between the northern and southern portion of the Patagonian Ice Sheet reflects the changing pressure gradients during the Last Glacial Cycle. This reflects the intensification and migration of the precipitation bearing westerlies, whose position is controlled by the Antarctic high pressure cell. The change in position of the location of maximum precipitation has caused the assymetic build up and decay of different portions of the Patagonian Ice Sheet recorded sediments and landforms from its former margins.

The timing of the last glacial cycle in southern Patagonia as deduced from TCN exposure dating, indicates maximum ice extent at around 26 ka yr BP and deglaciation by around 17 ka yr BP. With the precision of the technique this is indistinguishable from that of the last glacial period in the Northern Hemisphere. This similarity of moraine chronologies from mid-latitudes in both hemispheres infer a rapid mechanism of climate change, such as global atmospheric triggering being the principle method of global climate signalling during the LGIT.

Results from Antarctica indicate a much more complex picture, with the Antarctic Peninsula and the Shackleton Range Mountains producing very different patterns of glaciation. These data demonstrate that glaciation of the Antarctic Peninsula has been controlled predominately by eustatic sea level fluctuations, recording relatively early deglaciation in comparison to other sectors of the WAIS. Possibly reflecting that this relatively small ice mass, with its high accumulation and ablation rates, is perhaps the most sensitive part of the Antarctic Ice Sheet.

The pattern of deglaciation is very different in the Shackleton Range of Antarctica. In this more continental portion of the continent Quaternary Glacial fluctuations have been characterised by extreme stability. This study shows that ice thickening during the Quaternary has had little or no erosional effects at the altitudes of the summits of the Shackleton Range. Although these are

only preliminary results, they have important implications for glacial modelling studies and research regarding sinks and sources of global seawater during the last glacial interglacial cycle. One approach that may reveal a more detailed picture of glacial expansion would be the application of multiple stable and radiogenic isotopes. The application of these TCN techniques at various altitudes throughout the range could check for short periods of non-erosive ice cover (<100ka).

7.8 Conclusions

The application of the TCN technique using the radionuclides ^{10}Be and ^{26}Al is robust, and offers previously unobtainable insights into the history of exposed rock surfaces. This thesis has demonstrated that this technique is completely dependent on a holistic approach to answering the problems set. Without a sound understanding of both the field relationships of the surfaces in question, together with the intricacies of the chemical extraction and numerical calculation of the exposure model no tangible results will be obtained. This work also highlights the need for the results of TCN studies to be interpreted in conjunction with other available morphological, lithological and biological proxy records. This multiproxy approach can help reveal intractable events which may have occurred to individual samples during their exposure history such as exhumation and high erosion. Both of these effects have been demonstrated within this study.

This thesis has improved knowledge of the spatial and temporal patterns of environmental change in each of the study areas. However it is accpted that the possible precision of this technique could call into question when attempting to correlate interhemisperic climatic events, especially during the high frequency low amplitude events which have charcterised the last glacial interglacial transition. This is predominantly due to the determination of the local production rate of cosmogenic nuclides. This aspect of research is currently under a great deal of scrutiney by numerous research groups, who are working on both the theoretical and experimental aspects of this question. Improving the scaling functions will definatly make cosmogenic exposure dating a more precise tool of absolute dating. However until this day arrives the best approach is to obtain as many ages for the feature or landform under study as possible, inreasing the accuracy of the work, and demonstrating the repeatability of the measurements.

7.9 References

Caldenius C. 1932. Las glaciations cuaternarias en la Patagonia y Tierra del Fuego. Geografiska Annaler 14. 1-64.

Marden CJ. 1993. Late Quaternary glacial history of the South Patagonian Icefield, at Torres Del Paine, Chile. Ph. D Thesis, University of Aberdeen. 298pp.

Wenzens G. 1999. Fluctuations of outlet glaciers in the southern Andes (Argentina) during the past 13,000years. Quaternary Research. 51. 238-247.

Appendix 1

Sample Preparation Procedure for ^{10}Be and ^{26}Al.

Contents:

Chris Fogwill

June 2002

1.0 Initial Sample Preparation: Geography, main labs.

Using sample field description and Photographs attempt to reconstruct sample to allow further description of surface characteristics (i.e., weathering, polish, fracture planes, etc).

Clean all loose organic (lichen), and weathering products with a wire brush and reseal sample in a fresh sample bag.

1.1 Cutting, crushing and grinding: Geology Department cutting rooms.

Using small table saw, or large "clipper" saw, all weathered or leached surfaces and any left over organics on outer surface. Any thickness of surface removed must be recorded for eventual age calculation.

Once "clean" the sample must cut into suitable sized pieces for the jaw crusher available in the Geology labs (max. 3*3*2cm), after which sample must be thoroughly cleaned and dried to avoid any contamination from this environment being carried through to the crushing stage. If required a suitable piece of sample for thin section production should be taken at this point.

Clean, dry samples can now be crushed with the jaw crusher which has been previously thoroughly cleaned, and which must be cleaned between sample runs. Special care to avoid major contamination is required during this stage, and each sample should be crushed onto either clean paper or plastic covering bottom of the crushing draw below the jaws.

Once crushed the sample can be sieved through a sieve stack containing a 500μm, a 250μm sieve and a base to catch the <250μm fraction. In order to obtain enough sample further crushing is required. This can be either done in the jaw crusher, or alternatively with the "gyro-mill". Both of these methods have advantages and disadvantages:

Jaw-crusher: Avoids "powdering" sample, allowing greater return of "useful" fraction (i.e., 500-250μm), although this technique has greater likelihood of contamination.

Gyro-mill: Tends to "powder" sample very quickly, therefore it is best to use for a maximum of 30 seconds for the hardest rocks, and as little as 10 seconds for rocks such as granite.

Once this stage is complete all sample material should be returned to Geography.

1.2 Sieving & Cleaning: Geography main lab and sieve room.

Although the sample was sieved into 3 fractions (>500, 250 & <250μm) in Geology by hand, in order to reduce sample loss during the next few stages it is most efficient to re-sieve the fractions mechanically using a sieve shaker for 20 min. This also allowed the splitting of the 125μm fraction, which is important for ICPMS and GFAAS analysis.

In order to remove, dust and fines produced during the crushing process, the 500-250μm and the 250-125μm fraction were rinsed using 1000ml polypropylene beakers, in the following order:

-Rinse with tap water until clear
-Rinse twice with DI water
-Rinse once with 18mΩ pure water.

This stage removes fines, any left over organic material and a high percentage of micas by allowing them to float off during the early rinsing stages. Once complete the sample can be dried in the oven at approx. 40-50^{0}C, after which the samples can be bagged, labelled and stored.

2.0 Production of Quartz separates: Be/Al Laboratory.

Pure quartz separates are produced by chemical digestion of other minerals and the removal of the outer oxidised weathering surfaces of the quartz component. This is achieved by repetitive dissolution in weak HF and HNO_3, which together leach, dissolve and disperse the products of the feldspars, clays, and micas in the original sample. This process also serves to etch the pure quartz grains, removing any weathering material, together with any external meteoric ^{10}Be captured in this weathering rind.

- Take clean 1 Lt. Nalgene container, rinse once with 1:1 Nitric, and then three times with 18mΩ pure water. This can then be filled to the shoulder with 18mΩ pure water.
- Weigh out approx. 7.5 grams of 500-250μm fraction and place in bottle, recording sample name and weight on side of bottle.
- Add 20ml of HF (48%), and 15ml of 1:1 HNO_3.
- Place in ultra-sonic bath for 18hrs.
- Decant liquid, and use 18mΩ pure water to dissagregate clay by-products and quartz three times.
- Repeat whole process 4 times, to complete dissolution and grain etching.
- Once complete allow to dry in oven (40^0C), covering top to avoid dust contamination, and then weigh each sample to calculate percentage loss on acid dissolution.

Once complete the Quartz separate can be sealed and stored ready for production into Be and Al separates.

3.0 Estimation of minimum pure quartz required.

For the accelerator to obtain a detectable measurement of a low enough percentage error to be of use in the eventual age calculation a minimum number of atoms of cosmogenic Beryllium and Aluminium are required. This can be estimated by knowledge of the following variables:

- Exposure time (estimated / projected)
- Latitude of sample site
- Altitude of sample site

Therefore by calculating the expected production rates, and then using an "exposure age estimate" the volume of pure quartz required can be calculated. To obtain meaningful figures the minimum number of atoms of Beryllium (^{10}Be is used as it has a lower production rate than ^{26}Al), must be around 10^{-12}-10^{-13}, any lower than this will possibly be below the detection levels of the accelerator. Due to the lack of naturally occouring ^{10}Be in Quartz, a known volume of standard ^{9}Be carrier is used to calculate the ratio between this and the unknown concentration of ^{10}Be.

3.1 Production of Aluminium and Beryllium Separates: Be/Al laboratory.

Once enough pure Quartz sample has been produced (volume required dependant on projected age, and sample altitude and latitude (see section 3.0)), the process of separation of the Be and Al components of the Quartz can begin. In order to get an accurate idea of the elemental composition of the sample at this stage a sub-sample should be taken for analysis by ICP-AES. Thus providing multi-elemental analysis, with respect to the volume of Al, Be and feldspars present in the sample. This will help decide if there is a need for addition of an Aluminium carrier prior to the Anion column stage.

The sample should be weighed accurately, in the micro balance into a clean Teflon beaker, taking care to avoid sample loss due to static. Due to the lack of naturally occurring Be in Quartz, a Be carrier (Be Oxide warning) must be added at this stage to allow eventual calculation of the cosmogenic Be in the sample, relative to this known spike (o.5ml 10000ppm). To allow this standard solution to be used as a reference it must be an accurate known volume, this is achieved using a recently calibrated pipette.

3.1.1 Pipette Calibration:

Using 18mΩ pure water and a clean pipette tip, an average weight of the standard volume can be weighed using the balance. This weight should be recorded, and this process repeated 10 times to provide the Standard Deviation and mean average weight of this volume. As with ultra-pure water, its weight in grams should be the same as its volume (ml), it will allow for pipette calibration for the Be carrier used.

3.1.2 Weighing Quartz Sample.

Be Warning: Use Fume hood.

- The working area should always be cleaned with a damp cloth, before and between samples.
- Take clean Teflon container and write the sample I.D on sides and lids.
- Zero containers weight on balance.
- Anti-static gun should be used on both the sample and the Teflon container, prior to carefully transferring the sample into the container (care should be taken to avoid touching the sides with fingers or sample).
- Once complete, the base of the container should be wiped, and the sample replaced into the balance, and the weight recorded (this can be seen to change due to both static and air-movement).
- The Be carrier can now be added, using the recently calibrated pipette. The Carrier should be taken from a small sub-sample bottle Be Warning!!!!!, rather than the original to avoid contamination. The pipette should be filled and emptied once prior to sample transfer.

3.2 Quartz Dissolution:

-Once more HF (conc.) and HNO_3 (1:1) in a ratio of 2:1, are used to digest the SiO_2. This process should be repeated until the quartz has been dissolved, and finally full drying down, to

ensure all SiO_2 is digested. After this stage the sample could still contain Be, Al, Fe, Mg, Ca, Na and Fluorides.

$SiO_2+4HF=SiF_4+2H_2O$

Prior to any addition of HF or HNO_3 the sample should be left at room temperature for a few minutes to allow any sudden reactions to dissipate. Once on the hot-plate, the sample should be kept at 100^0C during working hours, and at a max of 80^0C outside working hours. The volumes of HF and Nitric added should always be recorded. When covered with acid approximately 5 grams of Quartz is dissovled in 24hrs, this can be used as a rough guide to the length of time required for a dissolution.

Opaque and/or translucent solids may remain after this procedure. X-ray diffraction has shown (at least in two cases) that the solids were corundum (Al_2O_3), xenotime (YPO4), and KClO4. Oxides in particular are often very resistant to dissolution. Such solids must be carefully removed from the teflon after washing carefully in HNO3 before proceeding to the Al aliquot stage. Dry the solids (wash in H_2O first), then weigh and subtract mass from the sample mass.

3.2.1 Fuming:

Three additions of HNO_3 (approx. 2.5ml), are now required, allowing the beaker fume and to dry fully between runs (hot plate temperature 150^0C/100^0C).

Three additions of HCL (approx. 2.5ml), are now required, allowing the beaker fume and to dry fully between runs (hot plate temperature 120^0C, $AlCl_3$is volatile at 183^0C).

Fume cupboard must be washed down before and after perchloric addition

Three additions of 1:1 perchloric ($HClO_4$) (approx. 2.5ml), are now required, allowing the beaker fume and to dry fully between runs (hot plate temperature 150-200^0C, although do not add $HclO_4$ to very hot Teflon). This stage should remove any ^{10}B (Boron, an interfering isobar), and Fluoride contamination.

Fume cupboard must be washed down before and after perchloric addition

Once these stages are complete, an aliquot for AA analysis can be taken, and if required a standard Al carrier can be added (depending on multi-element analysis results).

3.2.2 Aluminium aliquot procedure:

Requires two clean 100ml vol flasks for each sample.

- Using a small volume of 1:1 HNO_3, the fully dried down sample should be taken up into solution, the acid allows the Al to go into solution (if necessary this can be done on the hot plate).
- Taking a clean disposable pipette the sample should be homogenised and transferred into the first volumetic flask (2*100ml vol flasks required per sample, must be clean) NOTE: If any solids remain after fuming, dry down and weigh the solids. Subtract this weight from the sample weight. Great care must be taken to make sure that 100% of any Be or Al in solution is removed from the solid. This is achieved by multiple rinses with small volumes of HNO_3.
- 18mΩ pure water can then be used to ensure 100% sample transfer from the Teflon beaker, and fill the flask to the 100ml mark (care required!).
- Shake sample well to homogenise.
- Using a calibrated pipette (see earlier Be carrier addition), 2ml of sample should be transferred into the second clean 100ml vol flask (ie, 4*0.5ml pipettes).
- The remaining 98ml of sample can be replaced into the original teflon.
- The second flask containing the 2ml sample can be filled to the mark.
- This final solution should be transferred into one 30ml and one 60ml bottle, the first of which can be sent for analysis, and the second of which can be archived in case of sample loss. The 30ml sample can be sent off for analysis by ICP-AES.

After this the sample should be dried down, and when ready re-hydrated using <5ml 9N HCl, to rinse beaker thoroughly.

3.3 Anion Column:

This process is undertaken in order to remove the iron (Fe), from the solution, so as to avoid overloading the later cation column stage. Column conditioning should be undertaken before the first run and between each sample. This is undertaken with 3 column volumes (c.v.'s) of 9N HCl (using 20ml columns (i.e. 1cv=20ml)).

C.V.'s	Acid Used	Volume	Solution Contains:
Column conditioning	ultrapure H_2O	60 mL	Zn, Cl complexes
Column conditioning	9M HCl	60 mL	Previous Sample
Sample volume	9M HCl	5 mL	nothing
C.V.'s 1-2	9M HCl	40 mL	Al and Be
C.V.'s 3-6	0.5M HCl	80 mL	other anions

To run sample, in column in solution (<5ml 9NHCl), this should be collected, labelled and stored as sample volume (i.e., first 5ml to come through). Elute 3 c.v.'s of ultra pure H_2O through the column. This removes any Zn or Cl complexes present. Then put 2 c.v.'s of 9N HCl through column, collecting them in a savillex beaker. These cv's should contain Be and Al.

To elute remaining elements, 4 c.v.'s of 0.5N HCl are placed in column, which are then collected, bottled and labelled Bottle 1(c.v.'s 3-6).

3.4 Sample Clean Up:

- On hot-plate, the sample should be fully dried down at 150^0C.
- 2-3ml of HCl can now be added to the sample to ensure it is all in solution, then using ammonia solution and pH paper, the solution should be brought to a pH of 8, to allow precipitation of Al, and Be. This may also allows any left over Boron (^{10}B)and Mg and Ca to go into solution, if left to stand for 24-48 hours (Ivy-Ochs 1996).

- This can then be centrifuged (3000 rpm, time 15 min.), and then the supernatant decanted and kept in a marked bottle.

At this stage the sample is safe to leave in solution. If required, sample can be placed in capped and labeled centrifuge tube. Keep in dark place (photoreactive).

3.4.1 Optional cleaning procedures.

- Rinse with 18mΩ pure water, and conduct an HCl fume [both these stages are optional are depend on the "look" of the sample.
- HCl (<1N) can now be added, prior to cation column stage.

3.5 Cation Column.

This stage is undertaken to split the Be and Al into separates, using different acid strengths to elute the Be, and then the Al. The initial column conditioning, and the collection of the correct column volumes is critical at this stage.

Place sample on the column in the <1N HCl solution added in the last stage.

CV's	Description / Strength	Vol	Solution Contains:
Column conditioning	3 c.v.'s of H_2O	60 mL	complexes
Column conditioning	3 c.v.'s of 9M HCl	60 mL	Previous sample
Column conditioning	3 c.v.'s of 4.5M HCl	60 mL	nothing (equilibrate)
Column conditioning	3 c.v.'s of 1M HCl	60 mL	nothing (equilibrate)
Sample Volume	<1M HCl	<5 mL	nothing
c.v.'s 1-3	Bottle 2 (1M HCl)	60mL	elutant
c.v.'s 4-11	Savillex beaker(1M HCl)	160ml	Be

c.v.'s 12-15	Bottle 3 (1M HCl)	80ml	elutant
c.v.'s 16-19	Savillex beaker (4.5M HCl)	80ml	Al

If sample >40 g, dry down Be fraction. Dry down and put aside the Al fraction. For the Be fraction only, repeat cation column procedure including column conditioning. This will remove Al contaminating the Be fraction. Add the 80 mL Al elutant to the original Al fraction in the teflon.

If sample >70 g, repeat this procedure twice (for a total of 3 cation column runs).

Once collected the Al and Be samples should be dried down to c. 2ml, and the two elutant volumes kept and labelled. The columns should be capped and left until there next use, when they will be conditioned again and the conditioning elutant kept, containing any left over product of this sample.

Now the Al and Be are separate, great care must be taken to avoid cross contamination due to the air movement of the fume hood.

3.6 Hydroxide Formation, precipitation and oxidation:

This stage is the final one prior to the samples being sent off for production into targets at the AMS facility. Once again Nitric and ammonia are used in order to precipitate the hydroxides of Be and Al, which come out of solution at different known pH's.

- Using a small volume of 18mΩ pure water, the sample should be transferred into tapered centrifuge tube, to this c. 2-3 ml of 9M HCl is added, and the beaker is washed to ensure 100% sample removal.
- Using a clean pipette ammonia solution is added drop-wise until precipitate begins to form. The pH should be checked regularly with Beryllium precipitating at between pH 9-10, and Aluminium at a pH of about 8.

- Once reached the solution and the precipitate should be left overnight to complete precipitation and allow any Boron to go into solution. The sample can now be centrifuged at 3000 r.p.m. for 10 mins., and then the liquid decanted, bottled and labelled.
- Using a heater block set at a temperature of 70^0C, the sample can be dried over a period of 72hrs in the original centrifuge tube. This is undertaken due to problems with transfering the wet percipitate from the centrifuge tube to quartz vials. Once completely dry the precipitate can be carefully physically transferred into the clean quatz vials in the laminar flow hood.
- The samples can now be oxidised at high temperature in a furnace (850^0C for 2 hours), then packed in clean non-borosilicate glass sample bottles ready for sending to the AMS facility for pressing into targets.

If there are problems at the accelerator, then any Be or Al lost during the process could be recovered from the various bottles and supernatents kept during the process. Foe this reason it is necessary to keep these well logged and clearly marked for later reference.

4.0 Cleaning Protocol:

In order to reduce risks of contamination, all lab equipment coming into direct contact with the Al/Be solution should be cleaned in the following way:

- Rinse once with 1:1 HNO_3.
- Rinse 3 times with 18mΩ pure water.

Other items which require cleaning include pipette tips, quartz vials and the quartz sled. In order to avoid cross-contamination, 3ml disposable pipettes are used for all non-critical additions or liquid transfers, these are cleaned with aerosol air prior to use.
Items such as Tweezers can be rinsed with 1:1 HNO_3, and 18mΩ pure water, and gloves should be replaced regularly, and rinsed with 18mΩ pure water, between stages.

4.0.1 For all Teflon:

The Teflon lab-ware used in this process should be thoroughly cleaned by the following procedure:

- Place in 18mΩ pure water to neutralise any acid.

Just prior to use of Teflon in Procedure.

- Scrub with tissue to remove any solids on base of Teflon.
- Boil in 1:1 NHO_3 for 2hrs
- Boil in 1:1 HCl for 2hrs
- Rinse in 18mΩ pure water

4.0.2 Column Loading :

Using 20ml Bio-Rad Ion Exchange Resins:

- Take new polypropolene column, and ensure there is a foam disc in base.
- Mix resin with 18mΩ pure water, in a clean beaker, allow resin to settle slowly through the water removing problems due to air inclusions when the columns are in use.

4.0.3 Beryllium Hazard:

Any material that comes into contact with either Be carrier, BeOH, or BeO MUST either be rinsed with dilute HNO3 or bagged separately and placed in rubbish bin. This includes teflon beakers, pipette tips, disposable pipettes, spatulas, scissors, etc. All activities must be undertaken in the fume cupboard.